POLITECNICO DI TORINO

DIPARTIMENTO DI INGEGNERIA STRUTTURALE, EDILE E GEOTECNICA

Corso di Laurea Magistrale in Ingegneria Civile

Tesi di Laurea Magistrale

EFFECTS OF CORROSION ON REINFORCED CONCRETE BRIDGE PIERS IN SEISMIC ZONE

Relatore:
Prof. Marco Domaneschi
Correlatore:
Prof. Joan Ramon Casas

Candidata:
Mara Bartolozzi

Ottobre 2020

Contents

Abstract

This research deals with the effect of corrosion on reinforced concrete structures. In particular, it focuses on the consequences of bond strength deterioration. In a previous study (De Gaetano, 2019) the seismic capacity of a bridge pier subjected to corrosion was evaluated in time domain, considering the steel reinforcement cross-section reduction effect only. The aim of the present study is to deepen the previous investigation considering also the problem of loss of adherence between steel and concrete. Indeed, the analyzed structure is the same, so that a coherent comparison of the former results is possible. Furthremore, it is possible to assess to what extent the loss of bond can affect the bridge's strength and ductility. In the first part of the thesis a literature review of the main research results carried out on the topic and of the developed empirical models is presented. Then, one model has been chosen to be applied to the bridge case study, obtaining as result the effect of corrosion during the whole service life of the structure (100 years). The modification of strength capacity and ductility of the structural element are analyzed. In the last part of the thesis, a review of the most employed protective methods against corrosion is presented, for new and existing constructions. Moreover, a summary of corrosion monitoring techniques is reported, focusing on non-destructive methods.

Chapter 1

Introduction

The corrosion of steel reinforcement is the main reason of deterioration and shortening of the service life for reinforced concrete structures. It represents an issue affecting most of the existing structures that, if not constantly monitored and subjected to an immediate repairing intervention, may undergo to strong damages and even to complete failure. Environmental conditions and quality of the materials are key factors for the durability of a structure. Deterioration in an unavoidable process that, even in the best environmental conditions and using the higher quality materials, occurs. That is why the aim of a good design is to postpone the beginning of the deterioration process as much as possible in order to guarantee the functionality and the safety of the structure for a long time, taking into account the necessity of continuous maintenance interventions.

The collapse of the Morandi's Polcevera viaduct in Genoa (Italy) in 2018 is mentioned as example of a structure where the degraded conditions of the materials represented one of the causes of the failure (Figure 1.1). An active structural monitoring system could predict the behaviour of the structure in time. Performing a post-collapse study has been demonstrated that even a basic analysis, inclusive of fatigue and corrosion models, could be sufficient to predict the remaining life of the bridge (Domaneschi et al. 2020). Prediction of the structural behaviour is the only solution to avoid these disasters and to act on structures in time.

As showed in Figure 1.2, the three main corrosion effects of steel rebars are the reduction of the rebar cross-section, the cracking of the concrete cover and the decrease of the bond strength (Cairns, 2008). It is necessary to guarantee a sufficient bond between the concrete and reinforcing/prestressing steel in order to exploit the combination of the compressive strength of the concrete and the tensile strength of the steel. That is why it is fundamental to understand as better as possible how corrosion may change the bond properties. The use of truthful degradation models allows to know how the structural properties will change in time with specific boundary conditions.

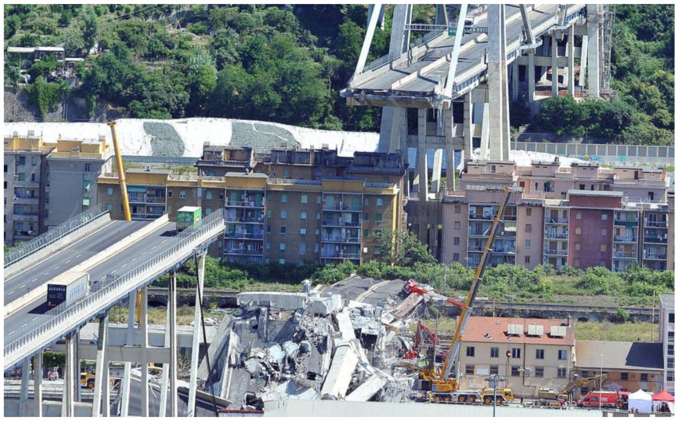

Figure 1.1: Collapse of Morandi bridge (Italy, 2018)

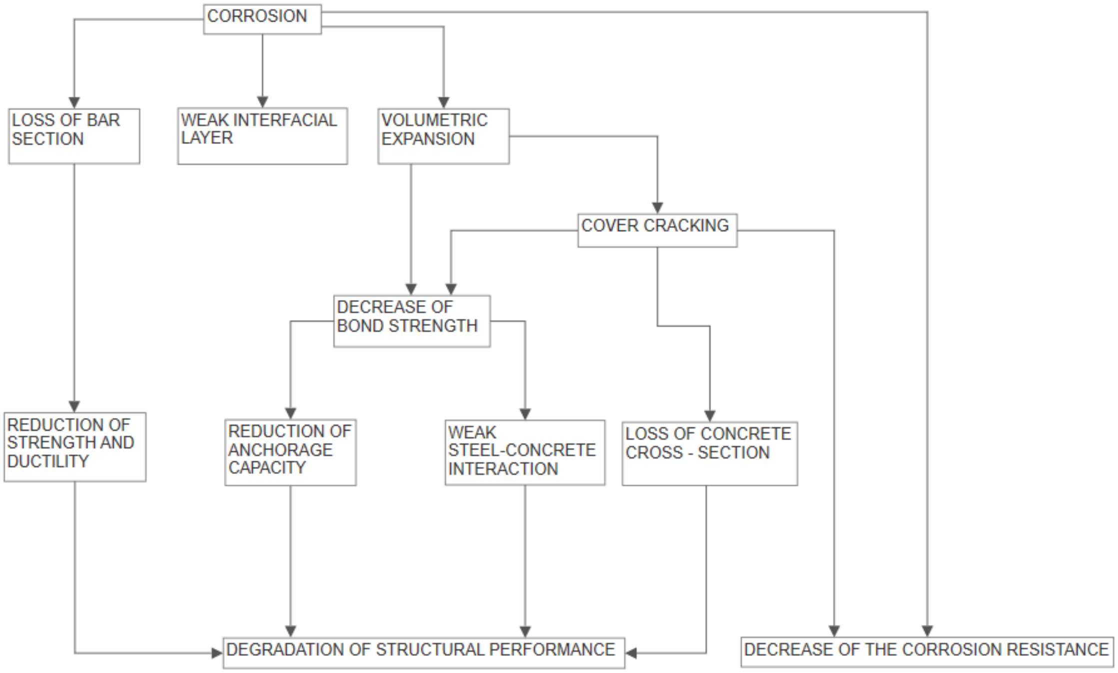

Figure 1.2: Effect of reinforcement corrosion on structural capacity (Cairns,2008)

Chapter 2

Literature review

2.1 Corrosion process

Corrosion is an electrochemical process where iron tends to return to its original form (oxidised) giving away electrons. Iron oxides (rust) are characterized by a higher volume than the initial material and create radial pressure that causes cracking, spalling and delamination in the concrete cover as shown in Figure 2.1 (Bilcik, 2013). In Figure 2.2. it is possible to see the important difference in volume between iron and corrosion products. The reactions of corrosion are reported below and are illustrated in Figure 2.3. It is a redox process that requires water and oxygen to occure.

$$2 \times (Fe \rightarrow Fe^{2+} + 2e^{-}) \quad Oxidation(anode) \tag{2.1}$$

$$O_2 + 2H_2O + 4e^{-} \rightarrow 4OH^{-} \quad Reduction(cathode) \tag{2.2}$$

$$2Fe + O_2 + 2H_2O \rightarrow Fe^{2+} + 4OH^{-} \rightarrow 2Fe(OH)_2 \tag{2.3}$$

$$Fe(OH)_2 + O_2 \rightarrow Fe(OH)_3 \rightarrow Fe_2O_3 \times H_2O \tag{2.4}$$

Concrete represents a physical and a chemical protection for the steel reinforcement. The functionality of the physical barrier depends on the thickness of the concrete cover and its quality. A high quality concrete presents low porosity and permeability and a high resistance against external and internal attacks. The chemical protection is exhibits trough the creation of an alkaline environment. In fact, due to the presence of calcium, potassium and sodium oxides and hydroxides in concrete's pores free water, in normal conditions the concrete has a $pH > 12$, that stabilizes the protective layer on the steel rebar surface. This layer consists of a passive oxide film that isolates the reinforcement from external attacks.

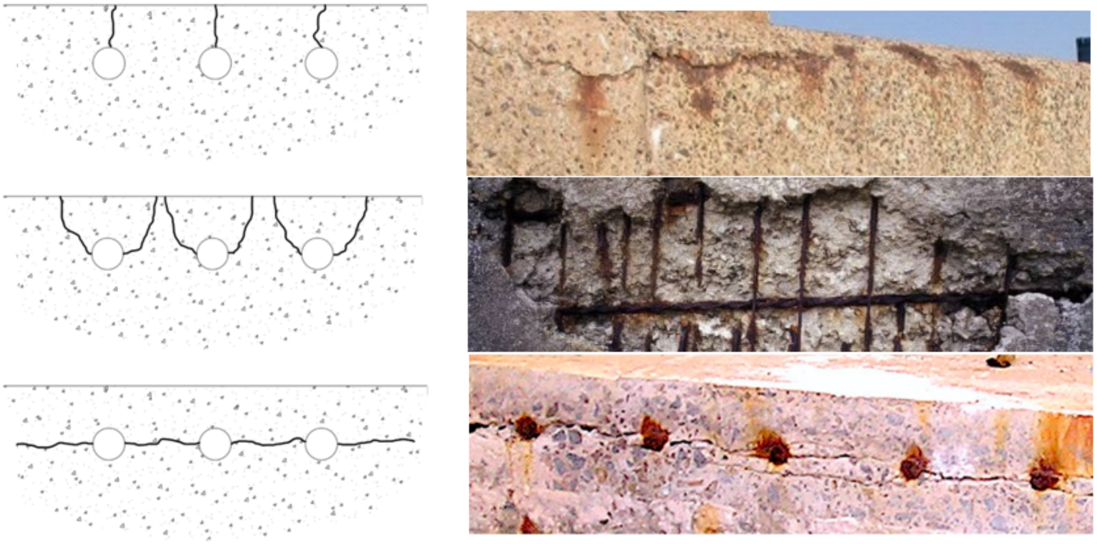

Figure 2.1: Effects of corrosion on concrete cover: cracking (top), spalling (center) and delamination(bottom).

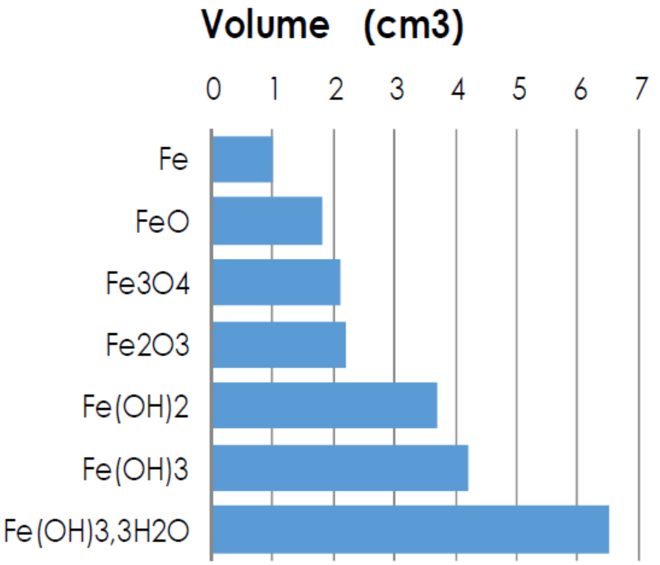

Figure 2.2: Oxidation states of iron.

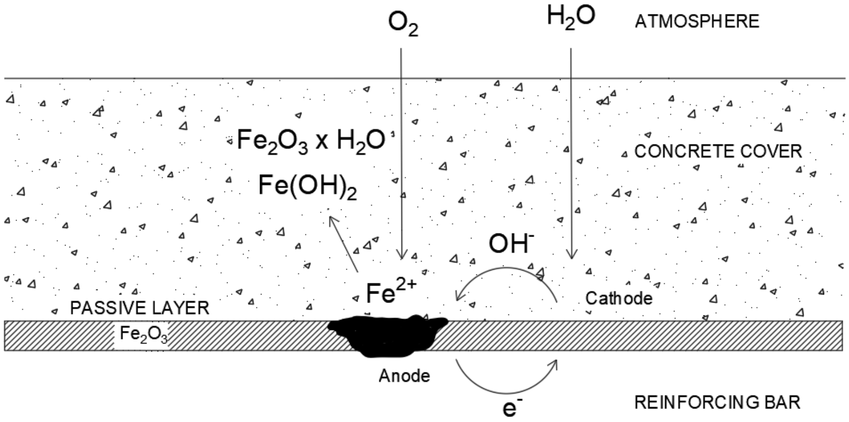

Figure 2.3: Corrosion mechanism.

The protection provided from the concrete can be threatened by chemical (carbonation and chloride penetration) and physical (tension) processes.

The carbonation (general corrosion) is due to the penetration of carbon dioxide from the atmosphere in the concrete. Ones in the pores, it reacts with the Portlandite $Ca(OH)_2$ (compound that maintain the alkalinity in the concrete) and leads to a reduction of pH (up to 8-9) that does not permit the existence of the passive layer. In Equation 2.5 is reported the corresponding chemical reaction.

$$Ca(OH)_2 + CO_2 \rightarrow CaCO_3 + H_2O \tag{2.5}$$

In the case of chloride attack (localized corrosion) the ions can penetrate and reach the reinforcement through the pores of the concrete or the cracks, in case they are already present in the structure. As showed in Figure 2.4 the corrosion occurs between the exposed steel (anode) and the passive steel (cathode), in presence of a big differential potential energy caused by the uneven distribution of chlorides on the reinforcement surface. The iron (anode) is consumed into iron ions (formation of pits). The redox process is reported below.

$$Fe + Cl^- \rightarrow FeCl_3^- + 2e^- \quad Oxidation(anode) \tag{2.6}$$

$$O_2 + 2H_2O + 4e^- \rightarrow 4OH^- \quad Reduction(cathode) \tag{2.7}$$

$$FeCl_3^- + 2OH^- \rightarrow Fe(OH)_2 + 3Cl^- \tag{2.8}$$

In the reaction chlorides are not consumed allowing to the process to continue and forming the typical pits on the steel surface.

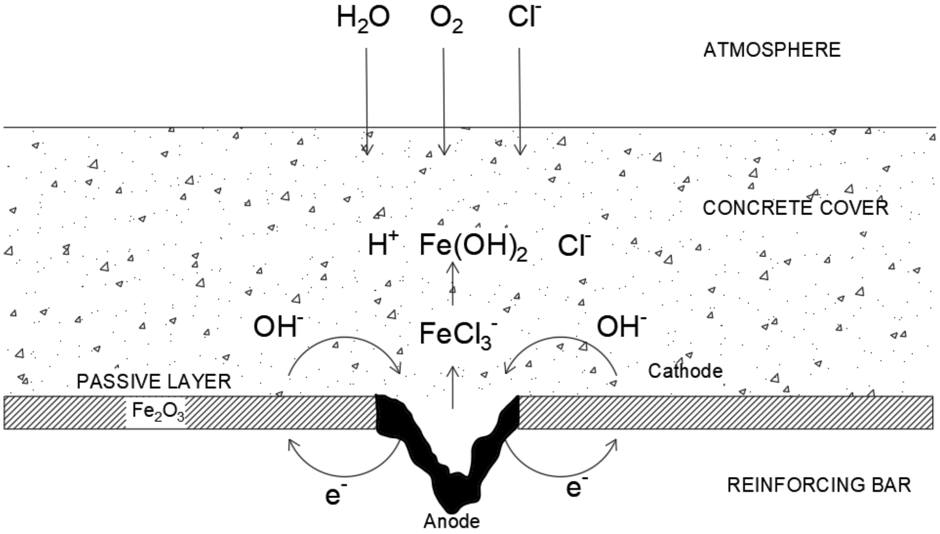

Figure 2.4: Chlorides corrosion mechanism.

2.2 Bond mechanism

The bond mechanism, between concrete and reinforcing steel bar, creates inclined forces that can be divided in a longitudinal component (bond stress) and a radial component (normal/splitting stress). The slipping mechanism between steel and concrete is defined as the relative displacement between the two materials. The bond forces are equilibrated by tensile stresses in the concrete cover that, if become higher than the tensile strength of the concrete, lead to the formation of cracks. If the concrete around the steel bar is cracked and there is no transversal reinforcement or if the longitudinal steel bar yields, bond stresses cannot be transferred, and a splitting failure can occur. If good confinement is provided to the reinforcing bar and it is not yielded, a pull-out failure is more probable (Lundgren, 2005). The first one leads to the formation of longitudinal and transversal cracks that, decreasing the bond strength, lead to the slipping of the rebar. Differently, the pull-out failure is characterized by the crushing of the concrete around the bar without cracks formation (Figure 2.5). In Figure 2.6 the bond-slip relationship of the two failure mechanisms are shown.

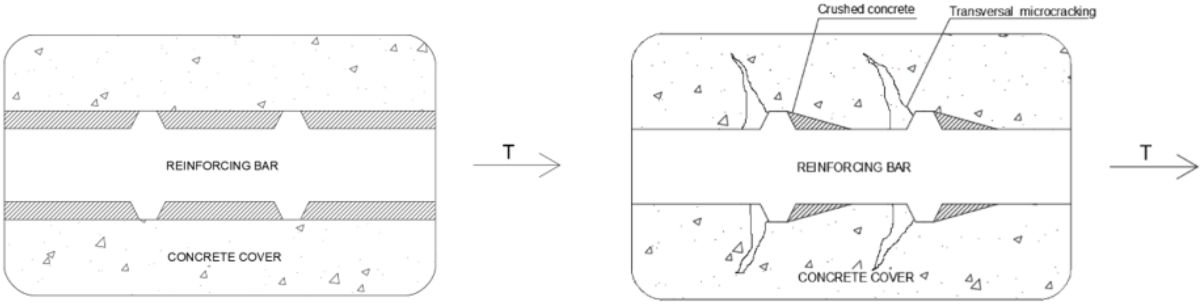

Figure 2.5: Pull- out failure (left) and splitting failure (right).

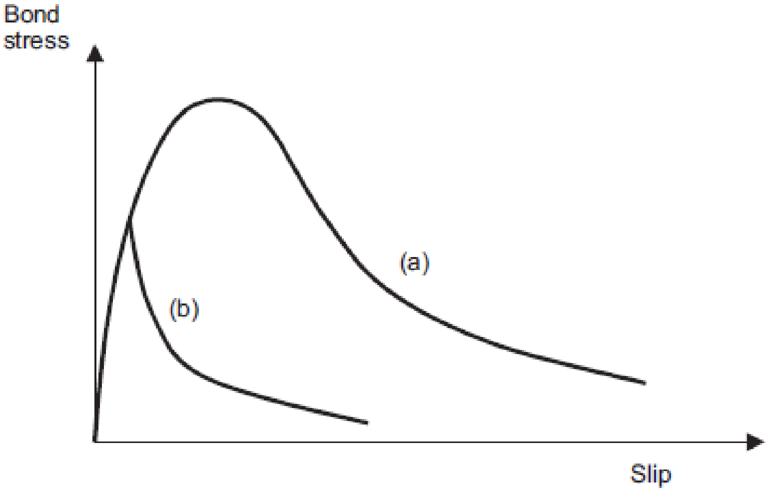

Figure 2.6: Bond -slip relationship in pull-out failure (a) and splitting failure or loss of bond due to reinforcement yielding (b) (Lundgren, 2005).

The factors that influence the bond strength are the concrete cover/ bar diameter ratio, the type of concrete and the steel confinement. The confinement provided by the stirrups can be threatened because of the stronger corrosion that they can undergo, due to the small cross-sectional area and the smaller concrete cover respect to the longitudinal bars. This may lead to a decrease of shear resistance capacity and so in a change of the failure mode, from ductile flexural to brittle flexural-shear failure mode.

The mechanisms that contribute to bonding are: chemical adhesion (low stress level), friction, and mechanical interaction (high stress level) between the steel and the concrete (Kabir, 2014). The adhesion is due to the chemical interaction and represents a small fraction of the total bond strength. The friction represents the main component of the bond strength in plain steel bars. When the bond stress overpass the concrete strength, longitudinal cracks appear (splitting failure) and is the friction that provides the resistance against the relative displacement between the two materials. It is influenced by the compressive force perpendicular to the contact surface, by the surface interface roughness and by the degree of confinement. The mechanical interaction consists in physical interlocking between the two materials (mainly due to the presence of ribs on the steel surface) and depends on the confinement of the steel rebar provided by the concrete cover and the stirrups. In Figure 2.7 the bond mechanisms are illustrated.

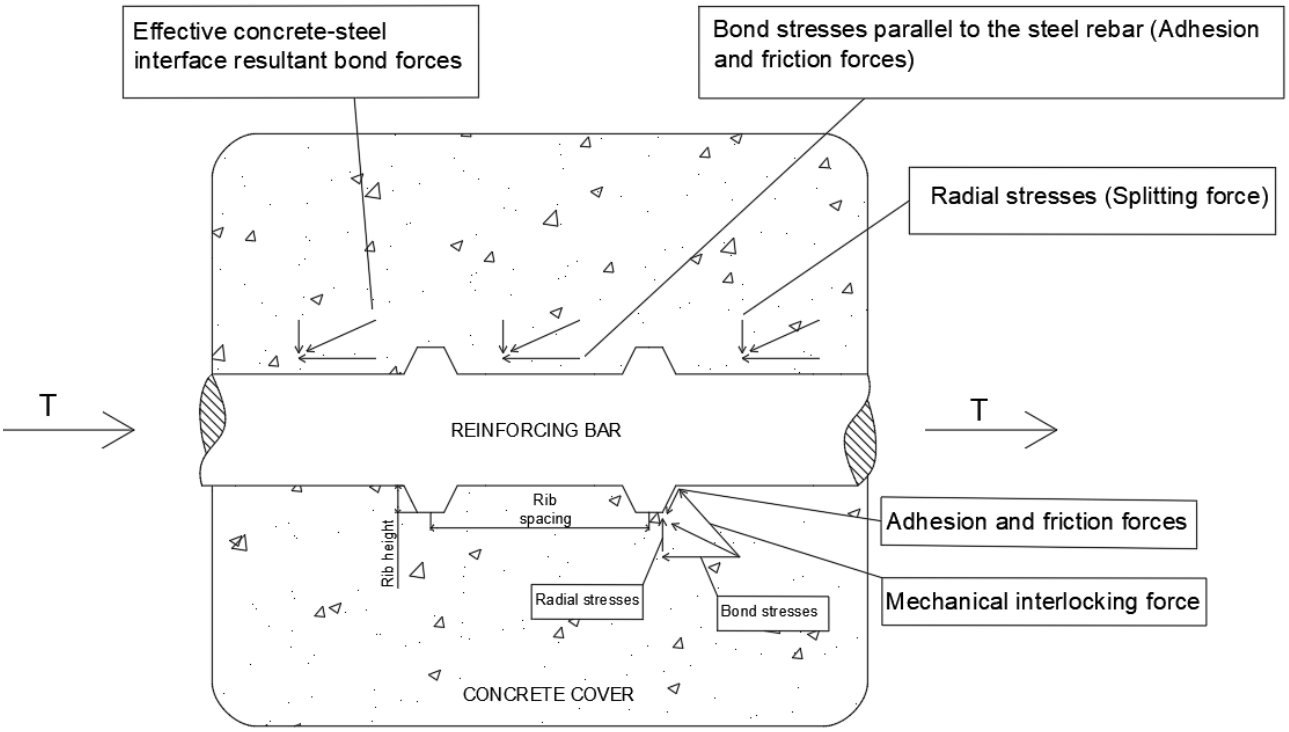

Figure 2.7: Components of the bond strength.

2.3 Determination of the bond strength

The main tests used to determine the bond strength in reinforced concrete elements are the pull-out and the beam test. Pull-out tests are the most used because of their execution simplicity. A steel rebar is placed in the centre of a cubic specimen and the pulling force is applied at one end, and the displacement in the other end are measured. The bond strength is obtained through equation 2.9 (RILEM RC5).

$$\tau = \frac{P}{\pi \phi L_a} \tag{2.9}$$

- τ: bond strength
- P: applied load
- ϕ: rebar diameter
- L_a: anchorage length

The beam test is a four-point bending test. The tested specimen consists in two concrete blocks connected by a steel reinforcement in the bottom part. The force is applied in the top part symmetrically on each concrete block in a continuous way and the movement of the bar is measured. The test is carried on until the bond strength is exceeded. The value of the bond strength can be obtained from Equation 2.10 (RILEM RC6).

$$\tau = \frac{F_a}{\pi \phi L_a} \tag{2.10}$$

- τ: bond strength
- F_a: rebar load $= 1.25P$
- P: applied load
- ϕ: rebar diameter
- L_a: anchorage length

Figures 2.8 and 2.9 show the characteristics of both tests stated by RILEM (International Union of Laboratories and Experts in Construction Materials, Systems and Structures). Despite the pull-out test is the most widespread, it slightly overestimates the bond strength. In fact, the rigid plate support increases it because of its bearing action on the specimen (compression of the concrete) and the friction that develop between it and the concrete, that provides confinement to shear deformations reducing the longitudinal cracking. Differently, the beam-test can represents the bond behaviour with higher accuracy. In fact, in this type of test the specimen is not compressed and this allow the developing of splitting cracks along the steel bar (Gudonis et al. 2014).

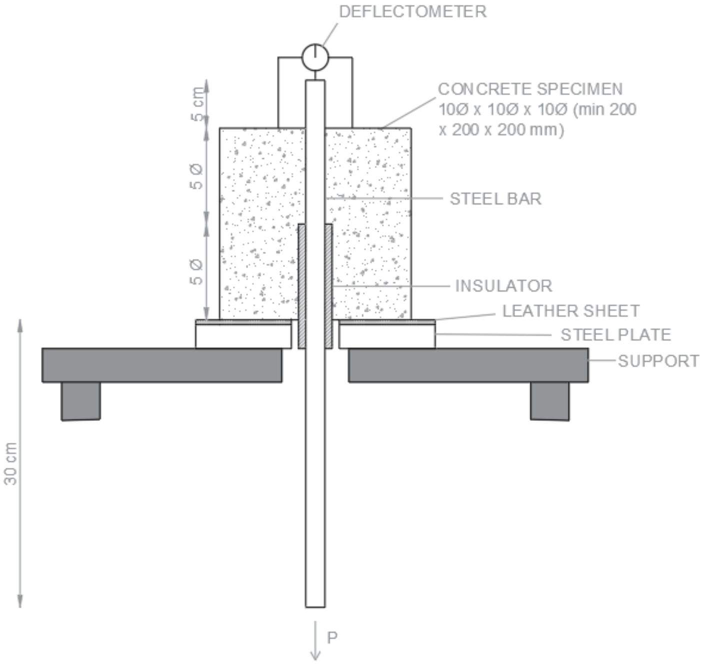

Figure 2.8: Pull-out test set-up.

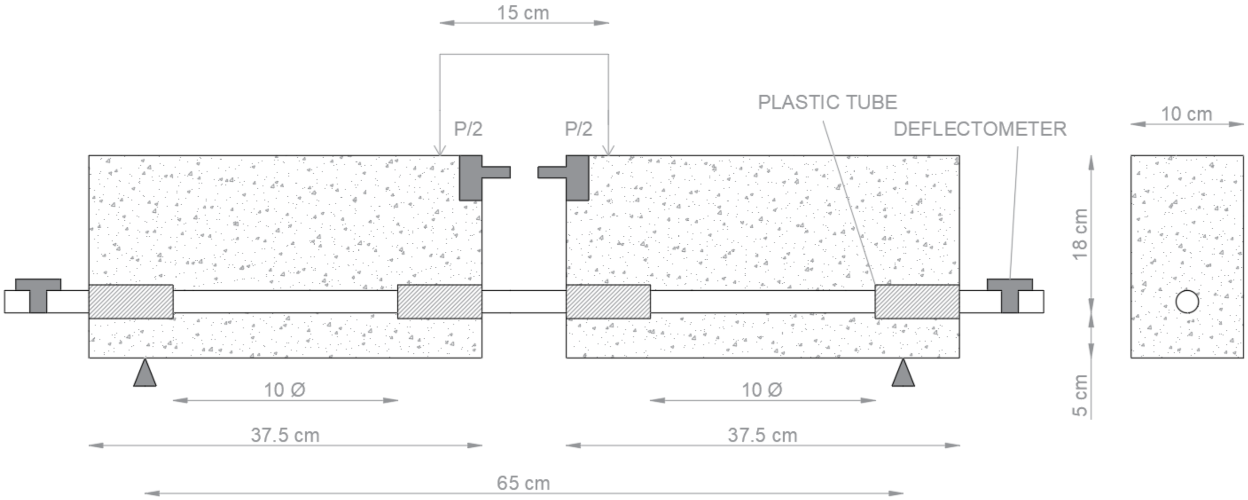

Figure 2.9: Beam test set-up.

2.4 Bond deterioration: State of the art

One of the first studies regarding the corrosion effect on the steel-concrete bond strength in RC structures was carried out by Al-sulaimani et al.(1990). Tests were conducted on beam and central pull-out specimens and was demonstrated that low level of corrosion, before the cracking of concrete (precracking stage), causes an increase in the bond capacity of the steel bars because of the increase of friction between steel and concrete, but rapidly it decreases with the advancing of the corrosion process. In Figure 2.10 it is possible to observe the initial increase of the bond strength, due to the formation of corrosion expansive products, and the following strong decrease, caused by the replacement of part of the steel with a weak layer of loose corrosion products and by the crack of the concrete cover. As presented in Zhao Y. and Lin H. (2018), this behaviour was demonstrated by Almusallam et al. (1996), Mangat et al. (1999), Stanish (1999), Yuan et al. (1999) and Zhao et al. (2013) too. Moreover, was proved that confined concrete exhibits less reduction in the bond strength respect to the unconfined case (Bhargava et al. (2007), Coronelli (2002), Lundgren (2002), Wang and Liu (2004) and Zhao et al. (2013)). As reported in Zhao Y. and Lin H. (2018), the studies of Fang et al. (2004) and Fischer et al. (2010) reveal that in presence of stirrups the effect of corrosion on the bond strength is limited and this result was confirmed by Al- Sulaimani et al. (1990), Cabrera (1992), Castel et al. (2016), Hanjari et al. (2011), Rodriguez et al. (1994) and Xia (2010).

As reported in Coronelli et al. (2004), in the empirical model of Rodriguez et al. (1994) the residual bond strength is formulated as:

$$\tau_{max}^{res} = \tau_{concrete} + \tau_{tie} = 0.6\left(0.5 + \frac{C}{d_b}\right) f_{ct}\left(1 - \beta X^{\mu}\right) + kA_{tr} f_y / \left(s d_b\right) \tag{2.11}$$

- f_{ct} concrete tensile strength [MPa]
- $\tau_{concrete}$ concrete contribution to bond [MPa]
- X corrosion attack penetration in the longitudinal bar [mm]
- τ_{tie} contribution to bond from the transverse reinforcement [MPa]
- $\frac{C}{d_b}$ cover to bar diameter ratio
- $\beta, \mu,\ k$ empirical constant
- A_{tr} section of a stirrup [mm2]
- f_y yield stress of a stirrup [MPa]
- S spacing of the stirrups [mm]

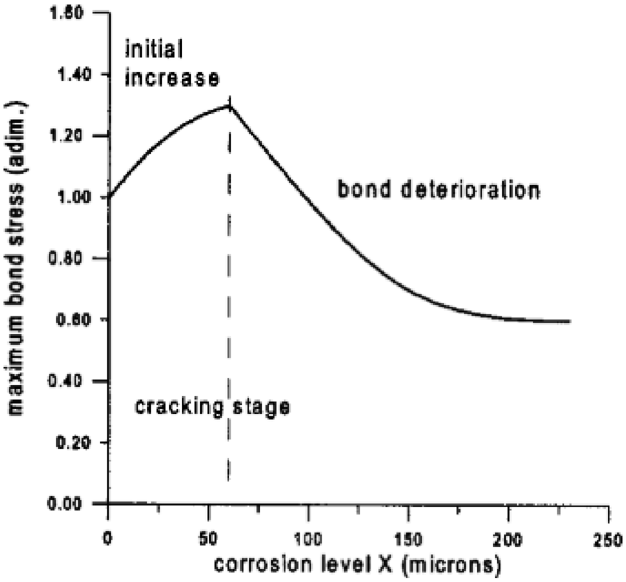

Figure 2.10: Variation of the bond strength with the corrosion level (Coronelli and Gambarova, 2004).

The relation is obtained performing bond tests on specimens with different concrete covers and amount of stirrups. In this model the same bond stress-bar slip relationship for the whole reinforcement is assumed, which means uniformly distributed corrosion on the bars, that is not fully representative of the reality. In addition, the reliability of the empirical model developed is linked to the arrangement of the steel rebars, in fact, the expression can be considered truthful only if the configuration considered is like the one used in the tests performed by Rodriguez at al.. Moreover, it does not consider stirrups corrosion, but this phenomenon can be taken into account by reducing their cross-sectional area.

Chung et al. (2008) performed tests on flexural slabs with corroded reinforcement and the results showed that the decrease of moment capacity is mainly due to the deterioration of the bond between concrete and steel bars and secondarily to the loss of cross sectional area of the steel bars.

Figure 2.11 shows the results of tests performed by different authors, plotting the relative bond strength (bond strength in case of corroded reinforcement divided by the non deteriorated bond strength) at different corrosion levels (expressed as mass loss percentage). The solid points represent the specimens provided with stirrups and the others those without. In the confined specimens it is possible to observe a high bond strength even for large amount of corrosion, while in the unconfined ones the initial increase in the strength is immediately followed by a strong decrease.

The experimental results obtained by different authors compared with several mathematical models are shown in Figure 2.12 and the models developed are reported in Table 2.1. The reliability of these models is not fully satisfactory because they don't consider the influence of confinement, corrosion rate, location of the reinforcement steel bar and loading method. Moreover, they do not show an increase of the bond strength at low corrosion level. The parameters present in the expressions are listed below.

- $\tau_u(\eta)$ bond strength of corroded specimens
- $\tau_u(0)$ bond strength of non-corroded specimens
- η percentage of steel mass loss
- c/d ratio concrete cover/bar diameter

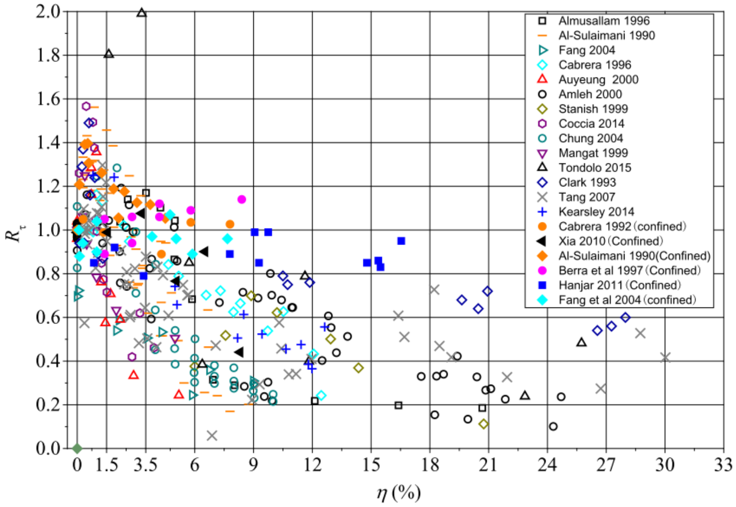

Figure 2.11: Tested relative bond strength (R_τ) at different corrosion level η (Zhao and Lin, 2018).

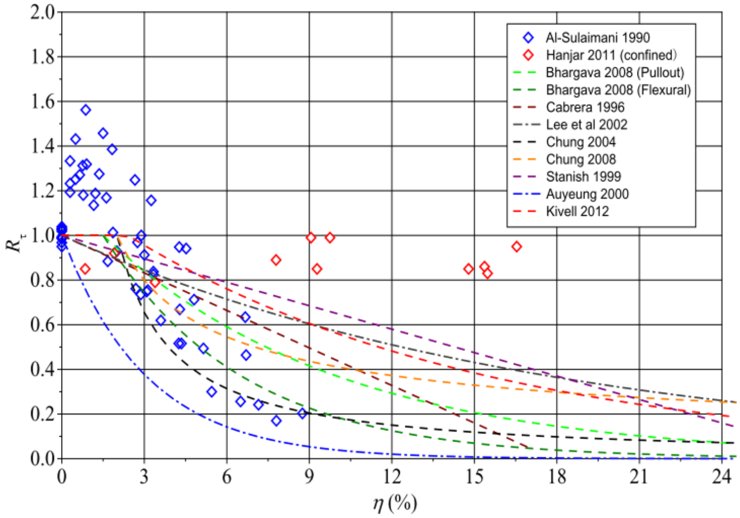

Figure 2.12: Variation of the relative bond strength (R_τ) with the corrosion level according to several models expressed as percentage of mass loss η of steel (Zhao and Lin, 2018).

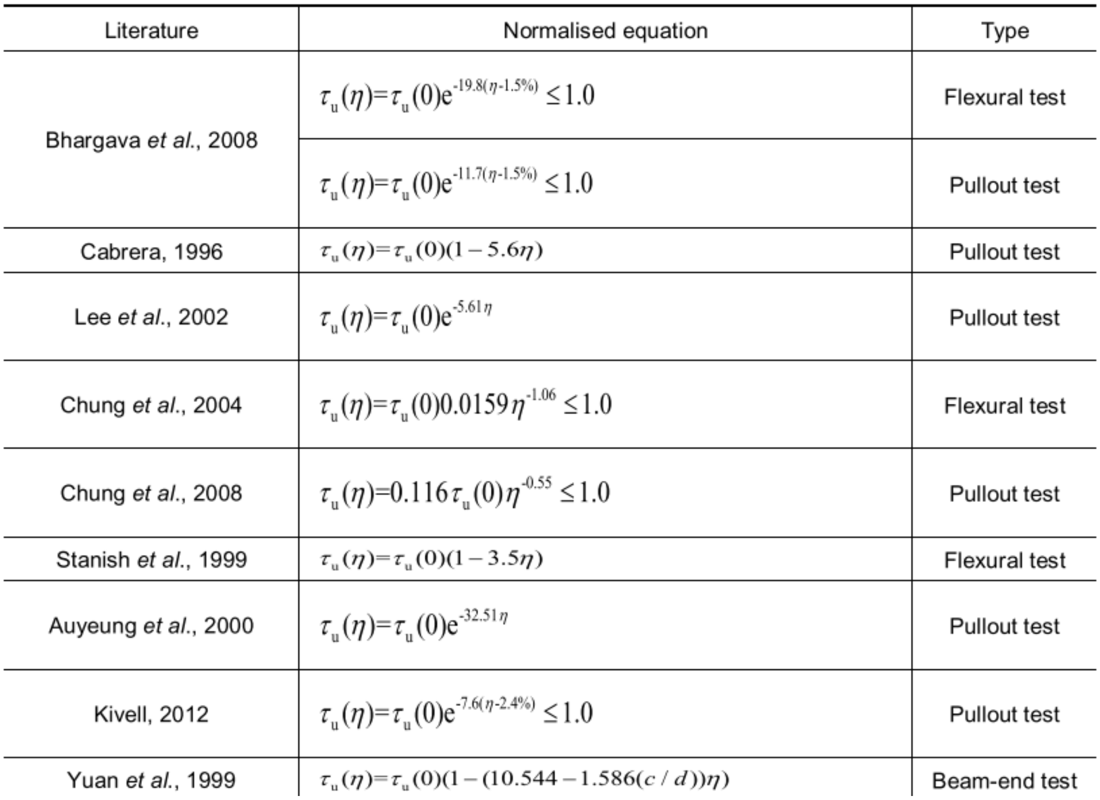

Literature	Normalised equation	Type
Bhargava *et al.*, 2008	$\tau_u(\eta)=\tau_u(0)e^{-19.8(\eta-1.5\%)} \leq 1.0$	Flexural test
	$\tau_u(\eta)=\tau_u(0)e^{-11.7(\eta-1.5\%)} \leq 1.0$	Pullout test
Cabrera, 1996	$\tau_u(\eta)=\tau_u(0)(1-5.6\eta)$	Pullout test
Lee *et al.*, 2002	$\tau_u(\eta)=\tau_u(0)e^{-5.61\eta}$	Pullout test
Chung *et al.*, 2004	$\tau_u(\eta)=\tau_u(0)0.0159\eta^{-1.06} \leq 1.0$	Flexural test
Chung *et al.*, 2008	$\tau_u(\eta)=0.116\tau_u(0)\eta^{-0.55} \leq 1.0$	Pullout test
Stanish *et al.*, 1999	$\tau_u(\eta)=\tau_u(0)(1-3.5\eta)$	Flexural test
Auyeung *et al.*, 2000	$\tau_u(\eta)=\tau_u(0)e^{-32.51\eta}$	Pullout test
Kivell, 2012	$\tau_u(\eta)=\tau_u(0)e^{-7.6(\eta-2.4\%)} \leq 1.0$	Pullout test
Yuan *et al.*, 1999	$\tau_u(\eta)=\tau_u(0)(1-(10.544-1.586(c/d))\eta)$	Beam-end test

Table 2.1: Mathematical models for bond strength of corroded reinforcement (Zhao and Lin, 2018).

Figure 2.13 shows the result of the research by Kivell (2012). His study confirms the results obtained in the past by other researchers. With the increase of the corrosion level an initial increase of friction and a decrease in the mechanical interaction between the materials can be observed.

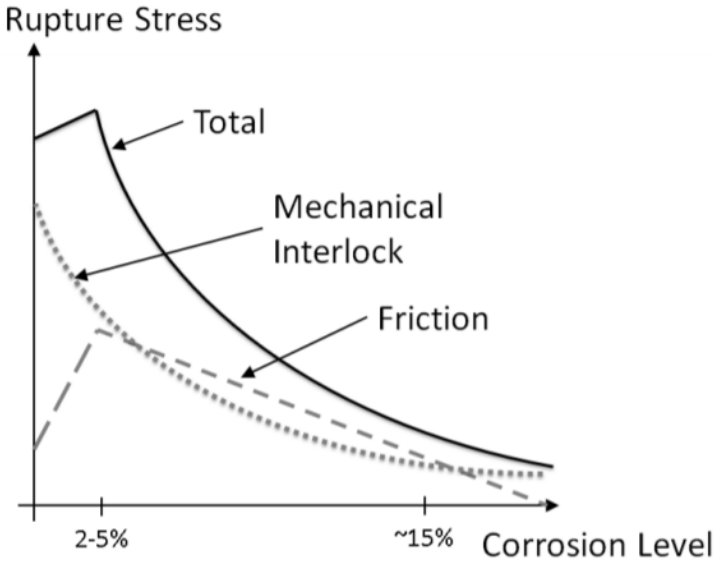

Figure 2.13: Variation of bond strength, friction and mechanical interaction with the corrosion level (Kivell, 2012).

In the study carried out by Coronelli (2002) the model of the bond strength for non-corroded bars proposed by Cairns and Abdullah (1996) is presented. The bond strength is expressed as the sum of the bond strength related to the splitting of the cover (splitting component) and τ_b^0, a term function of the interface cohesion (non- splitting component) (Eq. 2.12).

$$\tau_{bu} = kp^{max} + \tau_b^0 \tag{2.12}$$

- p^{max}: maximum pressure at bond failure [MPa]
- $\tau_b^0 = nA_r f_{coh} \left[cot\delta + \tan\left(\varphi + \delta\right)\right] / \left(\pi d_b s_r\right)$ [MPa]
- $k = nc_r tan(\varphi + \delta)/\pi$
- n: number of transverse ribs in the section considered
- s_r: rib spacing [mm]

- A_r: rib area in the plane at right angles to bar axis $[mm^2]$
- c_r: coefficient, depending on the rib shape and area
- δ: orientation of the ribs
- ϕ: friction angle between steel and concrete
- f_{coh}: adhesion strength [MPa]

Starting from the model of Cairns and Abdullah, a modified model has been developed by Coronelli (2002), in order to consider the effect of corrosion (Eq. 2.13). The changes in the friction and the adhesive stresses due to the reinforcement oxidation are considered by changing the adhesion strength and the friction angle, and the area of the steel rebars is modified reducing the rib height. The last term in Equation 2.13 represents an additional contribution to the bond strength, and it is obtained multiplying the pressure at the interface generated by the rust, by the friction coefficient of rusted steel.

$$\tau_{bu} = k(X)\, p^{max}\left(X\right) + \tau_b^0\left(X\right) + \mu\left(X\right) p_{corr}\left(X\right) \tag{2.13}$$

- X: depth of corrosion attack [μm]
- $\mu\left(X\right)$: friction coefficient of rusted steel
- $p_{corr}\left(X\right)$: pressure developed by corrosion products expansion [MPa]

When the corrosion level is low, the oxides adhere to the surface of the steel bar but with the progression of the phenomena the material between steel and concrete becomes weak. Using the results from the friction test carried out by Youlin (1992), the friction coefficient and the adhesion strength have been modelled in a linear way (Equations 2.14 and 2.15) with the introduction of X, the corrosion depth that exceeds the threshold that cause cracking of the concrete cover X_{cr}, both expressed in mm.

$$\mu = tan\phi = B - C\left(X - X_{cr}\right) \tag{2.14}$$

$$f_{coh} = D - E(X - X_{cr}) \tag{2.15}$$

The model parameters B, C, D, E have been obtained from experimental results (Rodriguez, Ortega and Garcia (1994)). Beam tests have been performed on RC cubic specimens and the four parameters have been found with the least-square method.

Lin and Zhao (2016), developed a mathematical model (Equation 2.16) that considers the confinement provided by the stirrups and the concrete, and the corrosion current density. Starting from tests results and previous studies, they formulate a model for the bond strength as:

$$\tau_u\left(\eta\right) = \tau_u\left(0\right) R_\tau \tag{2.16}$$

- $\tau_u\left(0\right)$: bond strength of non-corroded specimens
- $\tau_u\left(\eta\right)$: bond strength of corroded specimens
- Relative bond strength: $R_\tau = \begin{cases} 1 & \eta \leq\ 1.5\% \\ e^{-}\delta\left(\eta - 1.5\%\right) & \eta >\ 1.5\% \end{cases}$
- Degradation coefficient: $\delta = \begin{cases} \frac{k_1+k_2(c/d)}{k_4\xi_{st}+1} & i_{corr} \leq 200\frac{\mu A}{cm^2} \\ \frac{k_1+k_2(c/d)}{k_4\xi_{st}+1} \times (k_3 ln(\frac{i_{corr}}{200}) + 1) & i_{corr} > 200\frac{\mu A}{cm^2} \end{cases}$
- k_1, k_2, k_3, k_4: coefficients
- c/d: ratio of concrete cover to diameter
- i_{corr}: current density $[\mu A/cm^2]$
- ζ_{st}: stirrups index (Plizzari) $= A_{st}/nds_{st}$
- A_{st}: cross sectional area of stirrups
- n : number of tensile steel bar
- d : diameter of tensile steel bar
- s_{st}: longitudinal spacing of the stirrups

Subsequently, considering that the stirrups can be subjected to a higher corrosion than the longitudinal steel bars, the model has been modified in order to consider the influence of the degradation of the stirrups on the bond strength. The model was developed after several pull-out tests using specimens with corroded stirrups. The scale factor to consider the reduction of bond strength due to the corrosion of stirrups is considered as:

$$D_{st} = 1 - 0.68\eta_{stave} \tag{2.17}$$

η_{stave} : average mass loss percentage of stirrups
So, the final model becomes:

$$\tau_u\left(\eta, \eta_{stave}\right) = \tau_u\left(0\right) D_{st} R_\tau \tag{2.18}$$

The research of Nino Spinella et al. (2019), highlight the role of the transverse reinforcement in reinforced concrete beams and the effects of stirrups corrosion on the failure mode of RC elements that change from bending (ductile) to shear (brittle) failure. The effect of corrosion is considered modifying the yield strength of the steel stirrups. It is considered a linear relation between the yield strength of corroded and non-corroded rebars (Figure 2.14).

$$\frac{f_{y,c}}{f_y} = 1 - \alpha_y Q_c \tag{2.19}$$

- $f_{y,c}$: yield strength of the corroded steel rebars
- f_y: yield strength of the un-corroded steel rebars
- Q_c: average corrosion degree = $(A_{sv,c} - A_{sv}\ )/A_{sv}$
- $A_{sv,c}$: area of the transversal reinforcement in the corroded configuration
- A_{sv} : area of the transversal reinforcement in the un-corroded configuration
- α_y: empirical coefficient obtained by regression analysis (slope of the degradation model)

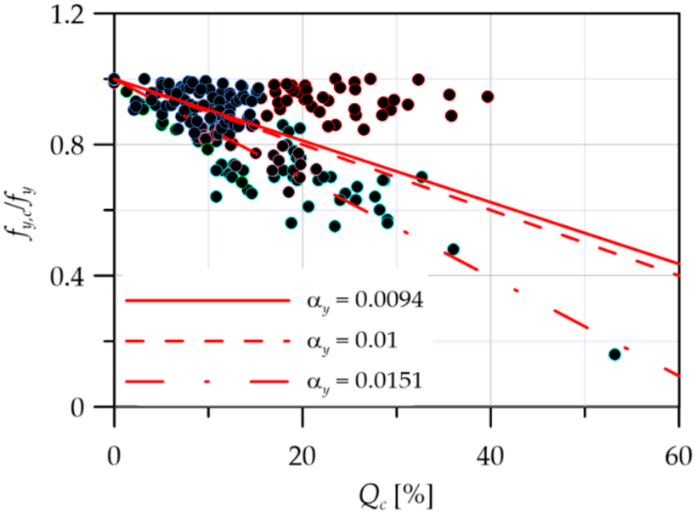

Figure 2.14: Experimental yield capacity ratio versus average corrosion degree of corroded steel rebar (Spinella et al. 2019).

2.4.1 Bond strength and crack width relationship

As presented by Chen and Nepal (2014), studies have been performed to evaluate the relationship between surface cracks width and bond strength of corroded rebars (Al-Sulaimani et al. 1990, Rodriguez et al. 1994, Almusallam et al. 1996, Fisher et al. 2010, Law et al. 2011, Li and Yuan 2013, Banba et al. 2014). In addition, some empirical relations based on experimental results have been proposed (Cairns et al. 2006).

The study of Fisher and Ozbolt (2013) concludes that the crack width can be a valid indicator of the corrosion bond degradation between concrete and steel, and, in addition, it is a parameter easier to determine respect to mass loss or section loss of steel bars. In the research, tests and numerical simulations are performed and then the change in the bond strength according to average corrosion penetration (x_{corr}) and the crack width are evaluated. The first one is computed from the mass loss as:

$$x_{corr} = \sqrt{\frac{m_0}{\pi L \rho}} - \sqrt{\frac{m_0 - \Delta m}{\pi L \rho}} \tag{2.20}$$

- m_0: original mass
- Δm: mass loss due to corrosion
- L: bond length
- ρ: density of the steel

The crack width was measured directly on the tested specimens subjected to artificial corrosion before the bar pull-out.

Figure 2.15 shows the normalized bond strength at different values of average corrosion penetration and crack width, compared with the results of Rodriguez et al (1994).

A good correlation was found using the crack width as parameter that, moreover, can be determined in a non-destructive way. The better correlation compared to the corrosion penetration is due to the fact that the corrosion products penetrate in the pores and cracks of concrete, so only a part of them is contributing to the increase in the pressure that cause the cracks in the surrounding concrete. Therefore, the corrosion penetration is a direct indicator of the total corrosion and the crack width of the loss of bond strength.

Figure 2.16 (Chen and Nepal, 2014) shows the normalized residual bond strength ratio of ultimate bond strength of the corroded element to non-corroded element versus the surface crack width according to the experimental results of several authors and compared to the empirical relations based on experimental results proposed by Cairns et al. 2006. Chen and Nepal (2014) developed a theoretical model to assess the structural conditions of RC corroded structures. They defined the bond strength deterioration due to the corrosion induced cracking as:

$$J_b = \frac{T_{ubo}(w_c) - T_{ubx}(w_c)}{T_{ubo}(w_c)} \tag{2.21}$$

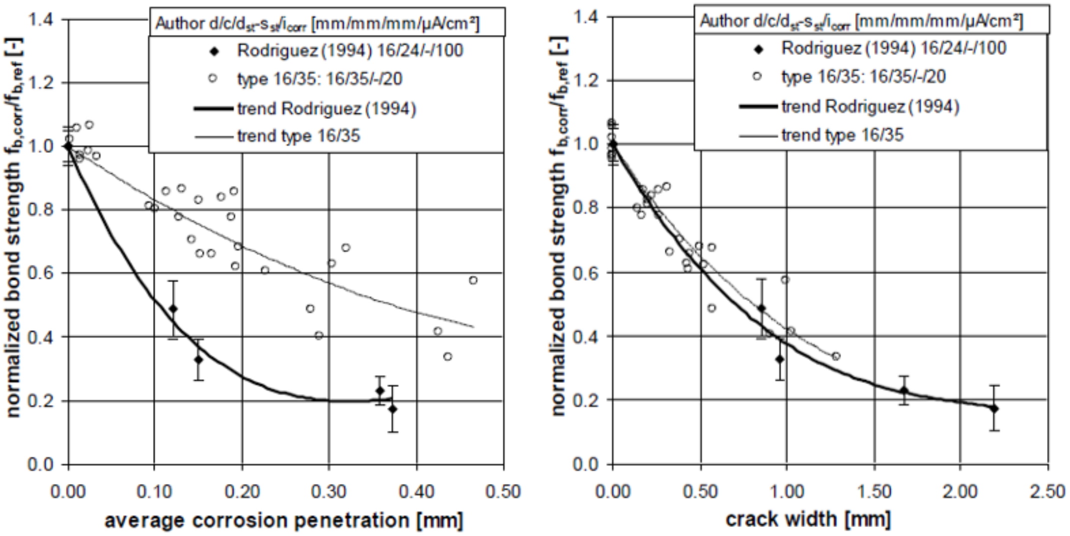

Figure 2.15: Comparison of bond strength values (Fisher and Ozbolt, 2013).

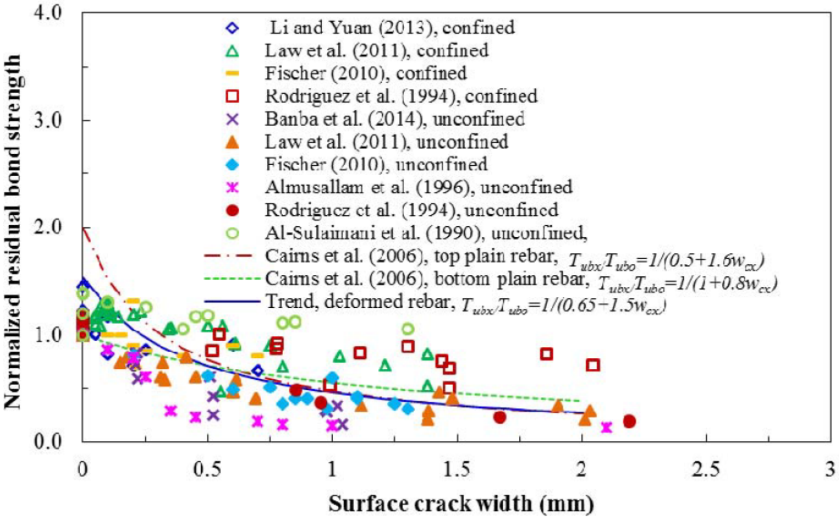

Figure 2.16: Normalized residual bond strength versus corrosion induced surface crack width (Chen and Nepal 2014).

- $T_{ubo}(w_c)$ residual bond strength at the onset of cracking
- $T_{ubx}(w_c)$ residual bond strength in correspondence of the ultimate cohesive value

The bond strength deterioration is assumed as a random variable with a gamma distribution.

The analytically predicted surface crack width versus the corrosion level (expressed in percentage of mass loss) obtained with the model of Chen and Nepal is plotted in Figure 2.17, and it is compared with accelerated and natural corrosion tests results of other authors. Figure 2.18 and Figure 2.19 show the predicted normalized residual bond strength (Eq 2.22) as function of the surface crack width compared with experimental results, respectively in the case of confined and unconfined concrete. In both cases there is a good agreement with the past experimental outcomes. It is possible to observe that in the case of unconfined concrete the residual bond strength is null in correspondence of a certain value of the crack width, due to the absence of containment provided by the transverse reinforcement.

$$Normalized\ residual\ bond\ strength = \frac{T_{ubx}(w_c)}{T_{ubo}(w_c)} \tag{2.22}$$

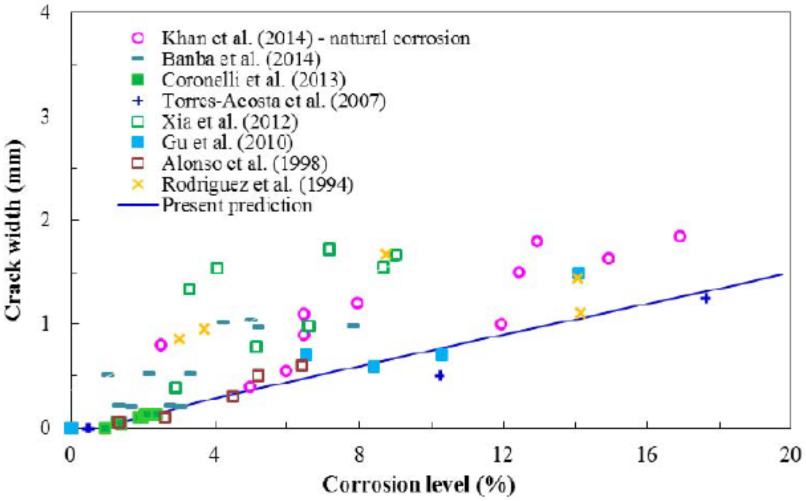

Figure 2.17: Analytical prediction of crack width versus corrosion level, compared with test results of other researchers (Chen and Nepal, 2014).

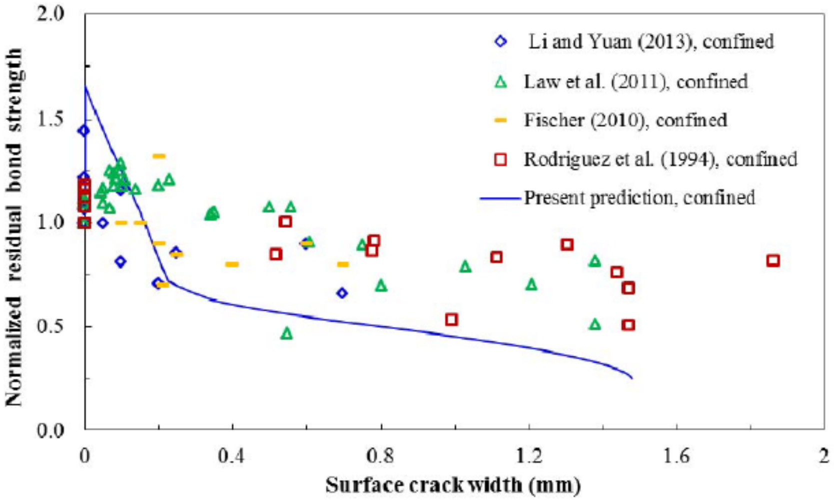

Figure 2.18: Analytical prediction of normalized residual bond strength versus surface crack width for confined concrete, compared with test results of other researchers (Chen and Nepal, 2014).

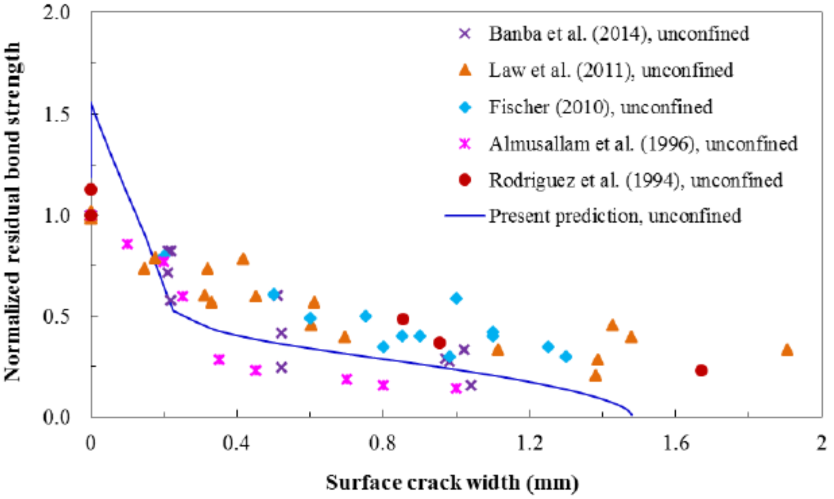

Figure 2.19: Analytical prediction of normalized residual bond strength versus surface crack width for unconfined concrete, compared with test results of other researchers (Chen and Nepal, 2014).

Zhao and Lin (2018) created an empirical model, based on pull-out tests, that estimates the bond strength starting from the crack width of longitudinal and lateral cracks:

$$\tau_u\left(W_{ave}\ ,W_{stave}\right)=\tau_u\left(0\right)D_{st}\left(1-0.9e^{-20\rho st}\left(1-e^{-1.73W_{ave}e^{-56.6\rho st}}\right)\right) \tag{2.23}$$

- $\tau_u\left(W_{ave}\ ,W_{stave}\right)$: bond strength of corroded specimens [MPa]
- W_{ave}: average longitudinal crack width [mm]
- W_{stave}: average lateral crack width [mm]
- ρst: stirrups index (ratio between the total area of stirrups and the total area of the longitudinal section of the principal steel bars)
- $D_{st}=1-0.68\left(\frac{w_{stave}d_{st}}{-0.29c_{st}+1.58d_{st}}+1-\left(1-\frac{\theta}{d_{st}}\left(7.53+9.32\frac{c_{st}}{d_{st}}\right)10^{-3}\right)^2\right)$
- c_{st}: concrete cover of stirrups [mm]
- d_{st}: diameter of stirrups [mm]
- θ: pit concentration factor (factor related to the cross-sectional loss of the corroded bar)

The recent experimental study of Yang et al. (2019) investigates the effect of corrosion-induced cracks, corroded rebar shape and rust around rebar on the bond properties. Tests were conducted on artificially corroded specimens varying corrosion degree, and it was highlighted that corrosion cracks are the most influential factor in the bond deterioration mechanism. In order to analyse separately the different factors, specimens have been divided in different groups. The one of normal corrosion, used to perform bond test directly after the corrosion and to investigate the combined effect of corrosion induced cracks, corroded rebar shape and rust. The second group was used to analyse only the effect of corroded rebar shape (the corroded rebar was taken out from the specimen; the rust was removed and then it was casted in new concrete). The third group was used to evaluate the effect of rust (corroded rebar was casted in new concrete without removing the rust).

Figure 2.20 shows the bond strength (the ultimate bond strength is normalized by the ultimate bond strength of non-corroded specimens), in the normal corrosion specimens (first group), versus the corrosion degree and the corrosion crack width. For the bond strength-corrosion degree relationship the results are compared with the empirical model of Bhargava et al. and show a good agreement. The ultimate bond strength initially improves and undergo to a degradation after 10% corrosion degree.

Figure 2.21 shows the results obtained for the specimens of the second and third group varying the corrosion degree. In absence of corrosion cracks the degradation of the bond is lower so that the formation of crack results to be major factor of bond degradation.

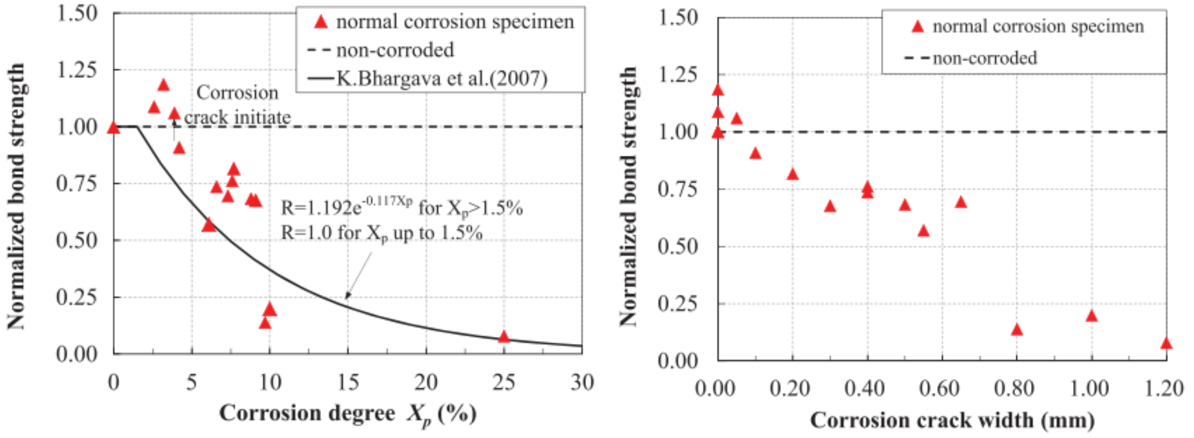

Corrosion degree-normalized bond strength

Corrosion crack width-normalized bond strength

Figure 2.20: Bond strength of normal corrosion versus corrosion degree (left) and corrosion crack width (right) (Yang at al. 2019).

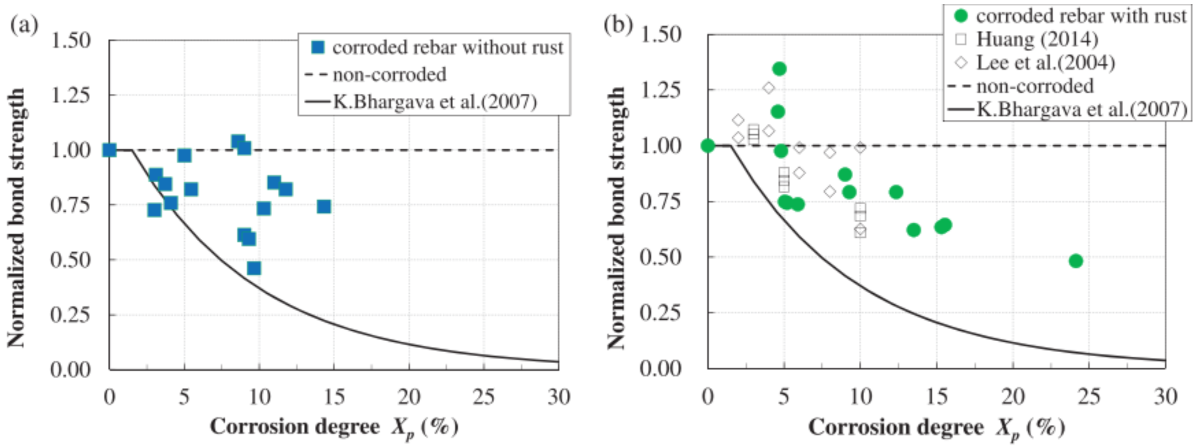

Corroded rebar without rust (group III)

Corroded rebar with rust (group IV)

Figure 2.21: Effect of corrosion degree on bond strength in absence of corrosion crack (Yang et al. 2019).

2.4.2 ARC 1990 and ARC 2010 models

ARC 1990 is an analytical one-dimensional model developed to assess the anchorage of reinforcing bars in corroded RC structures, developed by Lundgren et al. (2012). It comes from the modification of the local bond stress-slip model presented in Model Code 1990. The latter does not consider the corrosion so that it has been modified using the results of a parametric study (3D non-linear finite element). The model has been verified through tests results and a pilot study of two bridges in Stockholm.

The local bond stresses for monotonic loading, both in Model Codes 2010 and 1990, are calculated as a function of the relative displacement (slip) parallel to the bar axis:

$$\tau_b = \tau_{bmax} \left(\frac{s}{s_1} \right)^{\alpha} \; for \; 0 \leq s \leq s_1 \tag{2.24}$$

$$\tau_b = \tau_{bmax} \;\; for \; s_1 \leq s \leq s_2 \tag{2.25}$$

$$\tau_b = \tau_{bmax} - (\tau_{bmax} - \tau_{res})\,(s - s_2)\,/\,(s_3 - s_2) \quad for \; s_2 \leq s \leq s_3 \tag{2.26}$$

$$\tau_b = \tau_{bmax} - (\tau_{bmax} - \tau_{res})\,(s - s_2)\,/\,(s_3 - s_2) \quad for \; s_2 \leq s \leq s_3 \tag{2.27}$$

$$\tau_b = \tau_{res} \;\; for \; s_3 \leq s \tag{2.28}$$

As presented in Tables 2.2 and 2.3, in the local bond strength expression there is a differentiation between 'good bond conditions' and 'all other conditions'. The first apply to the bars with inclination of 45-90° respect to the horizontal during concreting and to the ones with inclination lower than 45° but at a distance up to 250 mm from the bottom and at least 300 mm from the top of the concrete layer.

Figures 2.22 and 2.23 show the bond-slip relationships present in Model Code 2010 and the comparison between the one in MC 2010 and MC 1990 respectively.

Table 2.4 reports experimental results regarding the reduction of the residual bond strength for corroded reinforcement from Model Code 2010. These are obtained from tests where accelerated corrosion is performed, so that cannot be considered completely truthful and should be taken into account only as indicative.

In Model Code 2010 the splitting bond strength is expressed as:

$$\tau_{bu,split} = \eta_2 * 6.5 * \left(\frac{f_{cm}}{25} \right)^{0.25} * \left(\frac{25}{\phi_m} \right)^{0.2} \left[\left(\frac{c_{min}}{\phi_m} \right)^{0.25} \left(\frac{c_{max}}{c_{min}} \right)^{0.1} + k_m * K_{tr} \right] \tag{2.29}$$

- c_{clear} clear distance between ribs
- η_2 is 1 for 'good bond conditions' and 0.7 for 'all other bond conditions'

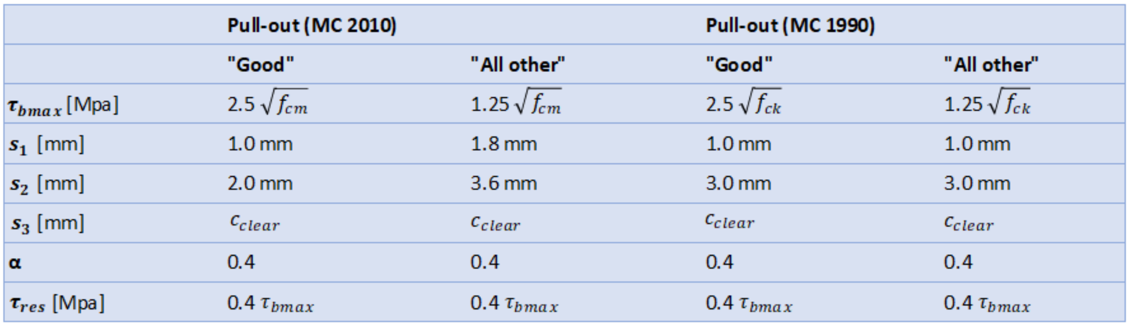

	Pull-out (MC 2010)		**Pull-out (MC 1990)**	
	"Good"	**"All other"**	**"Good"**	**"All other"**
τ_{bmax} [Mpa]	$2.5\sqrt{f_{cm}}$	$1.25\sqrt{f_{cm}}$	$2.5\sqrt{f_{ck}}$	$1.25\sqrt{f_{ck}}$
s_1 [mm]	1.0 mm	1.8 mm	1.0 mm	1.0 mm
s_2 [mm]	2.0 mm	3.6 mm	3.0 mm	3.0 mm
s_3 [mm]	c_{clear}	c_{clear}	c_{clear}	c_{clear}
α	0.4	0.4	0.4	0.4
τ_{res} [Mpa]	0.4 τ_{bmax}	0.4 τ_{bmax}	0.4 τ_{bmax}	0.4 τ_{bmax}

Table 2.2: Parameters for local bond stress-slip curve for pull-out failure for Model Code 2010 and 1990 (Coronelli et al. 2018).

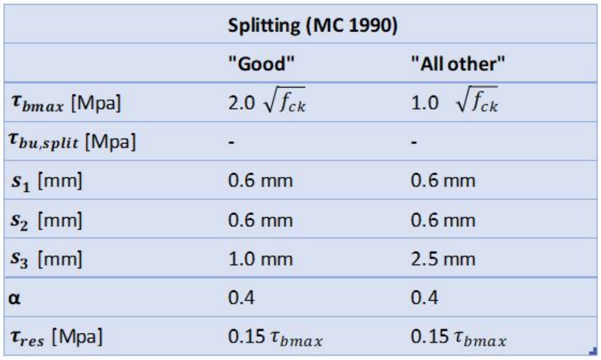

	Splitting (MC 1990)	
	"Good"	**"All other"**
τ_{bmax} [Mpa]	$2.0\sqrt{f_{ck}}$	$1.0\ \sqrt{f_{ck}}$
$\tau_{bu,split}$ [Mpa]	-	-
s_1 [mm]	0.6 mm	0.6 mm
s_2 [mm]	0.6 mm	0.6 mm
s_3 [mm]	1.0 mm	2.5 mm
α	0.4	0.4
τ_{res} [Mpa]	0.15 τ_{bmax}	0.15 τ_{bmax}

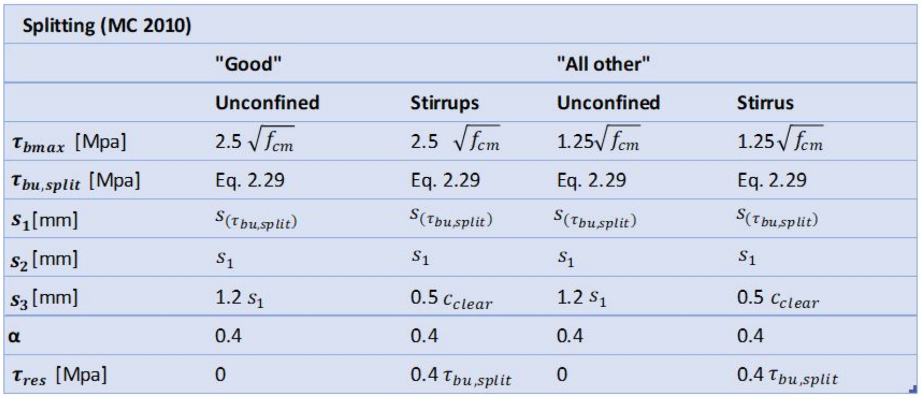

Splitting (MC 2010)				
	"Good"		**"All other"**	
	Unconfined	**Stirrups**	**Unconfined**	**Stirrus**
τ_{bmax} [Mpa]	$2.5\sqrt{f_{cm}}$	$2.5\ \sqrt{f_{cm}}$	$1.25\sqrt{f_{cm}}$	$1.25\sqrt{f_{cm}}$
$\tau_{bu,split}$ [Mpa]	Eq. 2.29	Eq. 2.29	Eq. 2.29	Eq. 2.29
s_1[mm]	$s(\tau_{bu,split})$	$s(\tau_{bu,split})$	$s(\tau_{bu,split})$	$s(\tau_{bu,split})$
s_2[mm]	s_1	s_1	s_1	s_1
s_3[mm]	1.2 s_1	0.5 c_{clear}	1.2 s_1	0.5 c_{clear}
α	0.4	0.4	0.4	0.4
τ_{res} [Mpa]	0	0.4 $\tau_{bu,split}$	0	0.4 $\tau_{bu,split}$

Table 2.3: Parameters for local bond stress-slip curve for splitting failure for Model Code 2010 and 1990 (Coronelli et al. 2018).

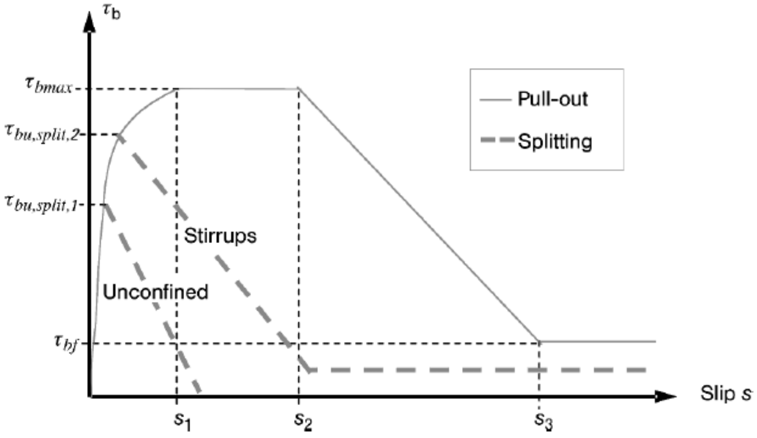

Figure 2.22: Analytical bond stress-slip relationship (monotonic loading) (Model Code 2010).

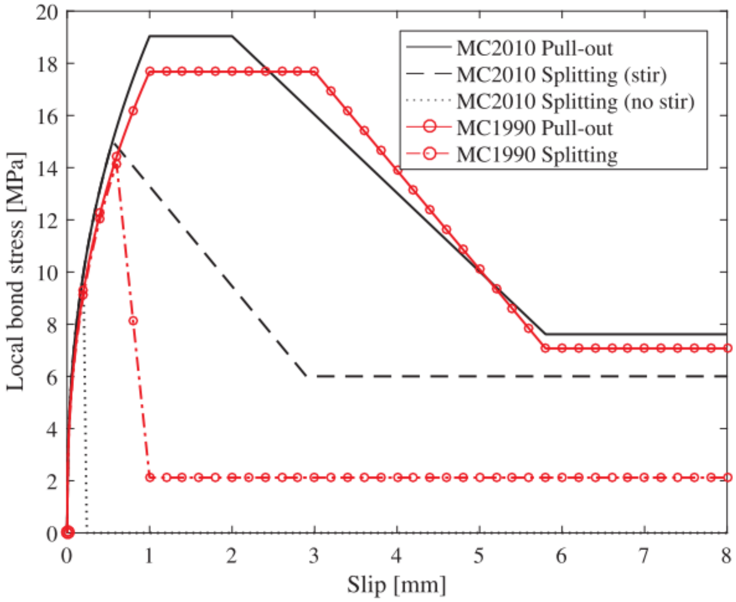

Figure 2.23: Comparison of local bond stress-slip expression for 'good bond condition' in Model Codes 2010 and 1990 for concrete C 50/60, $\emptyset_m = 20\ mm, k_m = 12,\ k_{tr} = 0.05, c = 40mm, c_{clear} = 5.8\ mmand\alpha = 0.4$ (Coronelli et al. 2018).

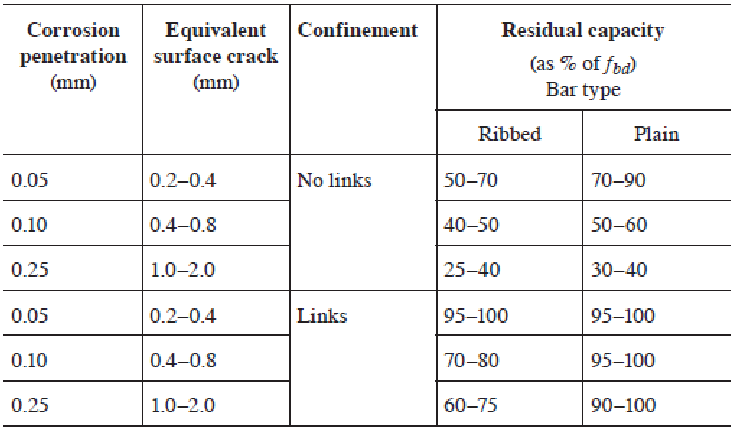

Corrosion penetration (mm)	Equivalent surface crack (mm)	Confinement	Residual capacity (as % of f_{bd}) Bar type	
			Ribbed	Plain
0.05	0.2–0.4	No links	50–70	70–90
0.10	0.4–0.8		40–50	50–60
0.25	1.0–2.0		25–40	30–40
0.05	0.2–0.4	Links	95–100	95–100
0.10	0.4–0.8		70–80	95–100
0.25	1.0–2.0		60–75	90–100

Table 2.4: The magnitude of the reduction in residual bond strength for corroded reinforcement (Model Code 2010).

- f_{cm} mean cylinder compressive strength [MPa]
- ϕ_m diameter of the anchored bar [mm]
- k_m confinement coefficient (12 for bars within $5\phi_m \leq 125\ mm$ from a stirrup corner, 6 if $c_s > 8c_y$ and 0 if $c_s < 8c_y$ or if a crack can propagate to the concrete surface without crossing transverse links (Figure 2.25)
- $c_{min} = min(c_s/2, c_x, c_y)$ (Figure 2.24)
- $c_{max} = max\left(\frac{c_s}{2}, c_x\right)$ (Figure 2.24)
- c_s clear spacing between main bars [mm]
- c_x, c_y cover in x and y directions [mm]
- K_{tr} amount of transverse reinforcement $= n_t A_{st} / \left(n_b \phi_m s_t\right) \leq 0.05$
- n_t number of legs of confining reinforcement crossing a potential splitting-failure surface at a section
- A_{st} cross - sectional area of one leg of a transverse bar [mm2]
- s_t longitudinal spacing of confining reinforcement [mm]
- n_b number of anchored bars or pairs of lapped bars in the potential splitting surface

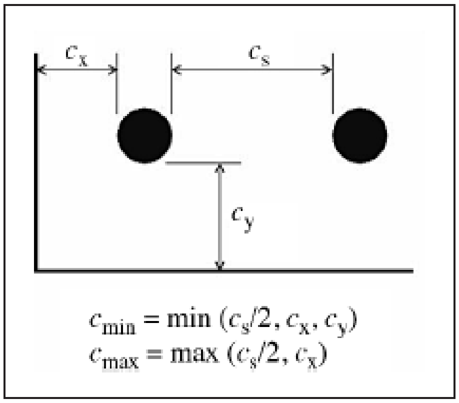

Figure 2.24: Notation for bar spacing and cover (Model Code 2010).

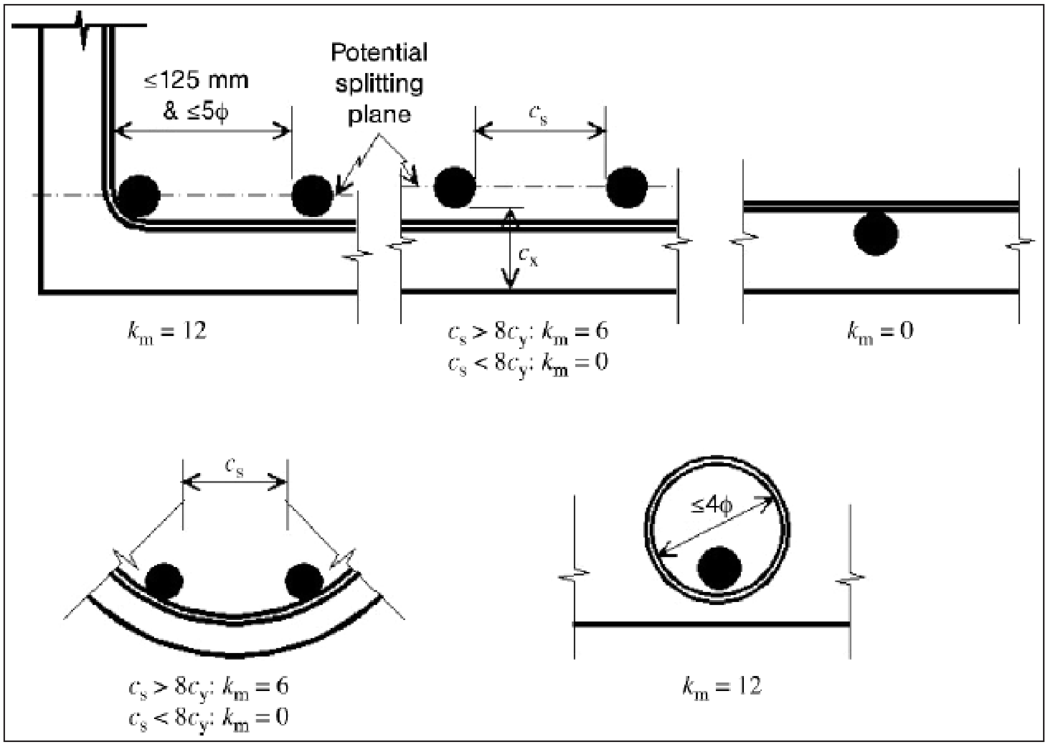

Figure 2.25: Confinement coefficients for transverse reinforcement (Model Code 2010).

ARC1990 models the bond strength in the 'unconfined' case and in the 'confined' case (uncorroded cases) as shown in CEB fib model Code 1990. For intermediate state it is used the following interpolation formula :

$$\tau_b = k\tau_{b,conf} + (1-k)\tau_{b,unconf} \tag{2.30}$$

$$k = max(k_{c/d}, k_{Asw}) \tag{2.31}$$

- $k_{c/d}$: factor dependent on the cover to bar diameter ratio (Figure 2.26)
- k_{Asw}: factor that depends on the amount of effective transverse reinforcement Asw/s (Figure 2.26)
- $\tau_{b,unconf}$: bond strength for 'unconfined case'
- $\tau_{b,conf}$: bond strength for 'confined case'

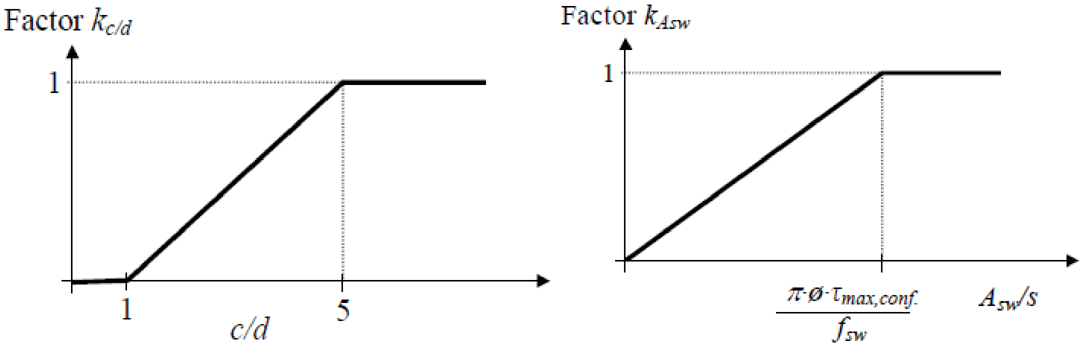

Figure 2.26: Interpolation factors between 'confined' and 'unconfined' case (Lundgren et al. 2012).

In the model the amount of transverse reinforcement that causes the pull-out failure is obtained assuming:

- yielding of the transverse reinforcement at the maximum bond stress for pull-out failure
- splitting stresses equal to bond stresses

$$l * \pi * d * \tau_{max,conf} = l * \frac{A_{sw}}{s} * f_{sw} \rightarrow \frac{A_{sw}}{s} = \frac{\pi * d * \tau_{max,conf}}{f_{sw}} \tag{2.32}$$

- A_{sw}: area of transverse reinforcement
- $\tau_{max,conf}$: maximum bond strength for confined case
- d : reinforcement bar diameter
- l : length
- s : distance between stirrups
- f_{sw}: stirrups tensile strength

The effect of corrosion is considered shifting the bond- slip curve of uncorroded reinforcement along the slip axis. This is introduced in the CEB-FIP bond -slip model considering the hardening parameter dependent on the plastic slip (s_p [mm]) and moreover on the corrosion penetration (x [mm]) as:

$$k = s_p + ax \tag{2.33}$$

a : constant parameter (adopted as 8.1 (Schlune 2006))

Moreover, in this model the change of failure mode (from pull-out to splitting) is taken into account using the interpolation factor k_{corr} that depends on the ratio x/x_{corr} (corrosion penetration/corrosion penetration that causes cracking). In this way it is considered that after the cracking only the transverse reinforcement contributes to the bond capacity, while before also the concrete cover contributes. In the model, the decrease of the capacity takes place when the corrosion penetration reaches 85% of cover cracking. As in the uncorroded case, the bond strength is formulated through the following correlation:

$$\tau_b = k_{corr}\tau_{b,conf} + (1 - k_{corr})\tau_{b,unconf} \tag{2.34}$$

It is a conservative evaluation because it considers no residual bond strength in the case of no transversal reinforcement. The value of k_{corr} is given from the graph in Figure 2.27.

The corrosion penetration that causes cracking (x_{cr}) is computed using a formula derived from curve fitting of analysis result on a 3D model (Lundgren 2005).

$$x_{cr} = 11 \ * \left(\frac{f_{cc}}{40}\right)^{0.8} * \left(\frac{c}{d}\right)^{1.5} * \ \left(\frac{d}{16}\right)^{0.5} \tag{2.35}$$

- f_{cc}: concrete cylinder compressive strength [MPa]
- c : concrete cover [mm]
- d : reinforcement bar diameter [mm]

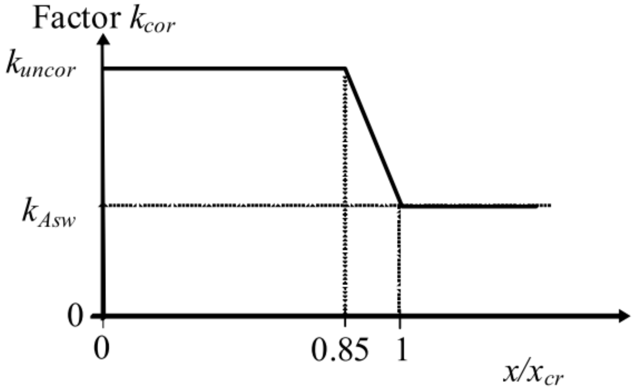

Figure 2.27: Factor that consider the change of failure mode for corroded reinforcement (Lundgren et al. 2012)

ARC2010 is the new model for anchorage assessment in concrete structures with corroded reinforcement and it is based on the local bond stress-slip relationship in Model Code 2010. It includes the following modifications with respect to ARC1990 model:

- Introduction of equivalent slip to account for bond degradation due to corrosion
- Change of failure mode due to corrosion-induced cracking of the concrete cover
- Modification of residual bond stress in case of low stirrup content

According to Figure 2.28, the local bond stress-slip curve of corroded reinforcement is approximated shifting the uncorroded curve in the slip direction and considering the minimum value of both, the original and the shifted curve. In this way an equivalent slip between steel and concrete is added and the effective slip is expressed as:

$$s_{eff} = s + s_{eq} \tag{2.36}$$

- s : mechanical slip
- s_{eq}: equivalent slip to take into account corrosion

The expression to compute the splitting strength from Model Code 2010 is used for corrosion level below the cracking limit. When this is overpassed the confinement provided by the cover decreases and this is considered reducing the factor of the concrete cover to 1. The expression for the reduced bond strength at splitting (cracked cover) is:

$$\tau_{bu,split,red} = \eta_2 * 6.5 * \left(\frac{f_{cm}}{25}\right)^{0.25} * \left(\frac{25}{\phi_m}\right)^{0.2} (1 + k_m * K_{tr}) \tag{2.37}$$

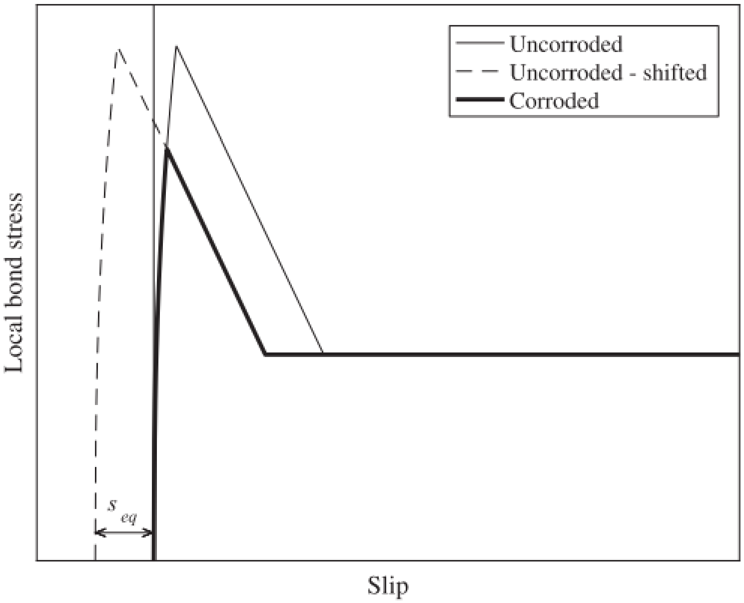

Figure 2.28: Equivalent slip to account for the effect of corrosion (Coronelli et al. 2018).

The residual bond capacity for specimens with low stirrups content is expressed as:

$$\tau_{res,mod}(K_{tr}) = \begin{cases} (0.16 + 12K_{tr}) \times \tau_{bu,split,red} & for 0 \leq K_{tr} \leq 0.02 \\ 0.4 \times \tau_{bu,split,red} & for 0.02 < K_{tr} \end{cases} \tag{2.38}$$

Figure 2.29 shows the bond-stress slip relationships of ARC2010 in the case of pull-out failure and splitting failure above or below the cracking limit and in presence and absence of transversal reinforcement.

The influence of several input parameters on the equivalent slip was studied and a correlation with the corrosion level was found. The equivalent slip increases with the corrosion level. Two function, Eq 2.39 (absence of stirrups) and Eq 2.40 (presence of stirrups), were determined through laboratory tests results, then calibrated with MATLAB software.

$$s_{eq,nostir} = 2.9W_c \tag{2.39}$$

$$s_{eq,stir} = 13.6W_c \tag{2.40}$$

W_c : corrosion level (weigth loss)

The two functions plus test and calibration data are plotted in Figure 2.30 and compared with the relationship of ARC1990 model.

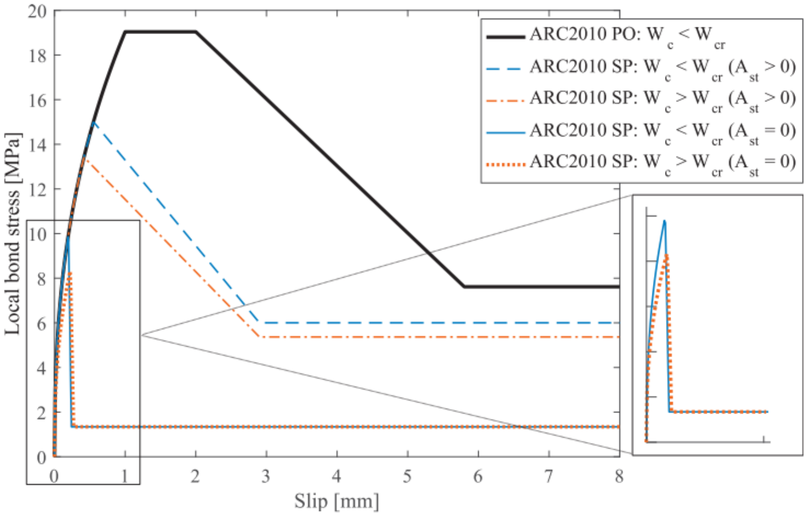

Figure 2.29: Change from pull-out failure (PO) to splitting failure (SP) due to corrosion for 'good bond conditions', C 50/60 concrete, $\emptyset_m = 20mm, K_m = 12, K_{tr} = 0.05, c = 40mm,\ c_{clear} = 5.8mmand\alpha = 0.4$ (Coronelli et al. 2018).

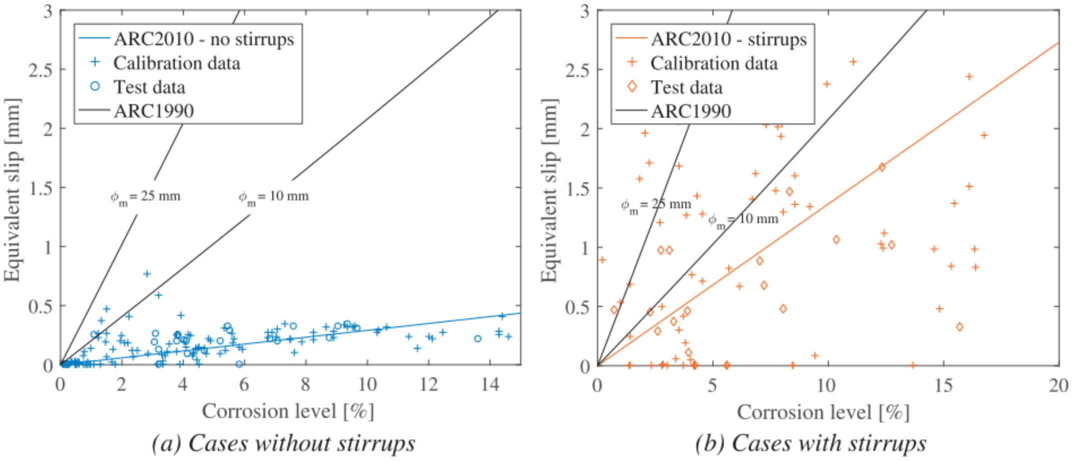

(a) Cases without stirrups

(b) Cases with stirrups

Figure 2.30: Equivalent slip-corrosion level relationships (Coronelli et al. 2018).

2.4.3 Considerations on the existing models

Many of the existing models developed to represent the corrosion bond degradation have been reported in the previous section. The majority of the less recent ones (Table 2.1) has several limitations. For example, the increase in the bond strength at low level of corrosion is not represented, that is a very well assessed behaviour demonstrated by many researchers. Moreover, the influence of the location of longitudinal reinforcement is not taken into account (Rodriguez et al. 1994) and in some of them neither the stirrups and concrete confinement effects.

As demonstrated by many authors, the confinement provided to the longitudinal reinforcement results to be the aspect that most affect the bond in reinforced concrete elements. That is why a truthful and complete model should represent the bond strength relating it to the concrete cover and transversal reinforcement characteristics. It is fundamental to take into account the state of the concrete cover (concrete strength, cover width and deterioration) and to consider the presence and/or degree of corrosion of the transversal reinforcement.

Recently, more precise and representative models have been developed (Lin and Zhao, 2016 and 2018), where, stirrups content, concrete cover and corrosion current density effects are considered. The limitation can be found in the complexity of the model parameters determination. Regarding the model based on bond strength and crack width relationship, both advantages and limitations are reported. Many studies demonstrate that surface cracks width is a direct indicator of the bond strength reduction. Anyway, models based on the measurement of this parameter results to be unusable for the present research, which aim is to compare the bond strength deterioration effect on the seismic capacity of a bridge with the results of a previous study based on the steel reinforcement cross-section reduction in time due to corrosion (De Gaetano, 2019). So, a suitable model should in some way correlate the bond strength reduction with the corrosion level expressed as steel area or weight loss.

ARC2010 results to be a complete model able to represent several scenarios. Different analytical expressions of the bond strength are provided for cracked and un-cracked concrete cover. The latter case corresponds to a reduced value of bond splitting strength. Both, pull-out and splitting failure can be represented and, in addition, it is possible to take into account the absence/ presence of stirrups and their degree of corrosion. Several configurations can be truthfully represented thanks to the possibility to take into account the position of the longitudinal steel bar with respect to the RC element cross-section. Moreover, the bond strength computed is related to the corrosion level (steel weight loss) through the equivalent slip empirical correlations for the cases of presence and absence of transversal reinforcement.

Chapter 3

Bridge case study

3.1 Bridge geometry

The bridge object of the study is a motorway overpass located in Sicily, close to the strait of Messina. The structure longitudinal profile is shown in Figure 3.1. The 55.5 meters length bridge, consist of two spans, each one of 27.75 m, so that the pier is positioned in the central part of the motorway. The longitudinal profile is convex with a coefficient of curvature $K_v = 2500$, in order to facilitate the water drainage. The deck consists of a solid slab in prestressed concrete with lightnings and variable depth as it is showed in Figure 3.2.

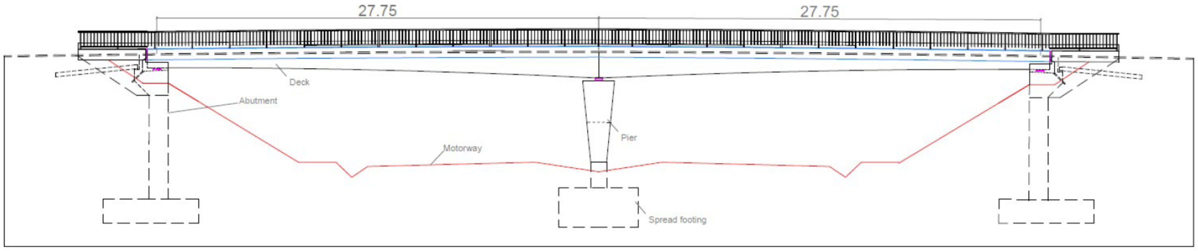

Figure 3.1: Bridge longitudinal profile (De Gaetano, 2019).

The study is focused on the bridge pier. This element presents a height of 6.70 m and at 1.6 m the cross-section start to increase developing then in a bifurcation that gives to it an Y shape. On the top of each arm is positioned a neoprene bearing. At the base it is supported by a 5x5x2.5 rigid footing (Figure 3.3).

CROSS-SECTION IN THE PIER

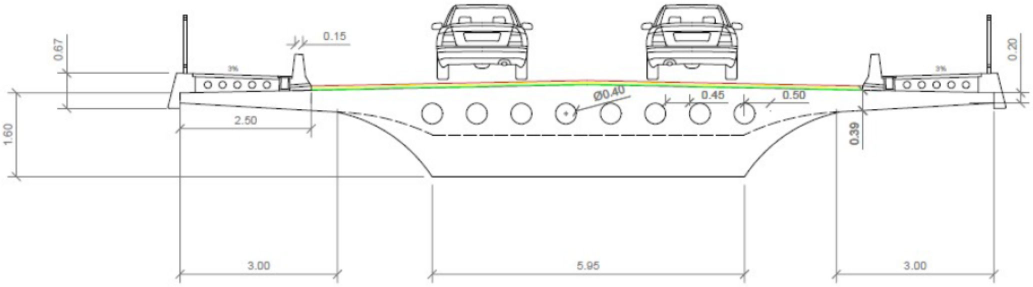

CROSS-SECTION IN THE ABUTMENTS

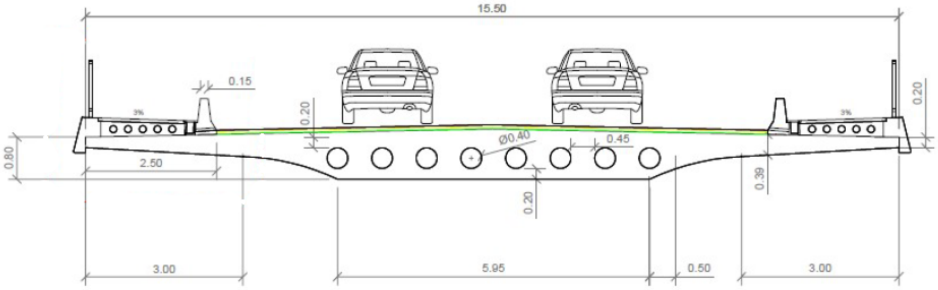

Figure 3.2: Deck cross-sections in correspondence of pier and abutments (De Gaetano, 2019).

3.2 Bridge seismic analysis

The structure has been modelled on SAP2000 in order to create a finite element model necessary to perform static loads and seismic analysis. The bridge has been modelled as a simple-supported beam. Both, the deck and the pier, have variable cross section so have been discretized in several parts and to each one different geometrical properties have been assigned. Loads have been defined according to IAP11 and includes vertical actions and horizontal actions, in the transverse and longitudinal directions.

In the present case study seismic and modal analysis are of high importance and interest because the bridge is located in high seismic hazard zone (Messina, Sicily). They have been performed according to the Italian (NTC2018) and European (EN 1998-2 Eurocode 8) regulations.

Applying to the bridge the seismic loads combination, has been possible to obtain the

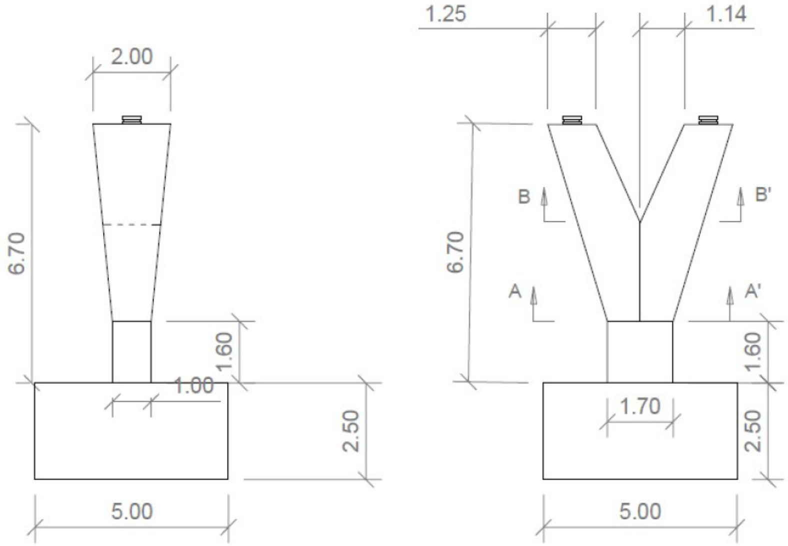

Figure 3.3: Pier geometry (De Gaetano, 2019).

values of axial force, moment and shear in the pier. The sections analysed are the two most critical (Figure 3.4):

- Section A: base of the pier
- Section B: base of the pier bifurcation

Solicitations in section A:

- N = - 18380 kN
- Mx= 3710 kNm
- My= 9415 kNm
- Vx= 536 kN
- Vy= 1409 kN

Solicitations in section B:

- N = - 8322 kN
- Mx= 16494 kNm

- My= 2833 kNm
- Vx= 4138 kN
- Vy= 704 kN

Knowing the applied actions, the dimensioning of the longitudinal and transversal reinforcement has been performed following the Italian regulation and the capacity design criteria. In fact, it is important that in a bridge the develop of a plastic mechanism occur in the pier and not in the deck or in the foundations.

The materials used are:

- Steel B450C
- Concrete C40/50

The amount and disposition of the reinforcement in the two sections is showed in Figures 3.5 and 3.6. Additional details regarding the bridge modelling and seismic analysis can be found in De Gaetano, 2019.

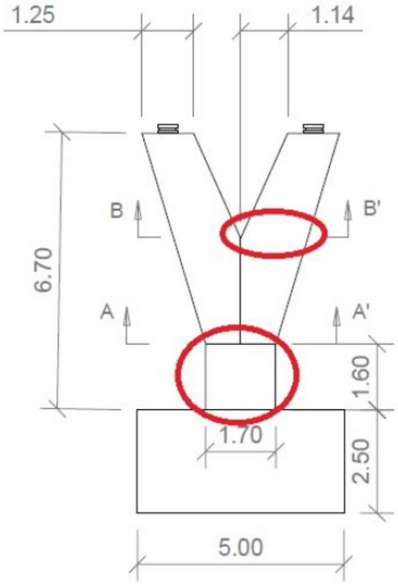

Figure 3.4: Sections of the pier (De Gaetano, 2019).

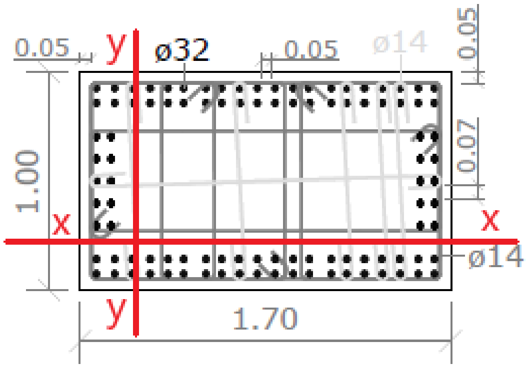

Figure 3.5: Section A (De Gaetano, 2019).

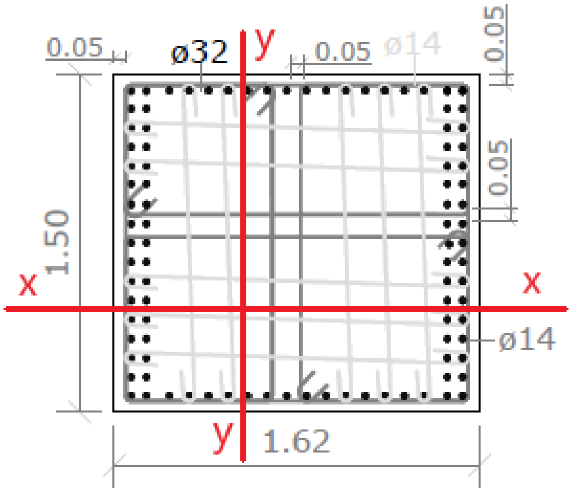

Figure 3.6: Section B (De Gaetano, 2019).

Chapter 4

Application of the bond deterioration model

4.1 Slip-bond strength relationship

ARC2010 model has been applied to the bridge pier case study and the slip - bond strength relationship has been plotted in MATLAB considering three different cases:

- Pull-out failure
- Splitting failure in absence of stirrups
- Splitting failure in presence of stirrups

In Table 4.1 are reported the properties of the two pier cross-sections analysed. Moreover, a differentiation between x-x and y-y section should be done because of the different number of legs of confining reinforcement and of longitudinal bars in the potential splitting surface. In Table 4.2 are reported the parameters of ARC2010 model related to A and B cross sections (Figure 2.24 and 2.25).

As shown in Tables 4.3, 4.4, 4.5 and 4.6 the bond strength-slip relationship parameters of ARC2010 model have been computed for the two cross-sections in x and y directions, considering the situation of 'good bond condition'. The derivation and explanation of the previous mentioned parameters can be found in Section 2.4.2 where the ARC2010 Model is presented. All the values refer to the instant t=0, when the corrosion attack didn't start yet. In fact, the amount of transversal reinforcement is an input parameter of the model and it is hypothesized that it undergoes the same corrosion deterioration as the longitudinal reinforcement cross-section. For this reason there will be different bond-slip curves per each corrosion level. In Figure 4.1, 4.2, 4.3 and 4.4 report the graphs corresponding to pull-out and splitting failures. The latter in the cases of presence and absence of transversal reinforcement.

$\boldsymbol{f_{cm}}$ [Mpa]	48
$\boldsymbol{c_s}$ [mm]	50
$\boldsymbol{c_x}$ [mm]	50
$\boldsymbol{c_y}$ [mm]	50
$\boldsymbol{n_t}$ *(section A,x)*	6
$\boldsymbol{n_t}$ *(section A,y)*	4
$\boldsymbol{n_t}$ *(section B)*	4
$\boldsymbol{n_b}$ *(section A,x)*	20
$\boldsymbol{n_b}$ *(section A,y)*	9
$\boldsymbol{n_b}$ *(section B,x)*	18
$\boldsymbol{n_b}$ *(section B,y)*	17
$\boldsymbol{c_{clear}}$ [mm]	5.8
$\boldsymbol{s_t}$ [mm]	60

Table 4.1: Cross-section properties.

$\boldsymbol{c_{min}}$ *(section A)* [mm]	25
$\boldsymbol{c_{min}}$ *(section B)* [mm]	25
$\boldsymbol{c_{max}}$ [mm]	50
$\boldsymbol{k_m}$	12

Table 4.2: ARC2010 model parameters.

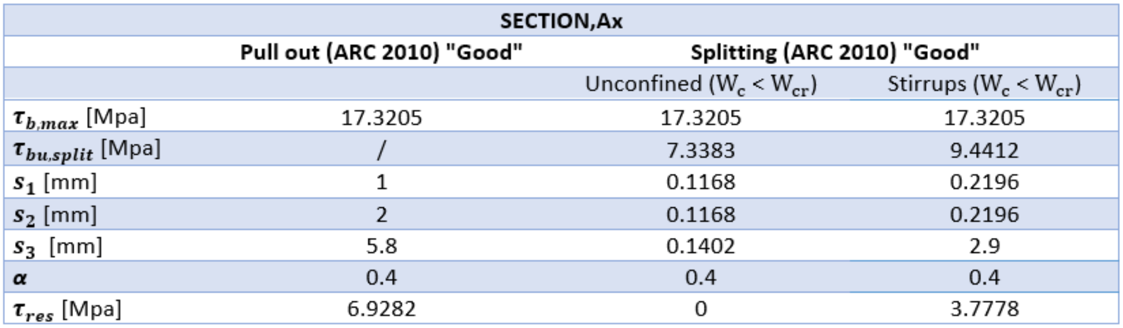

SECTION,Ax			
	Pull out (ARC 2010) "Good"	**Splitting (ARC 2010) "Good"**	
		Unconfined ($W_c < W_{cr}$)	Stirrups ($W_c < W_{cr}$)
$\tau_{b,max}$ [Mpa]	17.3205	17.3205	17.3205
$\tau_{bu,split}$ [Mpa]	/	7.3383	9.4412
s_1 [mm]	1	0.1168	0.2196
s_2 [mm]	2	0.1168	0.2196
s_3 [mm]	5.8	0.1402	2.9
α	0.4	0.4	0.4
τ_{res} [Mpa]	6.9282	0	3.7778

Table 4.3: Bond strength-slip relationship parameters of ARC2010 model for section A, x direction (t=0).

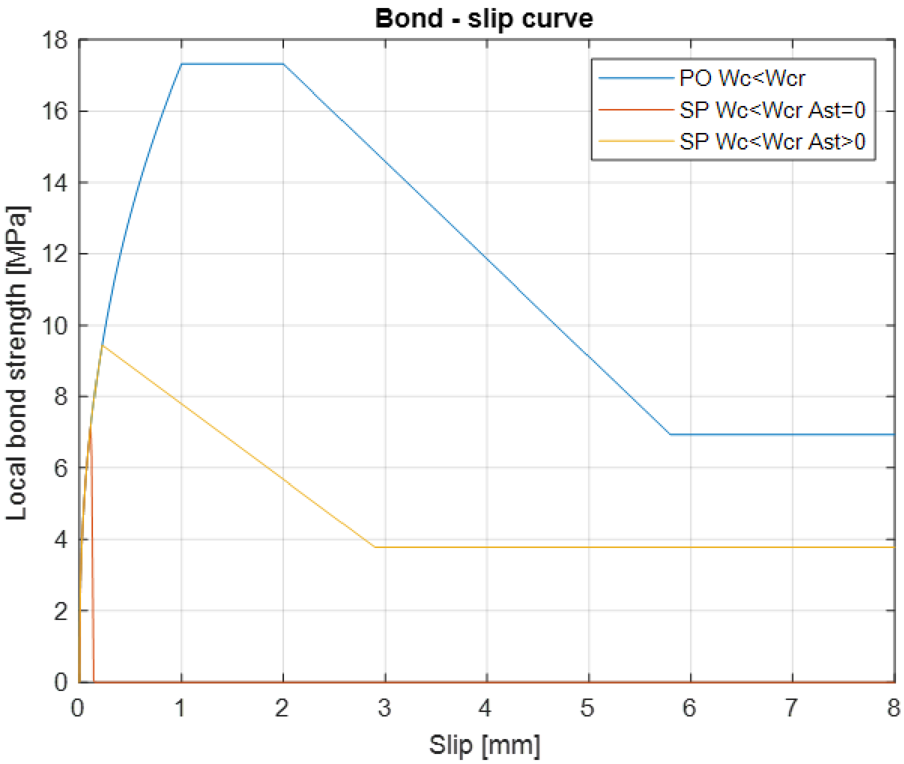

Figure 4.1: Bond strength-slip relationship ARC2010 model for section A, x direction (t=0).

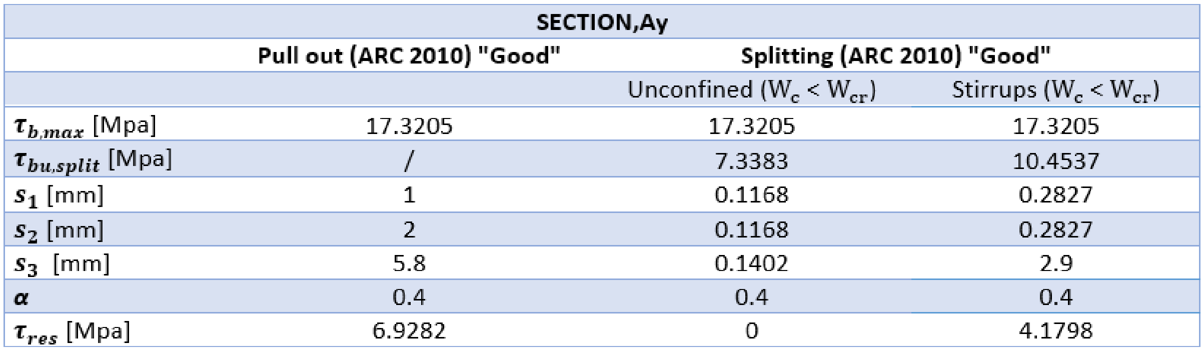

SECTION,Ay			
	Pull out (ARC 2010) "Good"	Splitting (ARC 2010) "Good"	
		Unconfined ($W_c < W_{cr}$)	Stirrups ($W_c < W_{cr}$)
$\tau_{b,max}$ [Mpa]	17.3205	17.3205	17.3205
$\tau_{bu,split}$ [Mpa]	/	7.3383	10.4537
s_1 [mm]	1	0.1168	0.2827
s_2 [mm]	2	0.1168	0.2827
s_3 [mm]	5.8	0.1402	2.9
α	0.4	0.4	0.4
τ_{res} [Mpa]	6.9282	0	4.1798

Table 4.4: Bond strength-slip relationship parameters of ARC2010 model for section A, y direction (t=0).

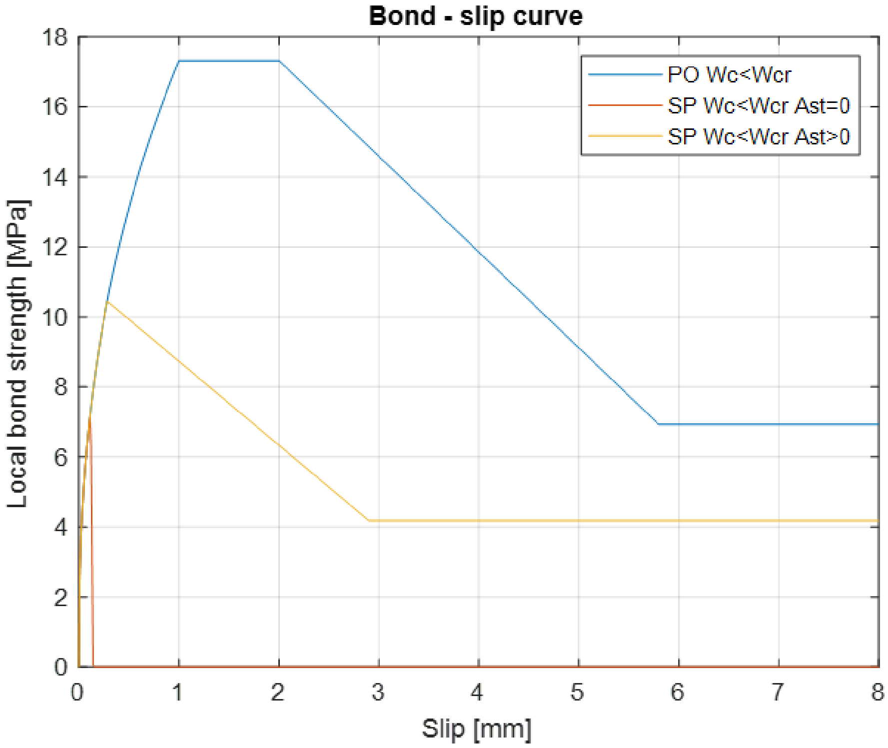

Figure 4.2: Bond strength-slip relationship ARC2010 model for section A, y direction (t=0).

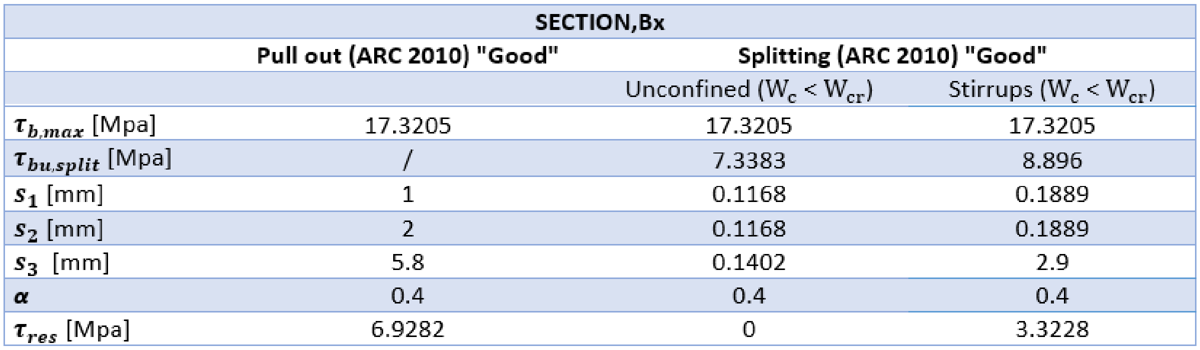

SECTION,Bx			
	Pull out (ARC 2010) "Good"	Splitting (ARC 2010) "Good"	
		Unconfined ($W_c < W_{cr}$)	Stirrups ($W_c < W_{cr}$)
$\tau_{b,max}$ [Mpa]	17.3205	17.3205	17.3205
$\tau_{bu,split}$ [Mpa]	/	7.3383	8.896
s_1 [mm]	1	0.1168	0.1889
s_2 [mm]	2	0.1168	0.1889
s_3 [mm]	5.8	0.1402	2.9
α	0.4	0.4	0.4
τ_{res} [Mpa]	6.9282	0	3.3228

Table 4.5: Bond strength-slip relationship parameters of ARC2010 model for section B, x direction (t=0).

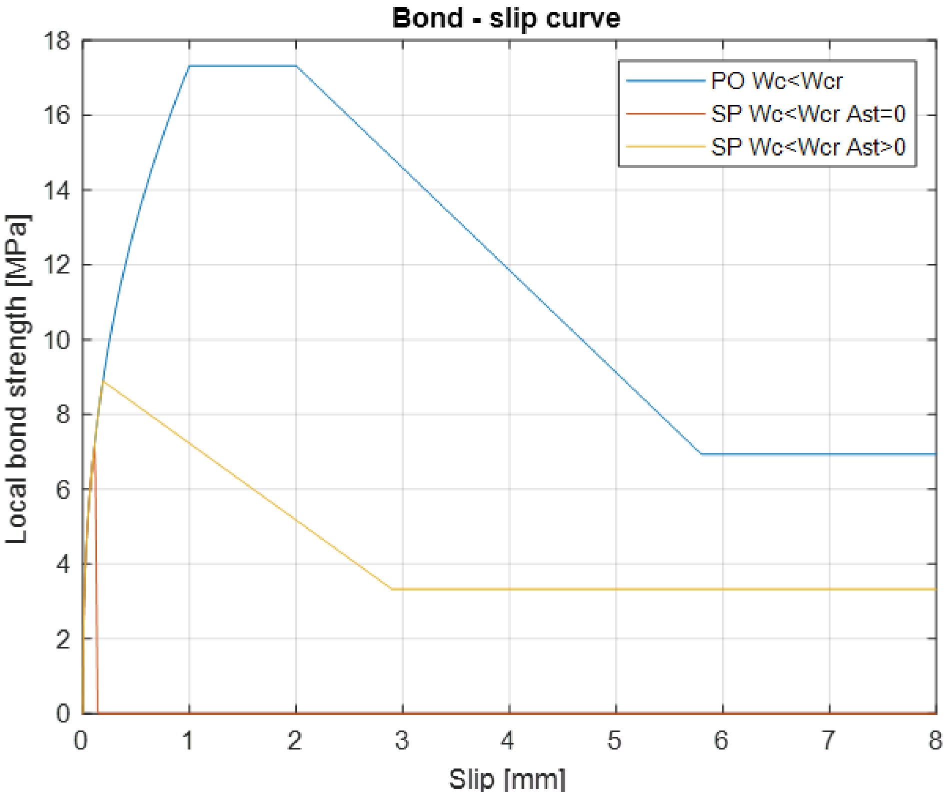

Figure 4.3: Bond strength-slip relationship ARC2010 model for section B, x direction (t=0).

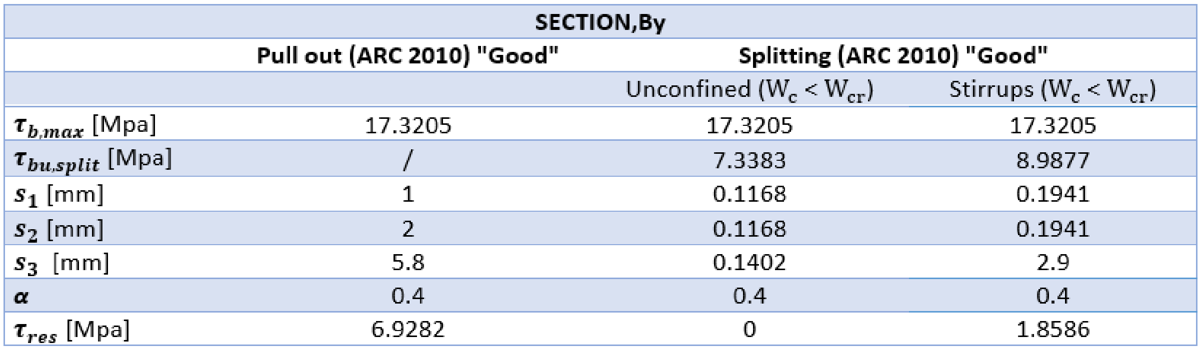

SECTION,By			
	Pull out (ARC 2010) "Good"	**Splitting (ARC 2010) "Good"**	
		Unconfined ($W_c < W_{cr}$)	Stirrups ($W_c < W_{cr}$)
$\tau_{b,max}$ [Mpa]	17.3205	17.3205	17.3205
$\tau_{bu,split}$ [Mpa]	/	7.3383	8.9877
s_1 [mm]	1	0.1168	0.1941
s_2 [mm]	2	0.1168	0.1941
s_3 [mm]	5.8	0.1402	2.9
α	0.4	0.4	0.4
τ_{res} [Mpa]	6.9282	0	1.8586

Table 4.6: Bond strength-slip relationship parameters of ARC2010 model for section B, y direction (t=0).

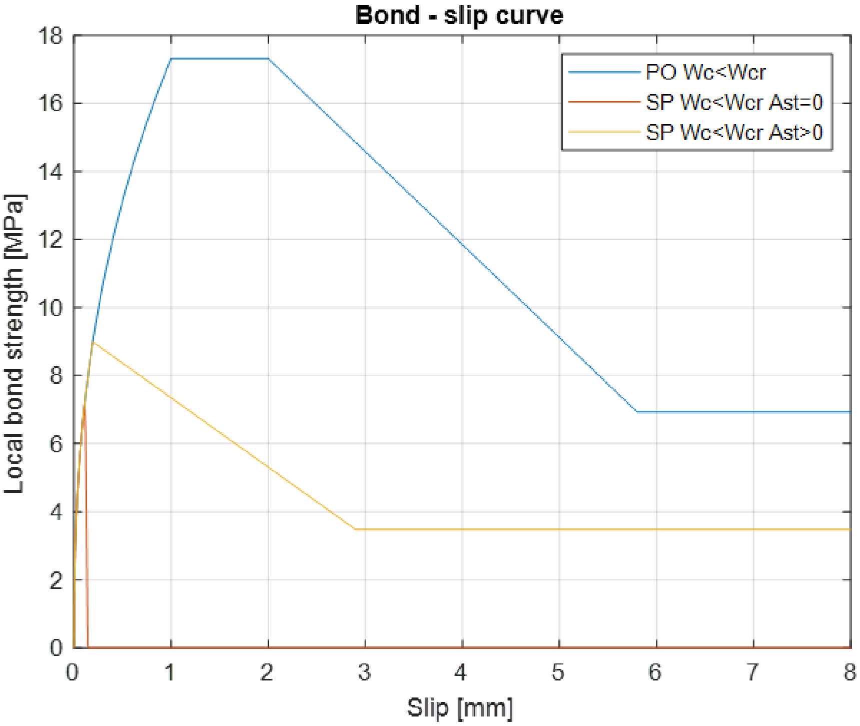

Figure 4.4: Bond strength-slip relationship ARC2010 model for section B, y direction (t=0).

4.2 Bond splitting strength

The reduction of the cross - sectional area of the longitudinal reinforcement is shown in Table 4.7 (De Gaetano, 2019). The percentage of reduction is reported and it is assumed equal for the stirrups. Once the variation of the stirrups area in time is known, the bond splitting strength has been computed for different values of K_{tr}, the parameter that takes into account the amount of transversal reinforcement (Table 4.8, 4.9, 4.10 and 4.11). The calculation has been performed for the two cross sections in both directions and for the two different type of corrosion, General and Pitting. In fact, in the two cases the reduction of the area in time is different. Moreover, the case of general and pitting corrosion acting at the same time has been considered.

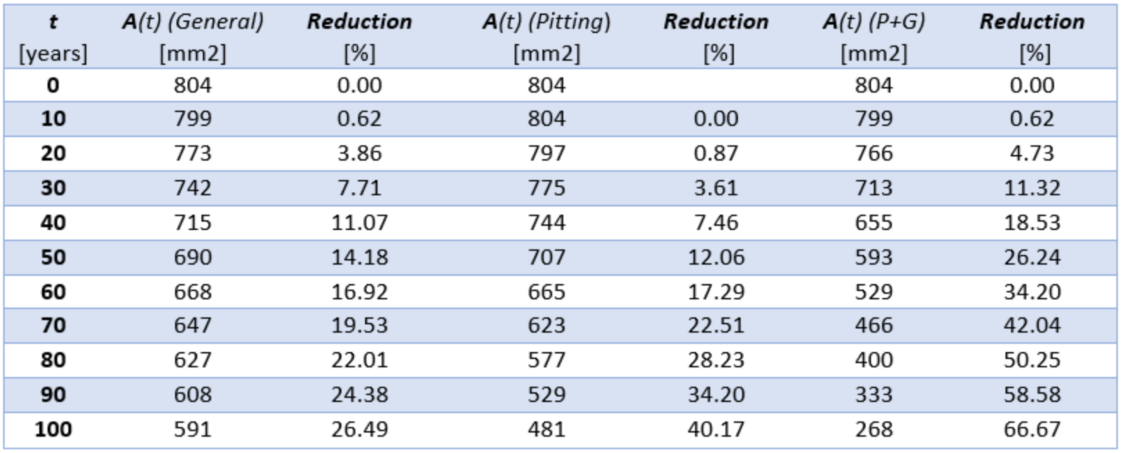

t [years]	***A(t) (General)*** [mm2]	**Reduction** [%]	***A(t) (Pitting)*** [mm2]	**Reduction** [%]	***A(t) (P+G)*** [mm2]	**Reduction** [%]
0	804	0.00	804		804	0.00
10	799	0.62	804	0.00	799	0.62
20	773	3.86	797	0.87	766	4.73
30	742	7.71	775	3.61	713	11.32
40	715	11.07	744	7.46	655	18.53
50	690	14.18	707	12.06	593	26.24
60	668	16.92	665	17.29	529	34.20
70	647	19.53	623	22.51	466	42.04
80	627	22.01	577	28.23	400	50.25
90	608	24.38	529	34.20	333	58.58
100	591	26.49	481	40.17	268	66.67

Table 4.7: Area reduction in the longitudinal reiforcement due to General, Pitting and General + Pitting corrosion.

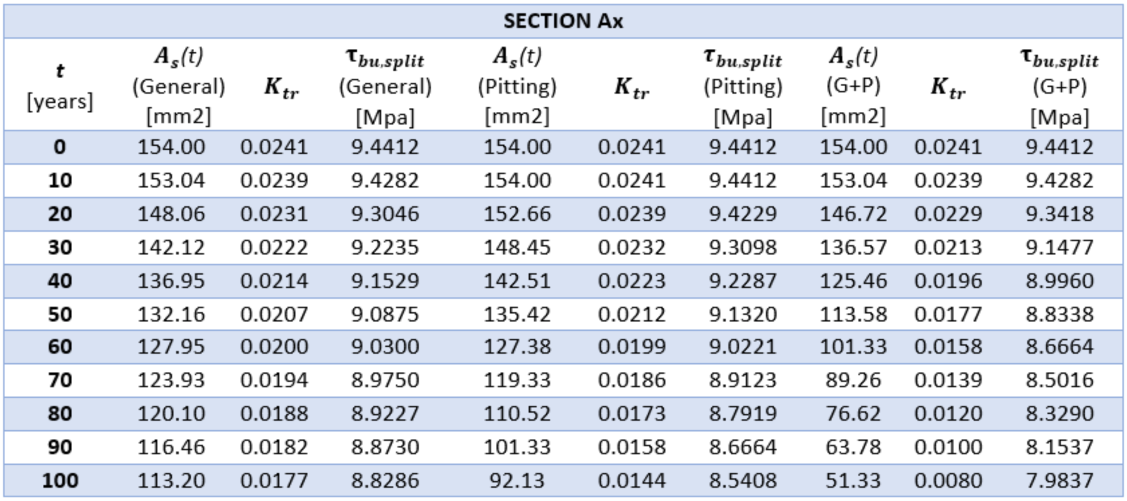

SECTION Ax									
t [years]	$A_s(t)$ (General) [mm2]	K_{tr}	$\tau_{bu,split}$ (General) [Mpa]	$A_s(t)$ (Pitting) [mm2]	K_{tr}	$\tau_{bu,split}$ (Pitting) [Mpa]	$A_s(t)$ (G+P) [mm2]	K_{tr}	$\tau_{bu,split}$ (G+P) [Mpa]
0	154.00	0.0241	9.4412	154.00	0.0241	9.4412	154.00	0.0241	9.4412
10	153.04	0.0239	9.4282	154.00	0.0241	9.4412	153.04	0.0239	9.4282
20	148.06	0.0231	9.3046	152.66	0.0239	9.4229	146.72	0.0229	9.3418
30	142.12	0.0222	9.2235	148.45	0.0232	9.3098	136.57	0.0213	9.1477
40	136.95	0.0214	9.1529	142.51	0.0223	9.2287	125.46	0.0196	8.9960
50	132.16	0.0207	9.0875	135.42	0.0212	9.1320	113.58	0.0177	8.8338
60	127.95	0.0200	9.0300	127.38	0.0199	9.0221	101.33	0.0158	8.6664
70	123.93	0.0194	8.9750	119.33	0.0186	8.9123	89.26	0.0139	8.5016
80	120.10	0.0188	8.9227	110.52	0.0173	8.7919	76.62	0.0120	8.3290
90	116.46	0.0182	8.8730	101.33	0.0158	8.6664	63.78	0.0100	8.1537
100	113.20	0.0177	8.8286	92.13	0.0144	8.5408	51.33	0.0080	7.9837

Table 4.8: Variation of the bond strength for different degree of corrosion of the stirrups in section Ax.

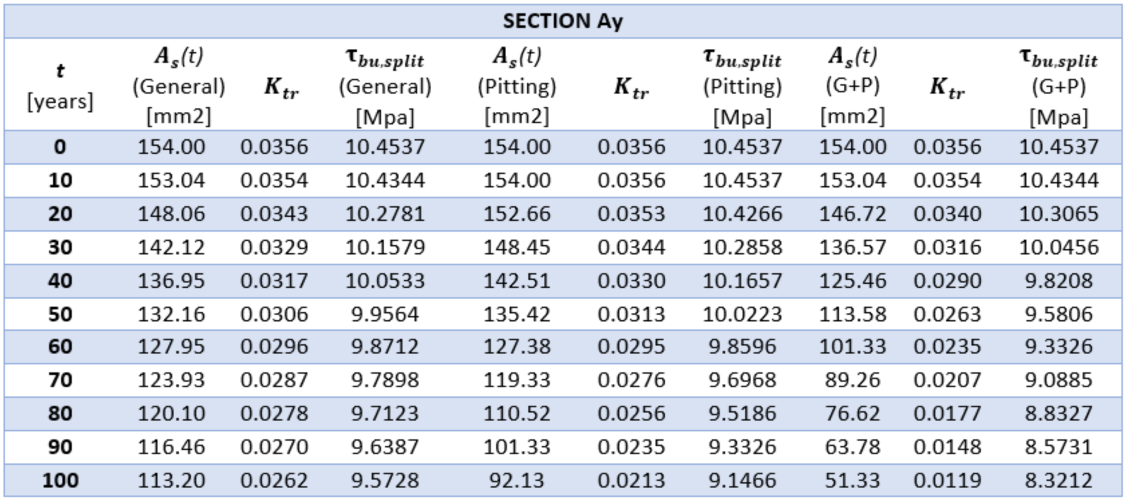

SECTION Ay									
t [years]	$A_s(t)$ (General) [mm2]	K_{tr}	$\tau_{bu,split}$ (General) [Mpa]	$A_s(t)$ (Pitting) [mm2]	K_{tr}	$\tau_{bu,split}$ (Pitting) [Mpa]	$A_s(t)$ (G+P) [mm2]	K_{tr}	$\tau_{bu,split}$ (G+P) [Mpa]
0	154.00	0.0356	10.4537	154.00	0.0356	10.4537	154.00	0.0356	10.4537
10	153.04	0.0354	10.4344	154.00	0.0356	10.4537	153.04	0.0354	10.4344
20	148.06	0.0343	10.2781	152.66	0.0353	10.4266	146.72	0.0340	10.3065
30	142.12	0.0329	10.1579	148.45	0.0344	10.2858	136.57	0.0316	10.0456
40	136.95	0.0317	10.0533	142.51	0.0330	10.1657	125.46	0.0290	9.8208
50	132.16	0.0306	9.9564	135.42	0.0313	10.0223	113.58	0.0263	9.5806
60	127.95	0.0296	9.8712	127.38	0.0295	9.8596	101.33	0.0235	9.3326
70	123.93	0.0287	9.7898	119.33	0.0276	9.6968	89.26	0.0207	9.0885
80	120.10	0.0278	9.7123	110.52	0.0256	9.5186	76.62	0.0177	8.8327
90	116.46	0.0270	9.6387	101.33	0.0235	9.3326	63.78	0.0148	8.5731
100	113.20	0.0262	9.5728	92.13	0.0213	9.1466	51.33	0.0119	8.3212

Table 4.9: Variation of the bond strength for different degree of corrosion of the stirrups in section Ay.

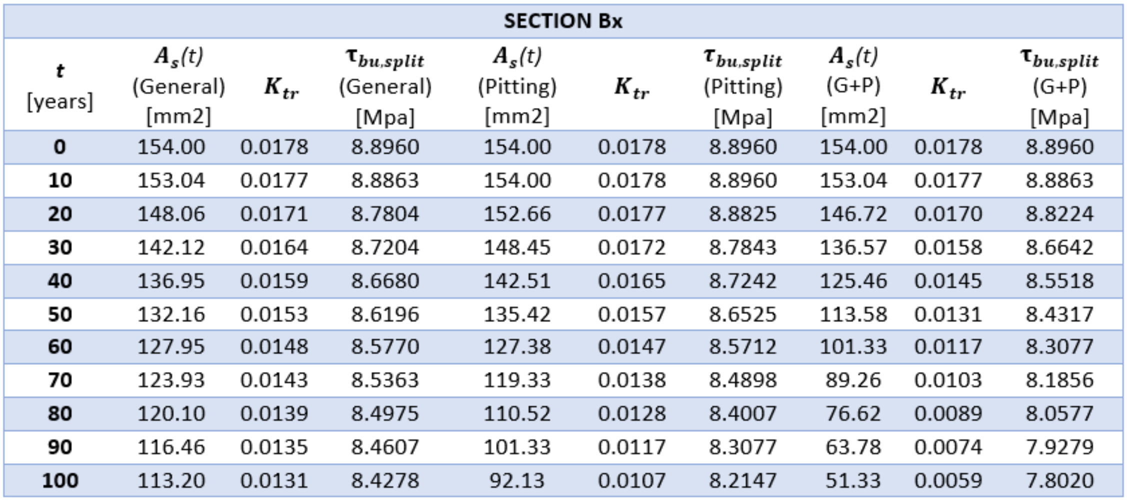

SECTION Bx									
t [years]	**$A_s(t)$** (General) [mm2]	**K_{tr}**	**$\tau_{bu,split}$** (General) [Mpa]	**$A_s(t)$** (Pitting) [mm2]	**K_{tr}**	**$\tau_{bu,split}$** (Pitting) [Mpa]	**$A_s(t)$** (G+P) [mm2]	**K_{tr}**	**$\tau_{bu,split}$** (G+P) [Mpa]
0	154.00	0.0178	8.8960	154.00	0.0178	8.8960	154.00	0.0178	8.8960
10	153.04	0.0177	8.8863	154.00	0.0178	8.8960	153.04	0.0177	8.8863
20	148.06	0.0171	8.7804	152.66	0.0177	8.8825	146.72	0.0170	8.8224
30	142.12	0.0164	8.7204	148.45	0.0172	8.7843	136.57	0.0158	8.6642
40	136.95	0.0159	8.6680	142.51	0.0165	8.7242	125.46	0.0145	8.5518
50	132.16	0.0153	8.6196	135.42	0.0157	8.6525	113.58	0.0131	8.4317
60	127.95	0.0148	8.5770	127.38	0.0147	8.5712	101.33	0.0117	8.3077
70	123.93	0.0143	8.5363	119.33	0.0138	8.4898	89.26	0.0103	8.1856
80	120.10	0.0139	8.4975	110.52	0.0128	8.4007	76.62	0.0089	8.0577
90	116.46	0.0135	8.4607	101.33	0.0117	8.3077	63.78	0.0074	7.9279
100	113.20	0.0131	8.4278	92.13	0.0107	8.2147	51.33	0.0059	7.8020

Table 4.10: Variation of the bond strength for different degree of corrosion of the stirrups in section Bx.

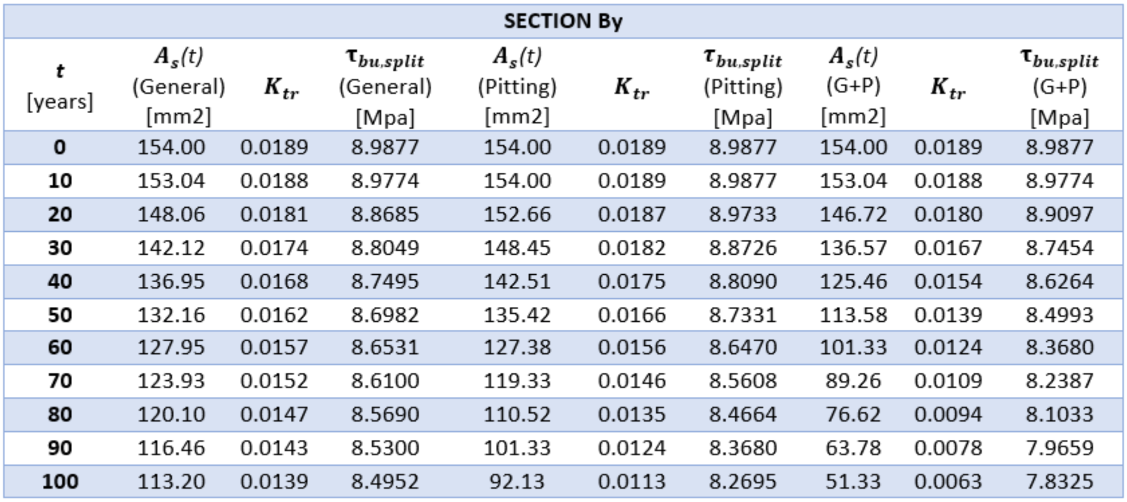

SECTION By									
t [years]	**$A_s(t)$** (General) [mm2]	**K_{tr}**	**$\tau_{bu,split}$** (General) [Mpa]	**$A_s(t)$** (Pitting) [mm2]	**K_{tr}**	**$\tau_{bu,split}$** (Pitting) [Mpa]	**$A_s(t)$** (G+P) [mm2]	**K_{tr}**	**$\tau_{bu,split}$** (G+P) [Mpa]
0	154.00	0.0189	8.9877	154.00	0.0189	8.9877	154.00	0.0189	8.9877
10	153.04	0.0188	8.9774	154.00	0.0189	8.9877	153.04	0.0188	8.9774
20	148.06	0.0181	8.8685	152.66	0.0187	8.9733	146.72	0.0180	8.9097
30	142.12	0.0174	8.8049	148.45	0.0182	8.8726	136.57	0.0167	8.7454
40	136.95	0.0168	8.7495	142.51	0.0175	8.8090	125.46	0.0154	8.6264
50	132.16	0.0162	8.6982	135.42	0.0166	8.7331	113.58	0.0139	8.4993
60	127.95	0.0157	8.6531	127.38	0.0156	8.6470	101.33	0.0124	8.3680
70	123.93	0.0152	8.6100	119.33	0.0146	8.5608	89.26	0.0109	8.2387
80	120.10	0.0147	8.5690	110.52	0.0135	8.4664	76.62	0.0094	8.1033
90	116.46	0.0143	8.5300	101.33	0.0124	8.3680	63.78	0.0078	7.9659
100	113.20	0.0139	8.4952	92.13	0.0113	8.2695	51.33	0.0063	7.8325

Table 4.11: Variation of the bond strength for different degree of corrosion of the stirrups in section By.

4.3 Deteriorated bond strength

In order to consider the effect of corrosion, the equivalent slip has been computed through the empirical relationships in Eq. 2.39 and 2.40. The two functions, representing the cases of presence and absence of stirrups, are plotted in Figure 4.5, where the corrosion level is expressed as weight loss. As it is possible to observe in the plot, the equivalent slip in case of presence of stirrups is higher then in case of absence. This is explicable observing the bond strength-slip plots of both cases. In absence of stirrups the reduction of the bond strength immediately after reaching the maximum value is stronger. This means that it is necessary a smaller equivalent slip to have the same decrement of bond strength that occurs in the case of presence of stirrups.

Once computed the equivalent slip, the bond strength-slip curves have been translated in order to find the intersection point between the original curve and the new one, representing the deteriorated bond strength at a specific corrosion level. The curve representing the splitting failure in presence of stirrups has been considered in this study and, according to experimental results, it is assumed that the cracking of the concrete cover occurs at a corrosion level of 2 %.

All the results obtained are reported in tables 4.12, 4.13, 4.14 and 4.15. The relative bond strength has been computed dividing the deteriorated bond strength by the non-corroded bond strength and has been plotted for different level of corrosion (Figure 4.6, 4.7, 4.8 and 4.9).

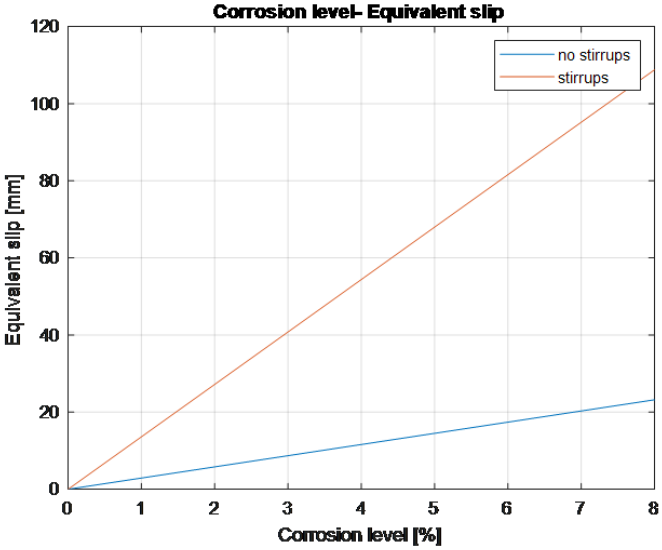

Figure 4.5: Corrosion level - Equivalent slip relationship.

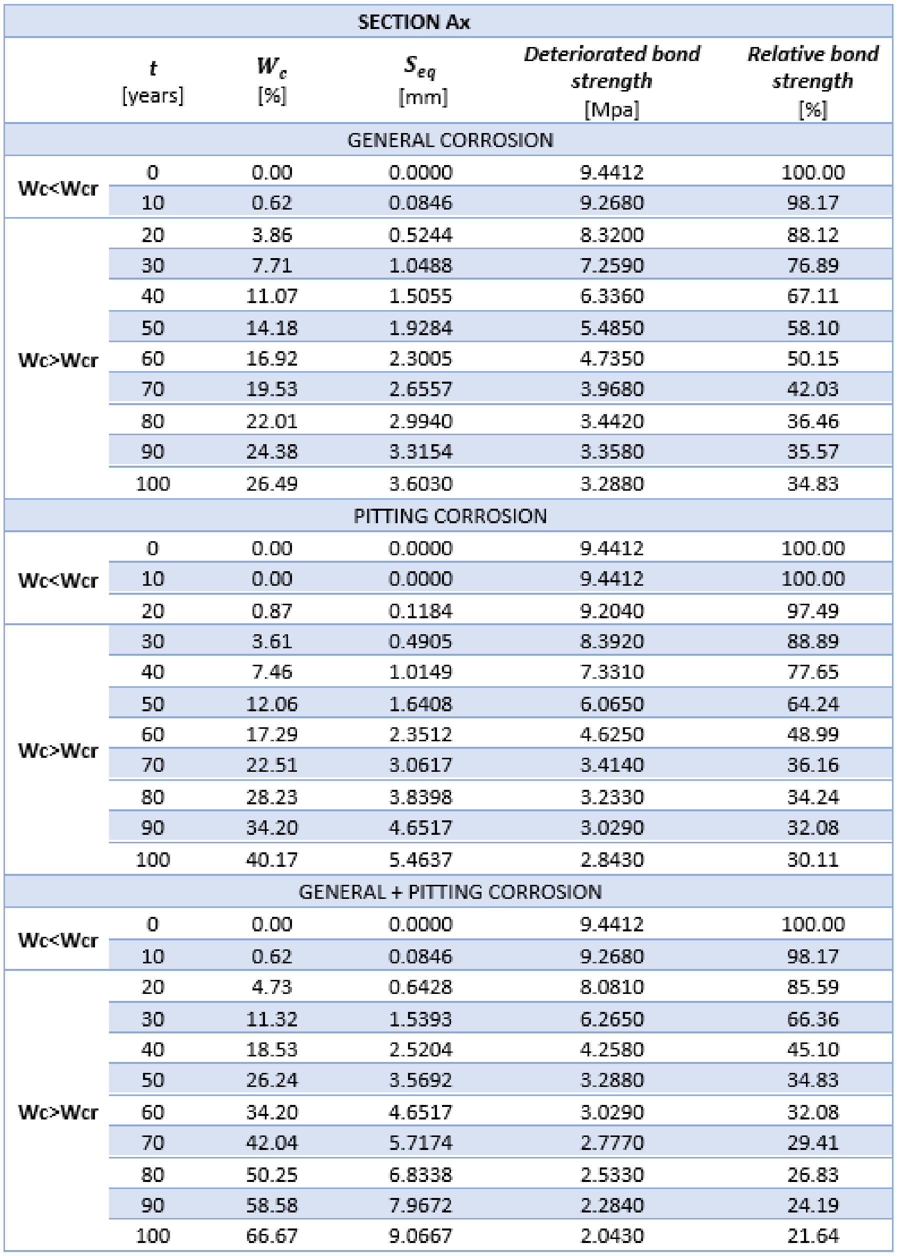

SECTION Ax					
	t [years]	W_c [%]	S_{eq} [mm]	*Deteriorated bond strength* [Mpa]	*Relative bond strength* [%]
GENERAL CORROSION					
Wc<Wcr	0	0.00	0.0000	9.4412	100.00
	10	0.62	0.0846	9.2680	98.17
Wc>Wcr	20	3.86	0.5244	8.3200	88.12
	30	7.71	1.0488	7.2590	76.89
	40	11.07	1.5055	6.3360	67.11
	50	14.18	1.9284	5.4850	58.10
	60	16.92	2.3005	4.7350	50.15
	70	19.53	2.6557	3.9680	42.03
	80	22.01	2.9940	3.4420	36.46
	90	24.38	3.3154	3.3580	35.57
	100	26.49	3.6030	3.2880	34.83
PITTING CORROSION					
Wc<Wcr	0	0.00	0.0000	9.4412	100.00
	10	0.00	0.0000	9.4412	100.00
	20	0.87	0.1184	9.2040	97.49
Wc>Wcr	30	3.61	0.4905	8.3920	88.89
	40	7.46	1.0149	7.3310	77.65
	50	12.06	1.6408	6.0650	64.24
	60	17.29	2.3512	4.6250	48.99
	70	22.51	3.0617	3.4140	36.16
	80	28.23	3.8398	3.2330	34.24
	90	34.20	4.6517	3.0290	32.08
	100	40.17	5.4637	2.8430	30.11
GENERAL + PITTING CORROSION					
Wc<Wcr	0	0.00	0.0000	9.4412	100.00
	10	0.62	0.0846	9.2680	98.17
Wc>Wcr	20	4.73	0.6428	8.0810	85.59
	30	11.32	1.5393	6.2650	66.36
	40	18.53	2.5204	4.2580	45.10
	50	26.24	3.5692	3.2880	34.83
	60	34.20	4.6517	3.0290	32.08
	70	42.04	5.7174	2.7770	29.41
	80	50.25	6.8338	2.5330	26.83
	90	58.58	7.9672	2.2840	24.19
	100	66.67	9.0667	2.0430	21.64

Table 4.12: Relative bond strength ARC2010, section Ax.

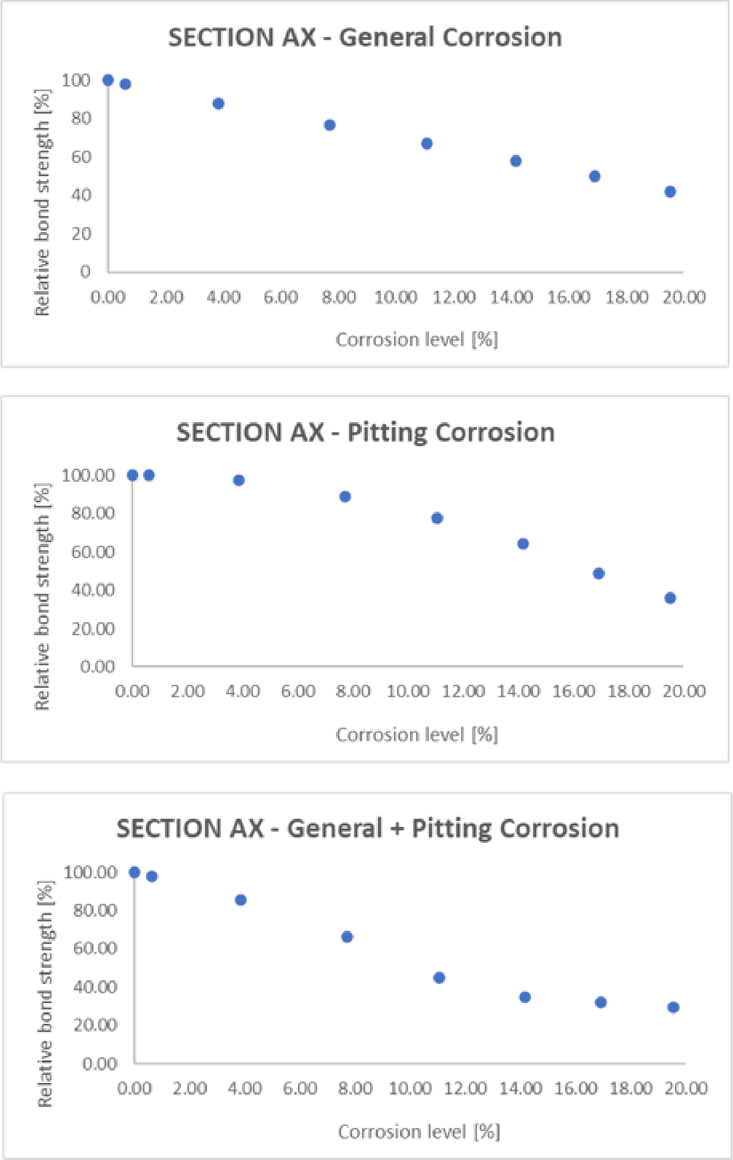

Figure 4.6: Relative bond strength ARC2010, section Ax.

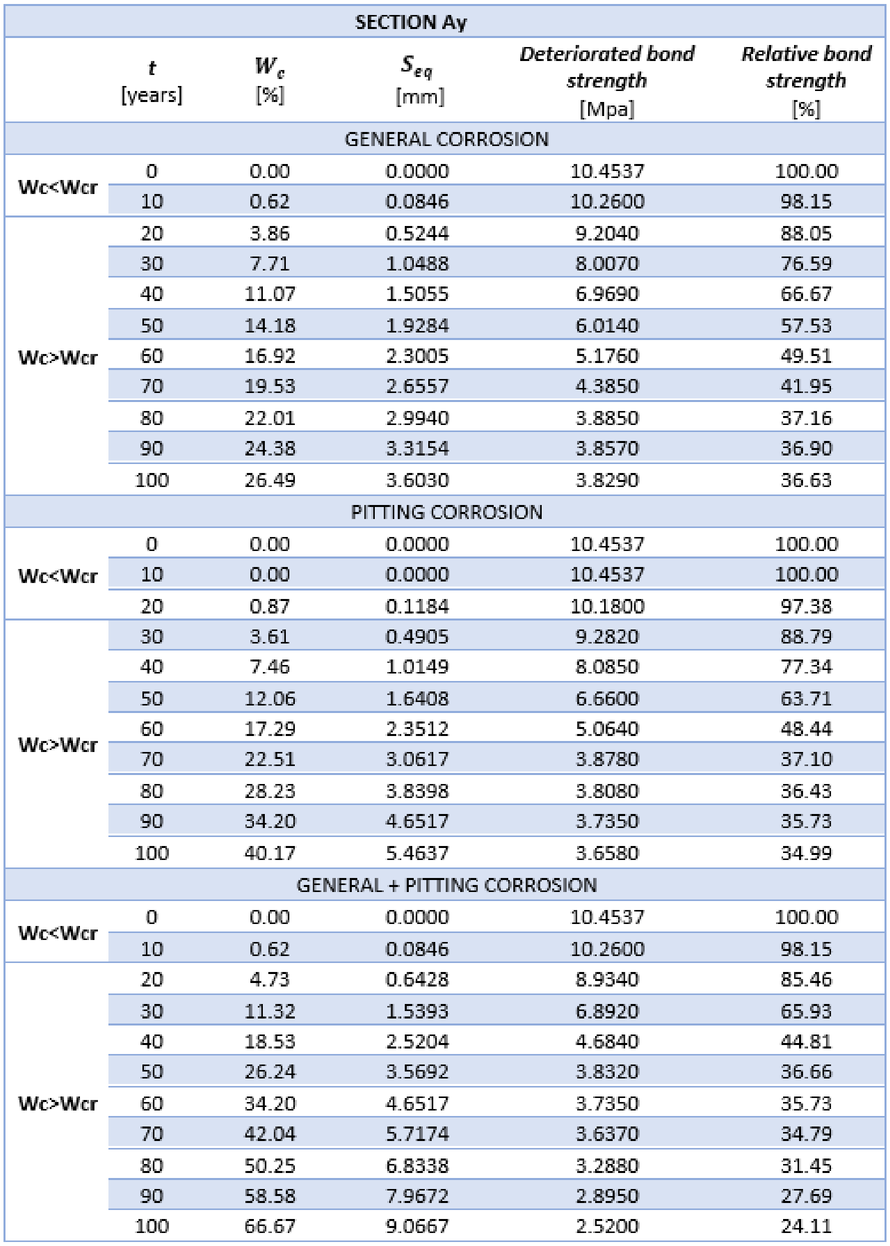

SECTION Ay					
	t [years]	***W_c*** [%]	***S_{eq}*** [mm]	***Deteriorated bond strength*** [Mpa]	***Relative bond strength*** [%]
GENERAL CORROSION					
Wc<Wcr	0	0.00	0.0000	10.4537	100.00
	10	0.62	0.0846	10.2600	98.15
Wc>Wcr	20	3.86	0.5244	9.2040	88.05
	30	7.71	1.0488	8.0070	76.59
	40	11.07	1.5055	6.9690	66.67
	50	14.18	1.9284	6.0140	57.53
	60	16.92	2.3005	5.1760	49.51
	70	19.53	2.6557	4.3850	41.95
	80	22.01	2.9940	3.8850	37.16
	90	24.38	3.3154	3.8570	36.90
	100	26.49	3.6030	3.8290	36.63
PITTING CORROSION					
Wc<Wcr	0	0.00	0.0000	10.4537	100.00
	10	0.00	0.0000	10.4537	100.00
	20	0.87	0.1184	10.1800	97.38
Wc>Wcr	30	3.61	0.4905	9.2820	88.79
	40	7.46	1.0149	8.0850	77.34
	50	12.06	1.6408	6.6600	63.71
	60	17.29	2.3512	5.0640	48.44
	70	22.51	3.0617	3.8780	37.10
	80	28.23	3.8398	3.8080	36.43
	90	34.20	4.6517	3.7350	35.73
	100	40.17	5.4637	3.6580	34.99
GENERAL + PITTING CORROSION					
Wc<Wcr	0	0.00	0.0000	10.4537	100.00
	10	0.62	0.0846	10.2600	98.15
Wc>Wcr	20	4.73	0.6428	8.9340	85.46
	30	11.32	1.5393	6.8920	65.93
	40	18.53	2.5204	4.6840	44.81
	50	26.24	3.5692	3.8320	36.66
	60	34.20	4.6517	3.7350	35.73
	70	42.04	5.7174	3.6370	34.79
	80	50.25	6.8338	3.2880	31.45
	90	58.58	7.9672	2.8950	27.69
	100	66.67	9.0667	2.5200	24.11

Table 4.13: Relative bond strength ARC2010, section Ay.

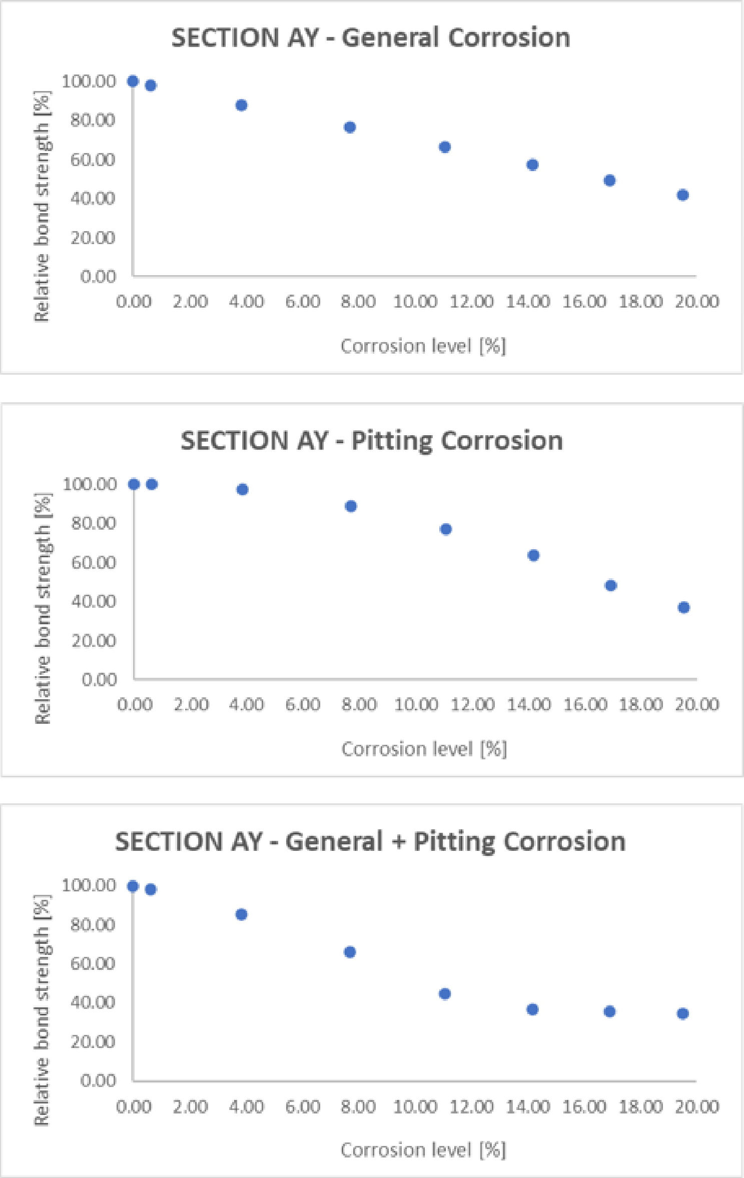

Figure 4.7: Relative bond strength ARC2010, section Ay.

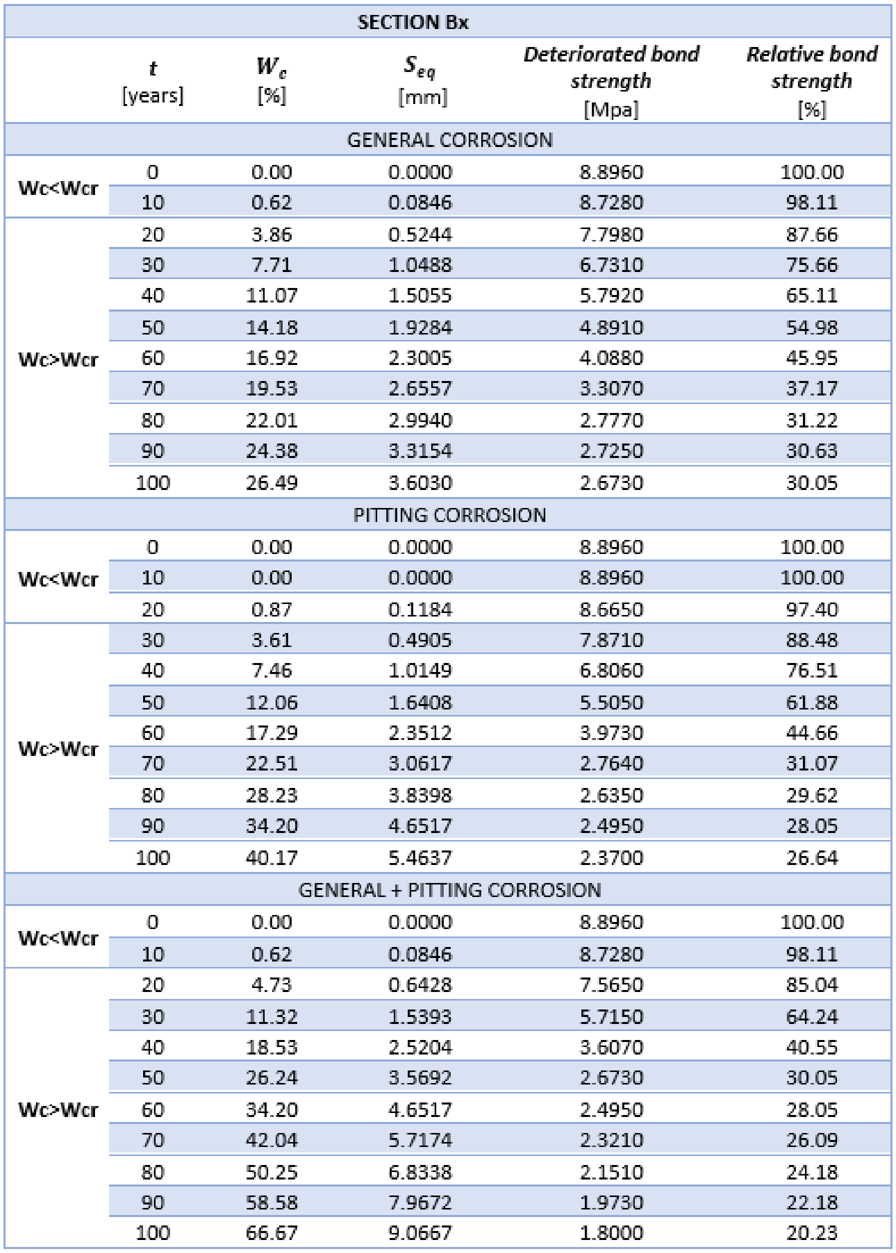

SECTION Bx					
	t [years]	W_c [%]	S_{eq} [mm]	*Deteriorated bond strength* [Mpa]	*Relative bond strength* [%]
GENERAL CORROSION					
Wc<Wcr	0	0.00	0.0000	8.8960	100.00
	10	0.62	0.0846	8.7280	98.11
Wc>Wcr	20	3.86	0.5244	7.7980	87.66
	30	7.71	1.0488	6.7310	75.66
	40	11.07	1.5055	5.7920	65.11
	50	14.18	1.9284	4.8910	54.98
	60	16.92	2.3005	4.0880	45.95
	70	19.53	2.6557	3.3070	37.17
	80	22.01	2.9940	2.7770	31.22
	90	24.38	3.3154	2.7250	30.63
	100	26.49	3.6030	2.6730	30.05
PITTING CORROSION					
Wc<Wcr	0	0.00	0.0000	8.8960	100.00
	10	0.00	0.0000	8.8960	100.00
	20	0.87	0.1184	8.6650	97.40
Wc>Wcr	30	3.61	0.4905	7.8710	88.48
	40	7.46	1.0149	6.8060	76.51
	50	12.06	1.6408	5.5050	61.88
	60	17.29	2.3512	3.9730	44.66
	70	22.51	3.0617	2.7640	31.07
	80	28.23	3.8398	2.6350	29.62
	90	34.20	4.6517	2.4950	28.05
	100	40.17	5.4637	2.3700	26.64
GENERAL + PITTING CORROSION					
Wc<Wcr	0	0.00	0.0000	8.8960	100.00
	10	0.62	0.0846	8.7280	98.11
Wc>Wcr	20	4.73	0.6428	7.5650	85.04
	30	11.32	1.5393	5.7150	64.24
	40	18.53	2.5204	3.6070	40.55
	50	26.24	3.5692	2.6730	30.05
	60	34.20	4.6517	2.4950	28.05
	70	42.04	5.7174	2.3210	26.09
	80	50.25	6.8338	2.1510	24.18
	90	58.58	7.9672	1.9730	22.18
	100	66.67	9.0667	1.8000	20.23

Table 4.14: Relative bond strength ARC2010, section Bx.

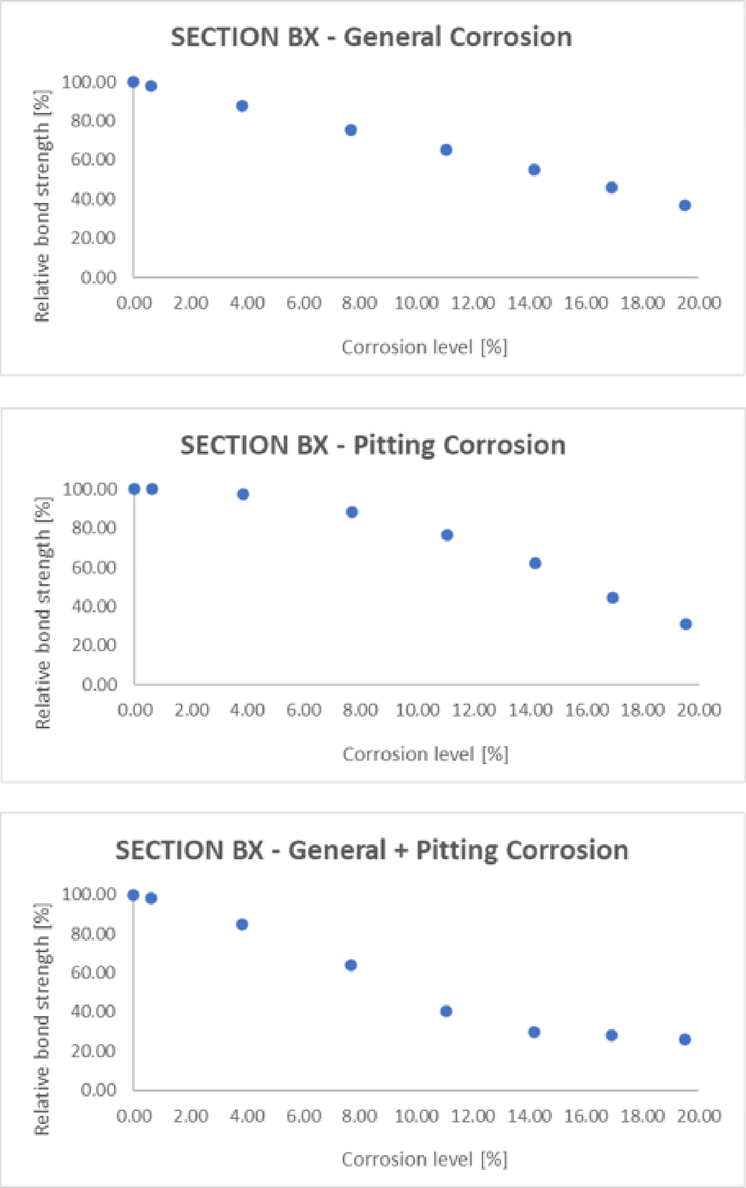

Figure 4.8: Relative bond strength ARC2010, section Bx.

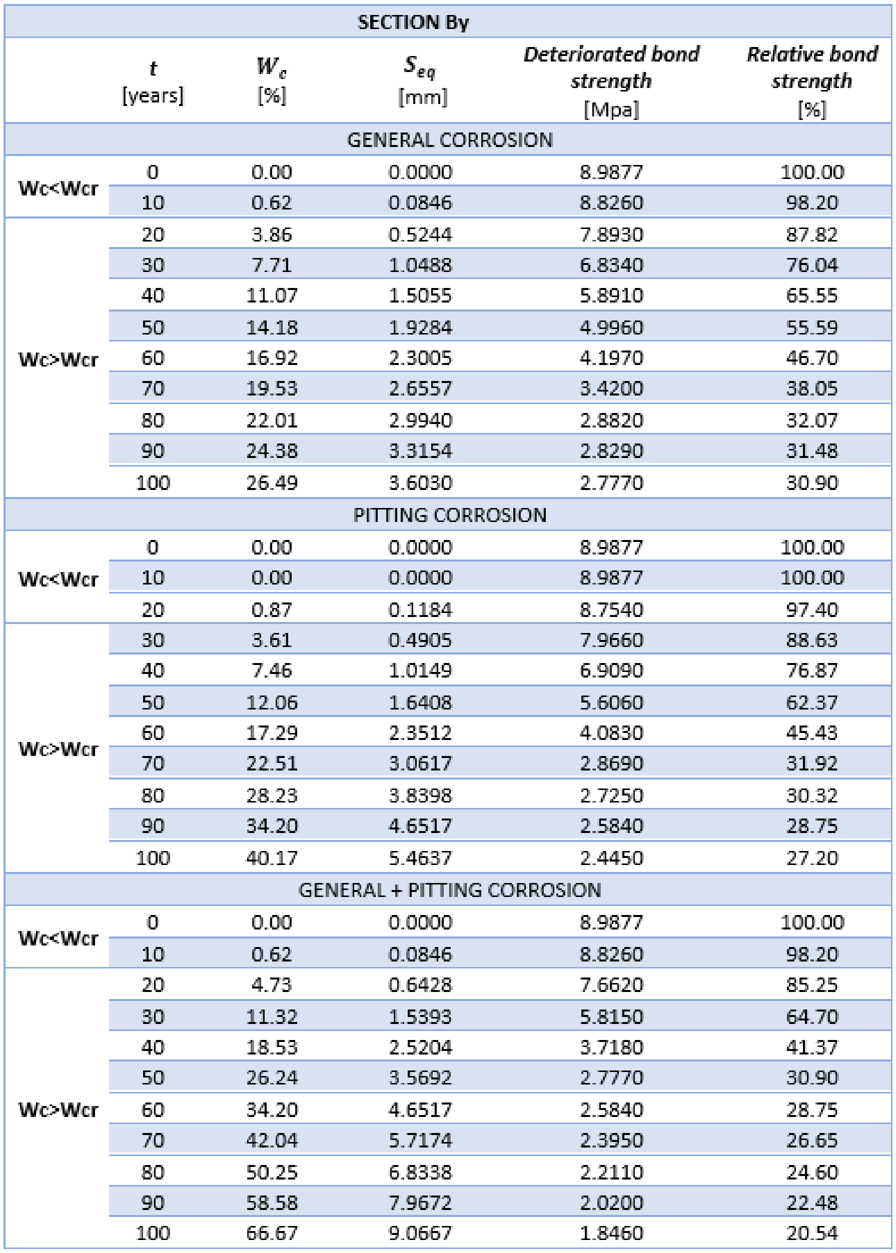

SECTION By					
	t [years]	W_c [%]	S_{eq} [mm]	*Deteriorated bond strength* [Mpa]	*Relative bond strength* [%]
GENERAL CORROSION					
Wc<Wcr	0	0.00	0.0000	8.9877	100.00
	10	0.62	0.0846	8.8260	98.20
Wc>Wcr	20	3.86	0.5244	7.8930	87.82
	30	7.71	1.0488	6.8340	76.04
	40	11.07	1.5055	5.8910	65.55
	50	14.18	1.9284	4.9960	55.59
	60	16.92	2.3005	4.1970	46.70
	70	19.53	2.6557	3.4200	38.05
	80	22.01	2.9940	2.8820	32.07
	90	24.38	3.3154	2.8290	31.48
	100	26.49	3.6030	2.7770	30.90
PITTING CORROSION					
Wc<Wcr	0	0.00	0.0000	8.9877	100.00
	10	0.00	0.0000	8.9877	100.00
	20	0.87	0.1184	8.7540	97.40
Wc>Wcr	30	3.61	0.4905	7.9660	88.63
	40	7.46	1.0149	6.9090	76.87
	50	12.06	1.6408	5.6060	62.37
	60	17.29	2.3512	4.0830	45.43
	70	22.51	3.0617	2.8690	31.92
	80	28.23	3.8398	2.7250	30.32
	90	34.20	4.6517	2.5840	28.75
	100	40.17	5.4637	2.4450	27.20
GENERAL + PITTING CORROSION					
Wc<Wcr	0	0.00	0.0000	8.9877	100.00
	10	0.62	0.0846	8.8260	98.20
Wc>Wcr	20	4.73	0.6428	7.6620	85.25
	30	11.32	1.5393	5.8150	64.70
	40	18.53	2.5204	3.7180	41.37
	50	26.24	3.5692	2.7770	30.90
	60	34.20	4.6517	2.5840	28.75
	70	42.04	5.7174	2.3950	26.65
	80	50.25	6.8338	2.2110	24.60
	90	58.58	7.9672	2.0200	22.48
	100	66.67	9.0667	1.8460	20.54

Table 4.15: Relative bond strength ARC2010, section By.

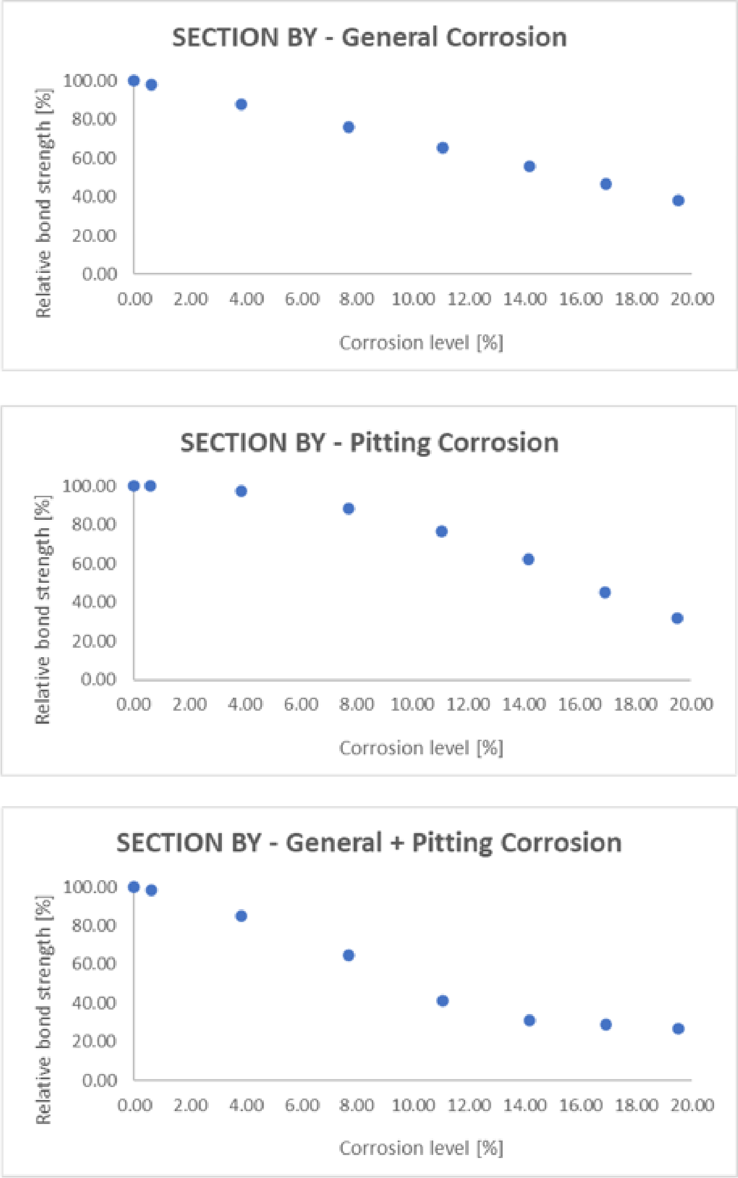

Figure 4.9: Relative bond strength ARC2010, section By.

4.4 Comparison between area loss and bond strength reduction

Plotting in the same graph the area and the bond strength reduction in time (Figure 4.10-4.21) it is possible to observe that the latter is always the most critical aspect. However, both reductions occur during the corrosion propagation phase, after the depassivation of the steel. This means that during the first years there will not be area and bond strength loss.

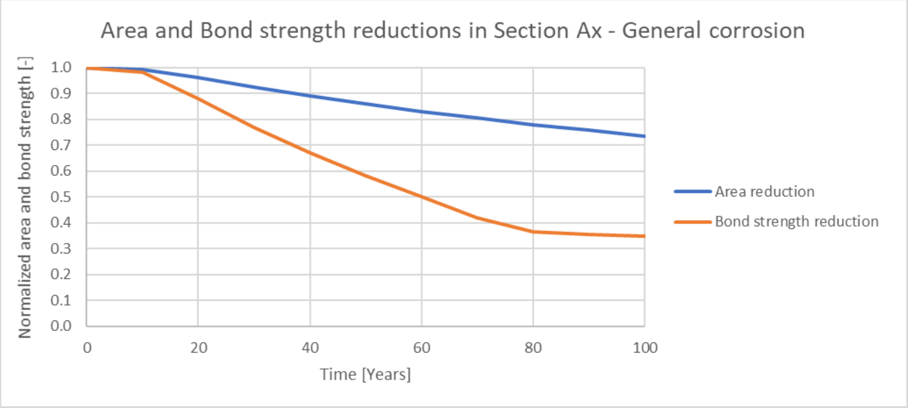

Figure 4.10: Comparison between area and bond strength reduction in time due to general corrosion for section Ax.

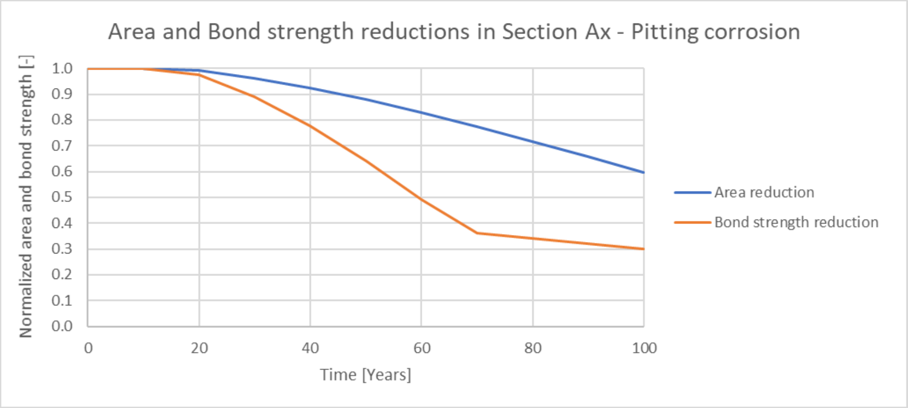

Figure 4.11: Comparison between area and bond strength reduction in time due to pitting corrosion for section Ax.

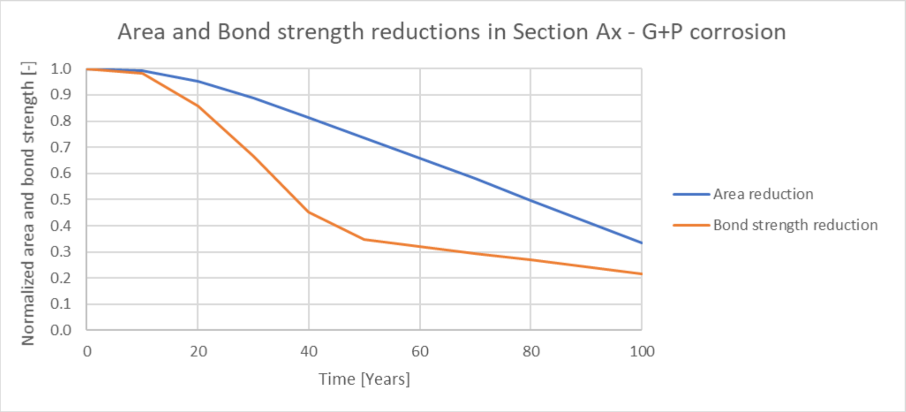

Figure 4.12: Comparison between area and bond strength reduction in time due to P+G corrosion for section Ax.

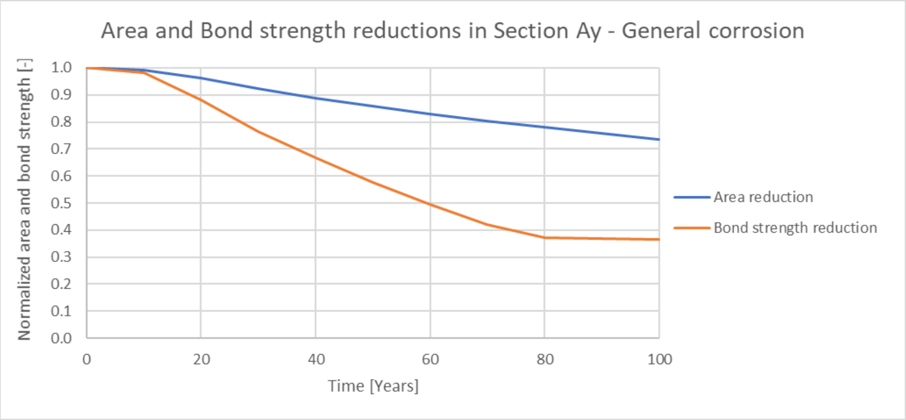

Figure 4.13: Comparison between area and bond strength reduction in time due to general corrosion for section Ay.

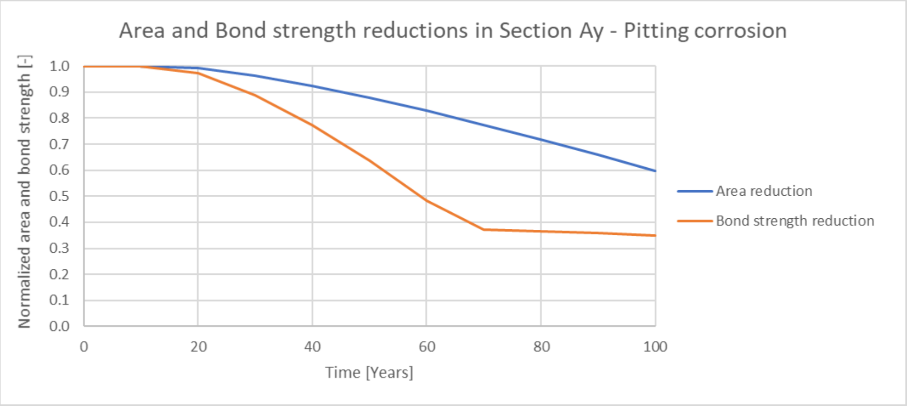

Figure 4.14: Comparison between area and bond strength reduction in time due to pitting corrosion for section Ay.

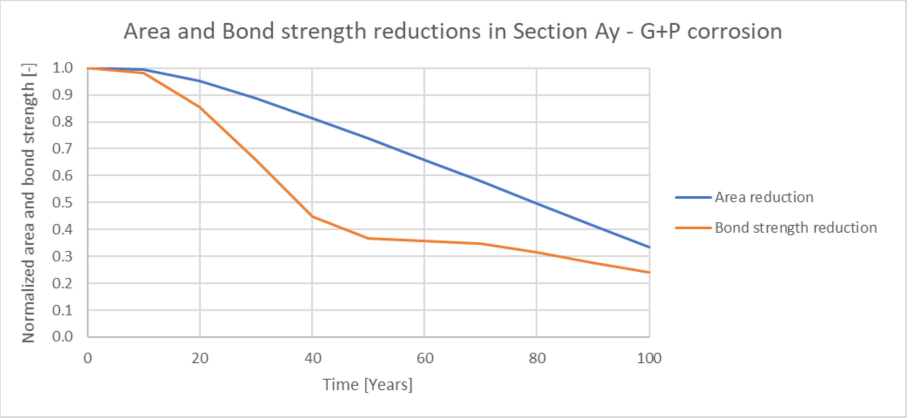

Figure 4.15: Comparison between area and bond strength reduction in time due to P+G corrosion for section Ay.

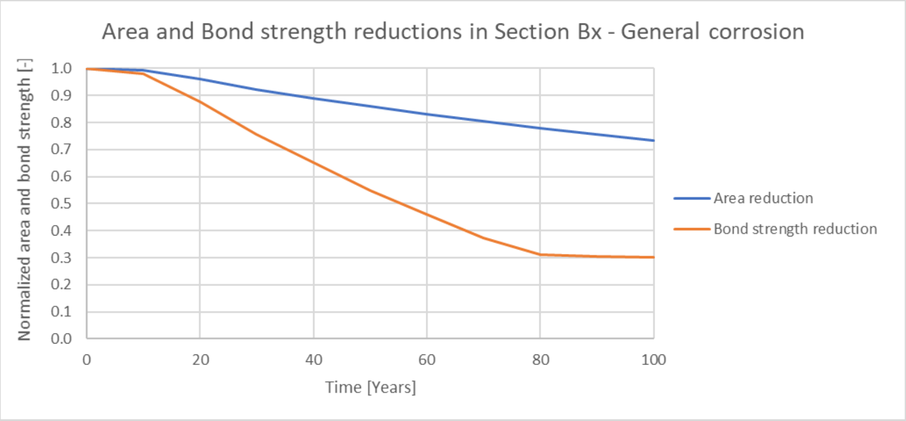

Figure 4.16: Comparison between area and bond strength reduction in time due to general corrosion for section Bx.

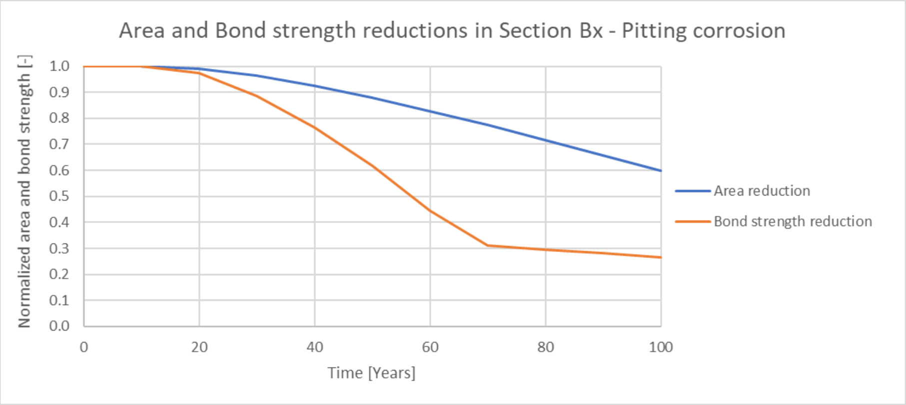

Figure 4.17: Comparison between area and bond strength reduction in time due to pitting corrosion for section Bx.

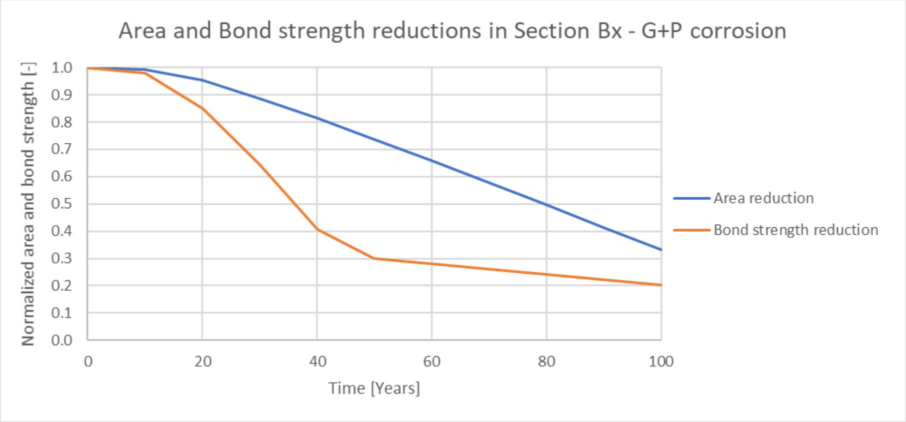

Figure 4.18: Comparison between area and bond strength reduction in time due to P+G corrosion for section Bx.

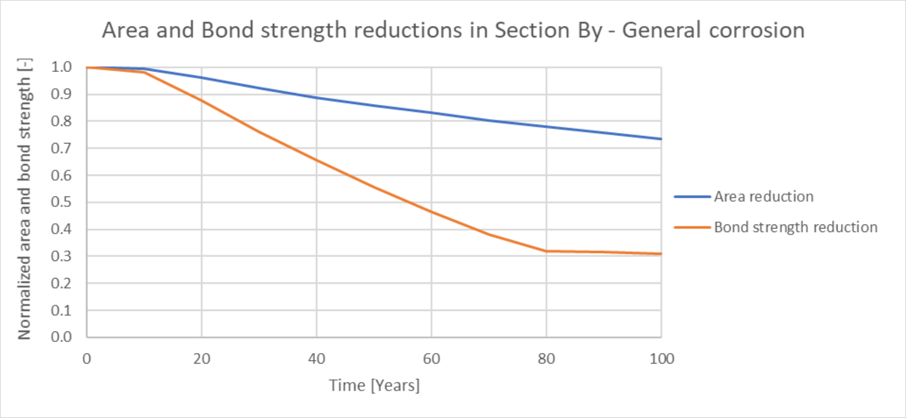

Figure 4.19: Comparison between area and bond strength reduction in time due to general corrosion for section By.

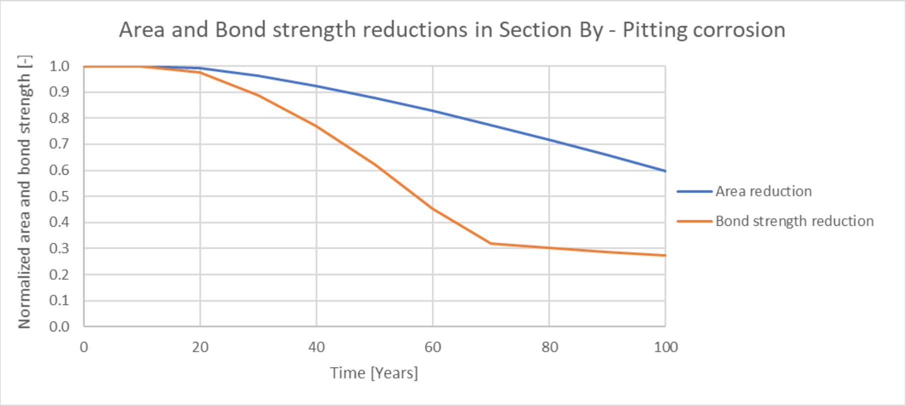

Figure 4.20: Comparison between area and bond strength reduction in time due to pitting corrosion for section By.

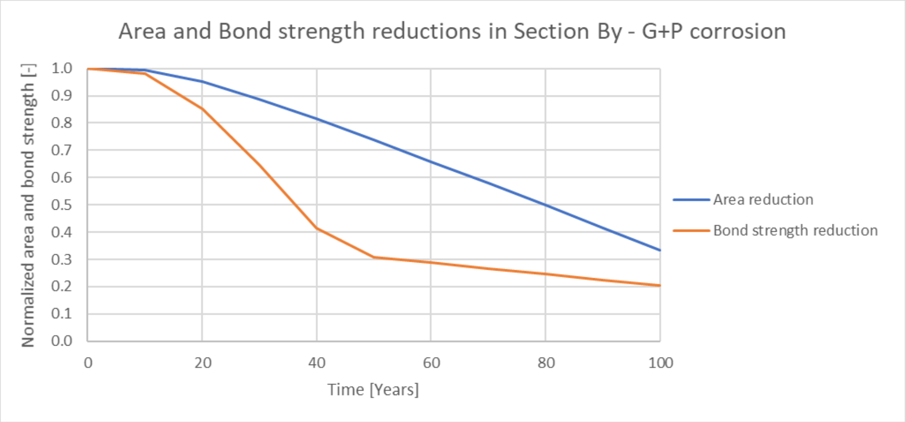

Figure 4.21: Comparison between area and bond strength reduction in time due to P+G corrosion for section By.

Chapter 5

Structural capacity and ductility

5.1 Interaction and Bresler's domains

Interaction domains are used for the assessment of elements simultaneously subjected to compressive and bending stress. These domains are realized from couples of M-N values that correspond to limit deformations in the materials of the section object of study. In a simple model the constitutive laws used for steel and concrete are parabola-rectangle and bilinear diagrams respectively (Figure 5.1).

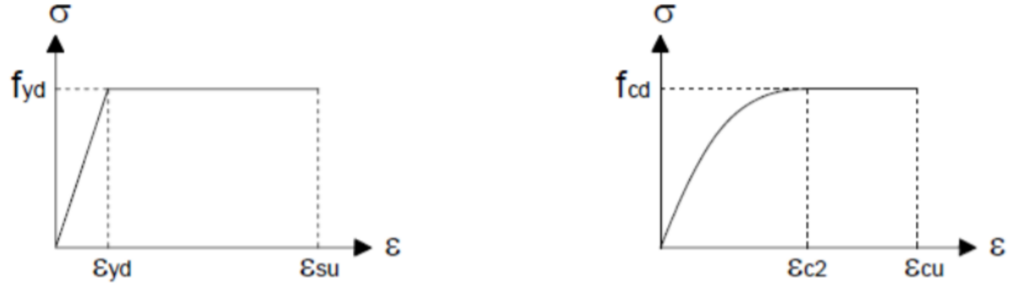

Figure 5.1: Constitutive law of steel (left) and concrete(right).

Stress-strain relationships parameters:

- $f_{yd} = 450/1.15 = 391.3 MPa$ (Steel B450C)
- $f_{cd} = 40/1.5 = 26.67 MPa$ (Concrete C40/50)
- $\epsilon_{yd} = f_{yd}/E_s = 0.001956$
- $\epsilon_{su} = 0.0675$

- $\epsilon_{c2} = 0.002$
- $\epsilon_{cu} = 0.0035$

The input parameters for the construction of the interaction domains that have been modified to consider the effects of corrosion in time are:

- Steel rebars cross-section
- Steel yield strength
- Steel ultimate strain

The reductions in time of these three parameters have been computed for the cases of general corrosion, pitting corrosion and the two corrosion types acting at the same time. The values have been obtained from empirical models and are the results of the research developed by De Gaetano, 2019 (Table 5.1).

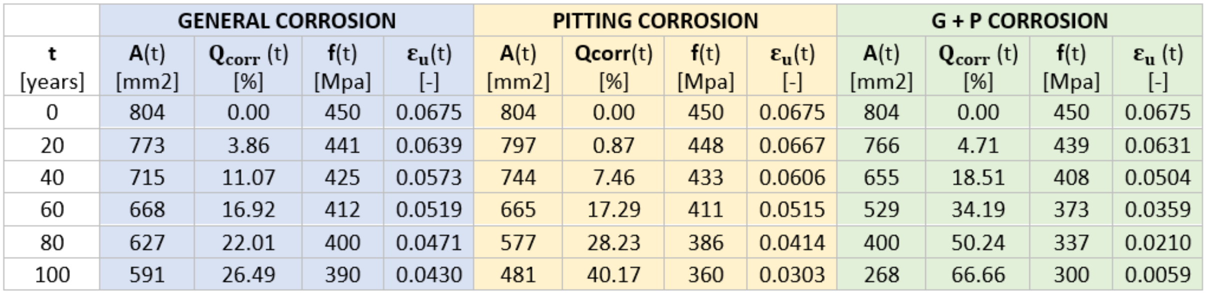

	GENERAL CORROSION				**PITTING CORROSION**				**G + P CORROSION**			
t [years]	**A**(t) [mm2]	**Q_{corr}** (t) [%]	**f**(t) [Mpa]	**ε_u**(t) [-]	**A**(t) [mm2]	**Qcorr**(t) [%]	**f**(t) [Mpa]	**ε_u**(t) [-]	**A**(t) [mm2]	**Q_{corr}** (t) [%]	**f**(t) [Mpa]	**ε_u** (t) [-]
0	804	0.00	450	0.0675	804	0.00	450	0.0675	804	0.00	450	0.0675
20	773	3.86	441	0.0639	797	0.87	448	0.0667	766	4.71	439	0.0631
40	715	11.07	425	0.0573	744	7.46	433	0.0606	655	18.51	408	0.0504
60	668	16.92	412	0.0519	665	17.29	411	0.0515	529	34.19	373	0.0359
80	627	22.01	400	0.0471	577	28.23	386	0.0414	400	50.24	337	0.0210
100	591	26.49	390	0.0430	481	40.17	360	0.0303	268	66.66	300	0.0059

Table 5.1: Interaction domain input parameters (De Gaetano, 2019).

In order to take into account the effect of bond strength degradation the following hypothesis was done. It is assumed that the initial bond strength in the undamaged state is the one that, taking into account the anchorage length or the lap splice of the rebars, is able to bond the rebar working at the yield strength. In fact, this can be considered as an optimum design of the anchorage or lap length of the rebar. Due to the degradation of the bond strength with increasing corrosion, the yield strength in the rebar can not be anymore accommodated by the rebar. According to equations 2.9 and 2.10 and not taking into account the reduction in the geometrical dimensions of the rebar because of the corrosion, we can assume that the percentage reduction in the bond strength is the same in the maximum tensile strength that the reinforcing steel can develop. Therefore, as the bond strength starts to degradate it is assumed that the maximum steel strength start to decrease, impeding the material to reach the yielding point and to exhibit its plastic behaviour. So, the same decrement that undergo the bond strength has been considered for the steel yield strength.

The percentages of reduction applied per each section and corrosion type in time are reported in Table 5.2. Figures 5.2-5.25 show the interaction domains for cross sections A and B at 0, 20, 40, 60, 80 and 100 years. Each figure that represents the variation of the domain in time, taking into account the bond deterioration, has been compared with the results obtained from the previous study based only on the effect of steel rebars area loss (De Gaetano, 2019).

The new domains obtained show that the decrease in adherence strongly affects the structural capacity of the pier. Comparing the resistant domains obtained whit the ones of the previous study, a substantial reduction can be observed in the ones where the bond strength deterioration is considered. So, this effect cannot be neglected in the computation of the strength capacity. Section Ax and By are in both cases the ones that undergo to early failure. The results obtained considering bond deterioration effect show that section Ax, in the cases of general and pitting corrosion, is not able to reach 60 years of service life and not even 40 years if the two corrosion effects act simultaneously. While, it undergoes early failure only in the case of general + pitting corrosion attack (80 years), if only the steel area loss effect is taken into account. As it is possible to see from the plots, section By is not able to reach 40 years of service life in all the corrosion cases analysed. While, if the bond strength reduction is not considered, it can reaches 80 and 70 years of service life in the cases of general and pitting corrosion respectively, and 40 years in the case of the two corrosion types combined attack.

Comparing the new diagrams obtained with the ones of the previous research it is possible to note many differences. The domains where the effect of bond deterioration is considered, undergo a reduction in time that is not proportional as the ones where only the area loss is taken into account. This is explicable observing the trend of steel cross-section and bond strength in time (Figures 4.10-4.21). In the study of De Gaetano (2019), the domains input parameters that have been modified are the steel cross section, the steel yield strength and the steel ultimate strain, and all of them are subjected to a proportional decrease in time, as it is possible to see in Table 5.1. In order to consider the bond degradation the steel yield strength has been subjected to the same reduction that the bond strength undergoes. The way it decreases depends on the bond strength-slip plot, that shows how after a certain value of slip (high level of degradation), the bond strength assumes a constant value equal to the residual bond strength. In this study, where the corrosion of stirrups has been considered too, the value of the bond strength for high level of corrosion is not constant but undergoes a small decrease. That is why it is possible to observe that domains undergo a stronger reduction during the first decades (low corrosion level), while reduce more slowly when an high level of corrosion is reached.

Moreover, it is possible to observe that the reduction of resistant domains differs for the different section considered (Ax, Ay, Bx, By). In fact, the percentage reduction of steel yield strength is different for each one because is the same decrement that the bond strength undergoes. This is related to the amount of longitudinal and transversal reinforcement in the splitting surface, that vary for each section.

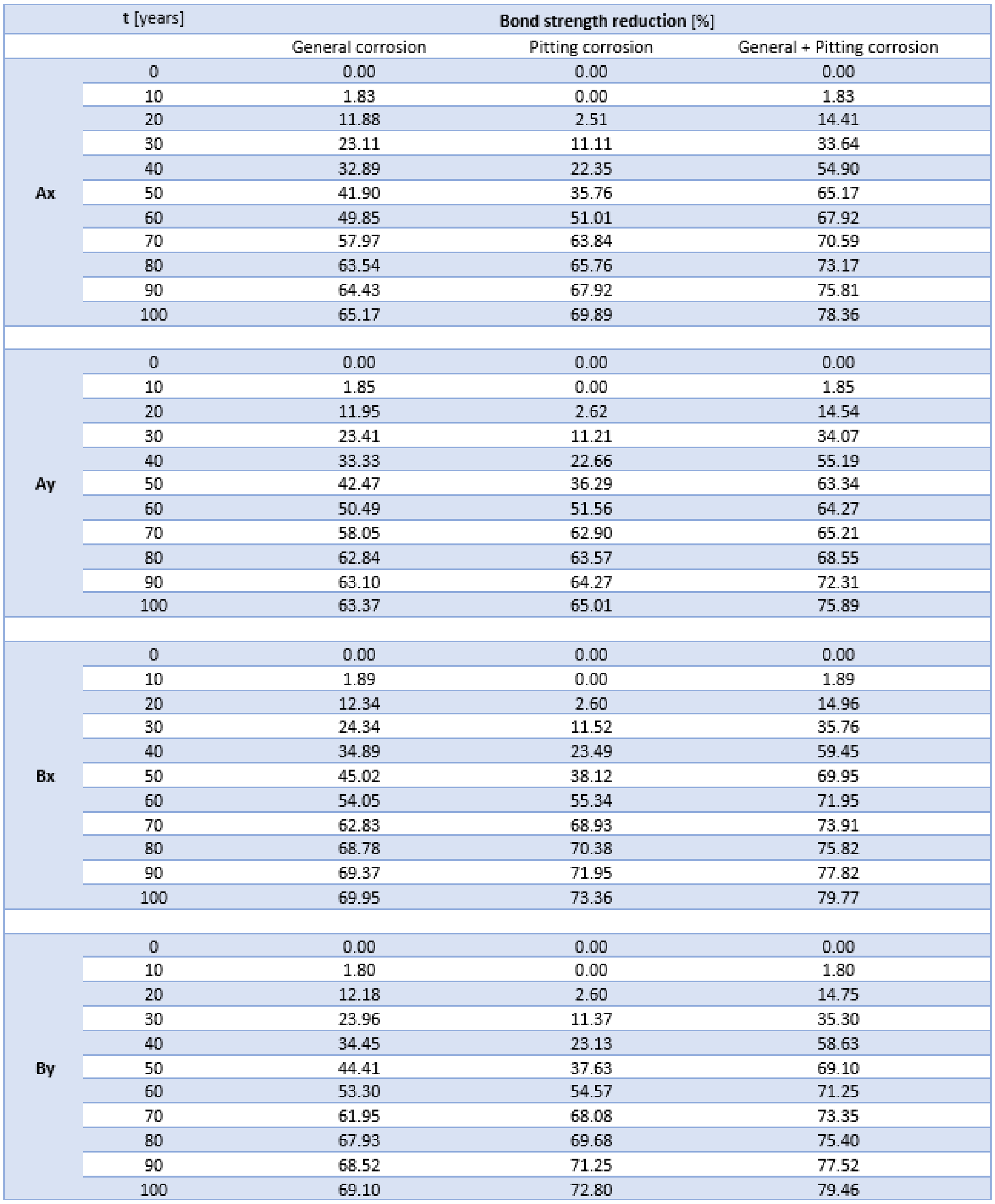

	t [years]	Bond strength reduction [%]		
		General corrosion	Pitting corrosion	General + Pitting corrosion
Ax	0	0.00	0.00	0.00
	10	1.83	0.00	1.83
	20	11.88	2.51	14.41
	30	23.11	11.11	33.64
	40	32.89	22.35	54.90
	50	41.90	35.76	65.17
	60	49.85	51.01	67.92
	70	57.97	63.84	70.59
	80	63.54	65.76	73.17
	90	64.43	67.92	75.81
	100	65.17	69.89	78.36
Ay	0	0.00	0.00	0.00
	10	1.85	0.00	1.85
	20	11.95	2.62	14.54
	30	23.41	11.21	34.07
	40	33.33	22.66	55.19
	50	42.47	36.29	63.34
	60	50.49	51.56	64.27
	70	58.05	62.90	65.21
	80	62.84	63.57	68.55
	90	63.10	64.27	72.31
	100	63.37	65.01	75.89
Bx	0	0.00	0.00	0.00
	10	1.89	0.00	1.89
	20	12.34	2.60	14.96
	30	24.34	11.52	35.76
	40	34.89	23.49	59.45
	50	45.02	38.12	69.95
	60	54.05	55.34	71.95
	70	62.83	68.93	73.91
	80	68.78	70.38	75.82
	90	69.37	71.95	77.82
	100	69.95	73.36	79.77
By	0	0.00	0.00	0.00
	10	1.80	0.00	1.80
	20	12.18	2.60	14.75
	30	23.96	11.37	35.30
	40	34.45	23.13	58.63
	50	44.41	37.63	69.10
	60	53.30	54.57	71.25
	70	61.95	68.08	73.35
	80	67.93	69.68	75.40
	90	68.52	71.25	77.52
	100	69.10	72.80	79.46

Table 5.2: Bond strength reduction for general, pitting and G+P corrosion.

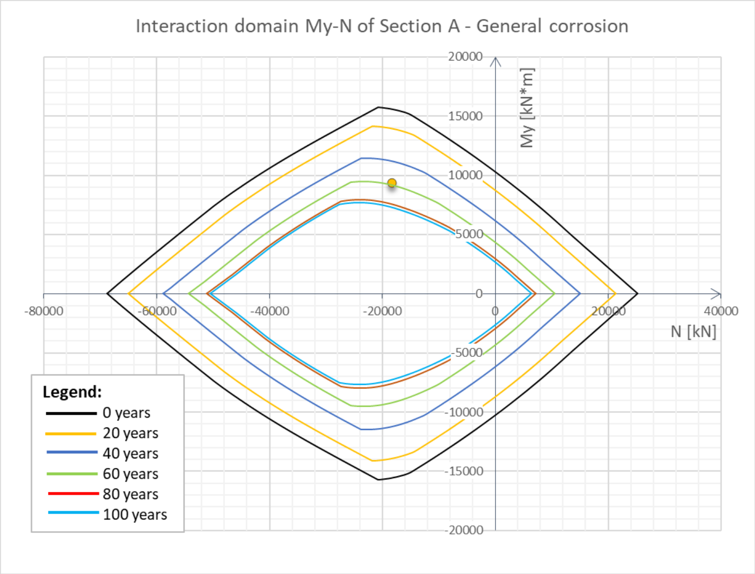

Figure 5.2: Interaction domain My-N of section A due to general corrosion, including bond reduction effect.

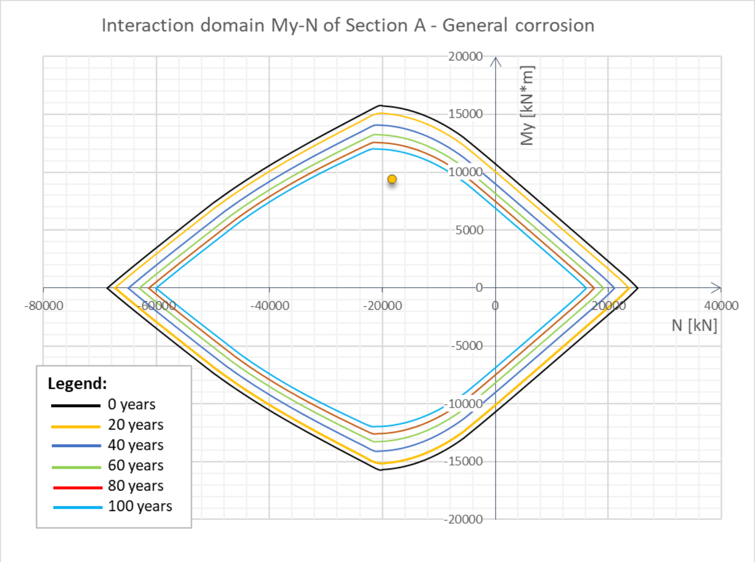

Figure 5.3: Interaction domain My-N of section A due to general corrosion (De Gaetano, 2019).

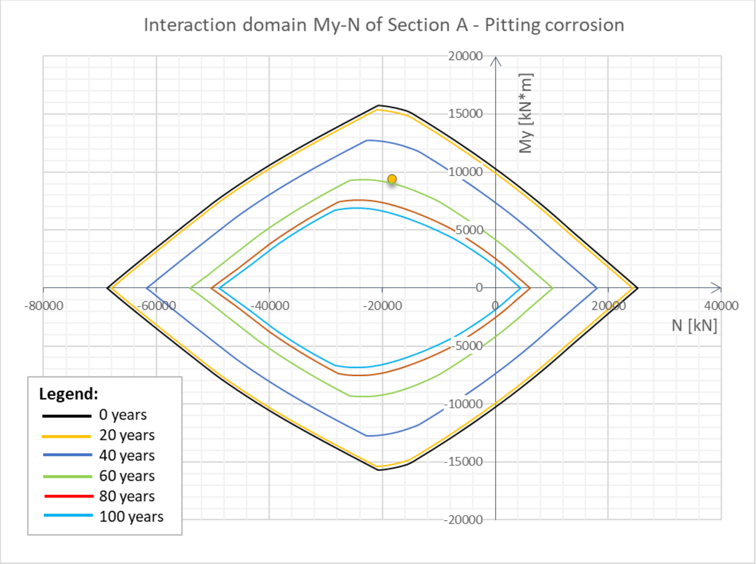

Figure 5.4: Interaction domain My-N of section A due to pitting corrosion, including bond reduction effect.

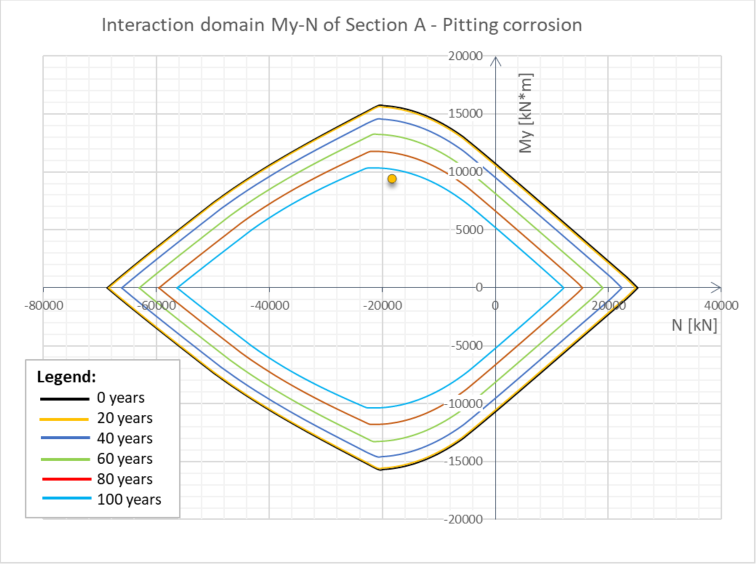

Figure 5.5: Interaction domain My-N of section A due to pitting corrosion (De Gaetano, 2019).

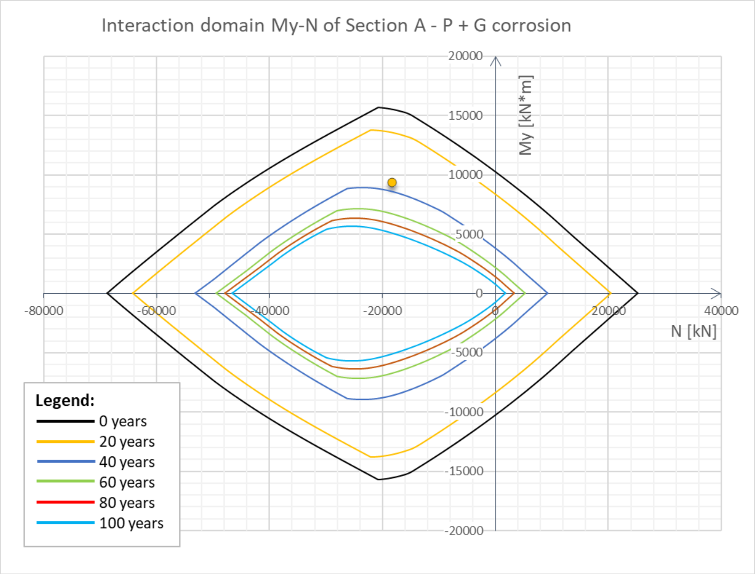

Figure 5.6: Interaction domain My-N of section A due to general and pitting corrosion, including bond reduction effect.

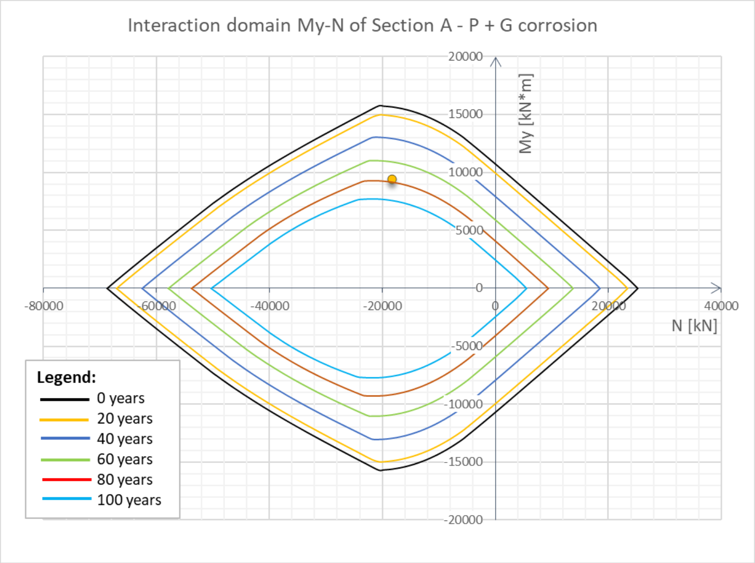

Figure 5.7: Interaction domain My-N of section A due to general and pitting corrosion (De Gaetano, 2019).

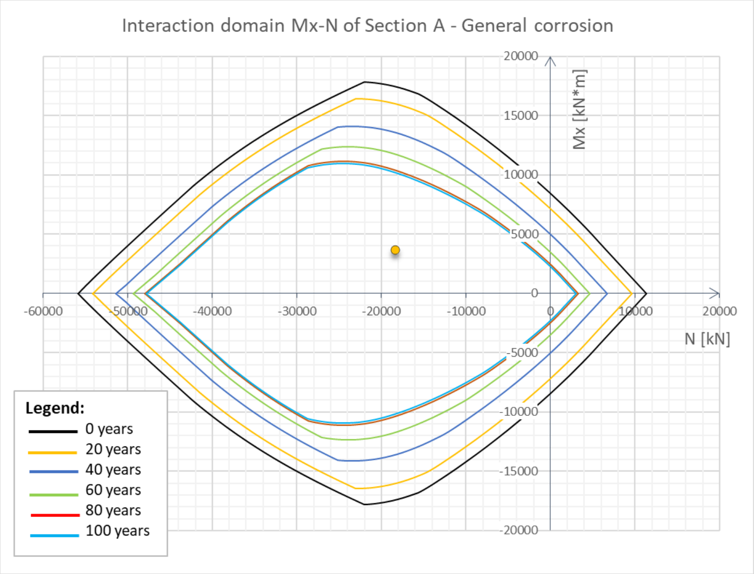

Figure 5.8: Interaction domain Mx-N of section A due to general corrosion, including bond reduction effect.

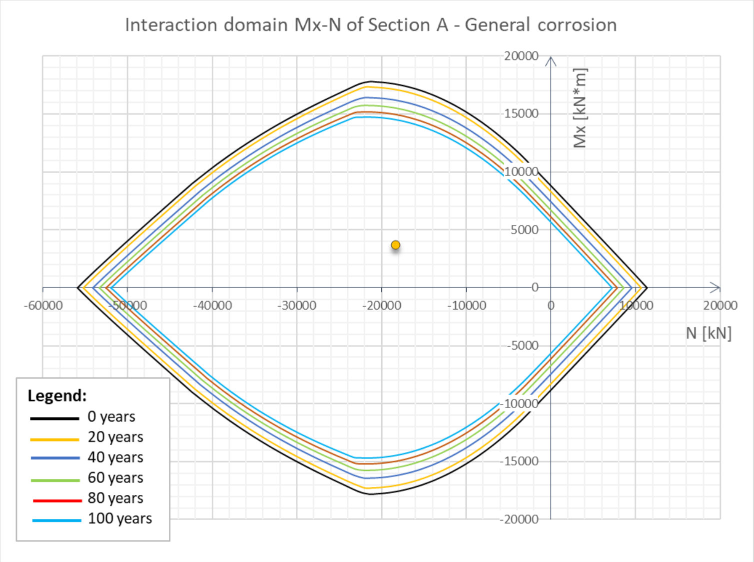

Figure 5.9: Interaction domain Mx-N of section A due to general corrosion (De Gaetano, 2019).

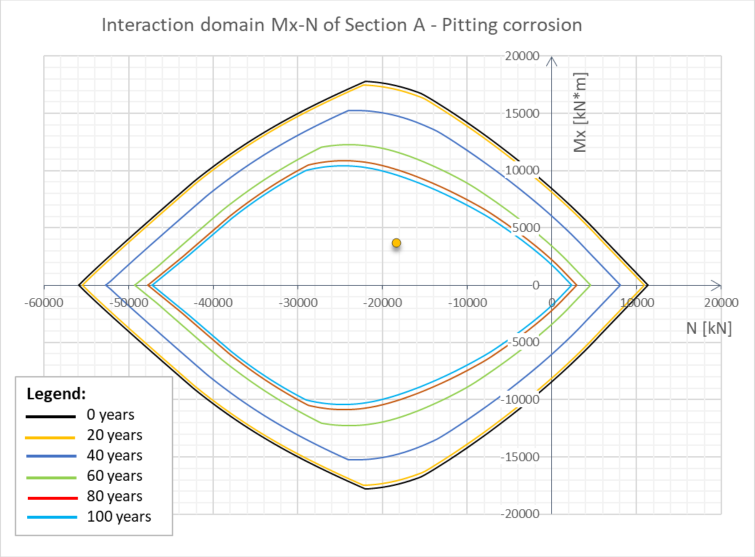

Figure 5.10: Interaction domain Mx-N of section A due to pitting corrosion, including bond reduction effect.

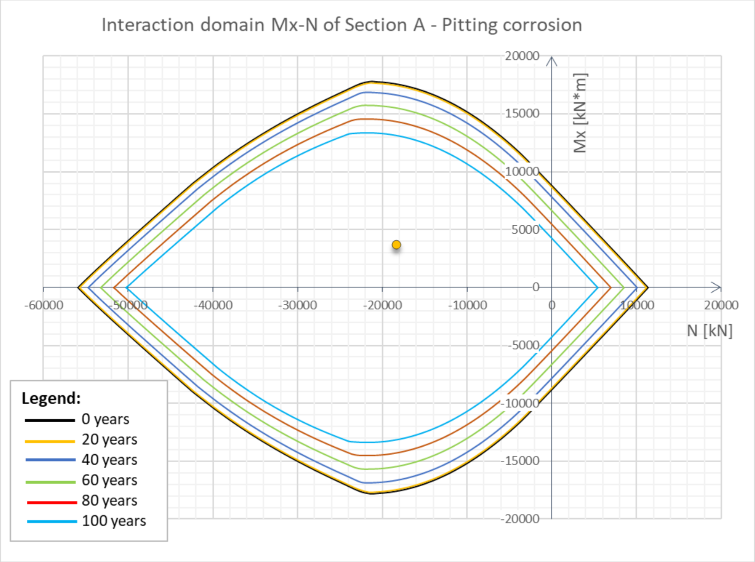

Figure 5.11: Interaction domain Mx-N of section A due to pitting corrosion (De Gaetano, 2019).

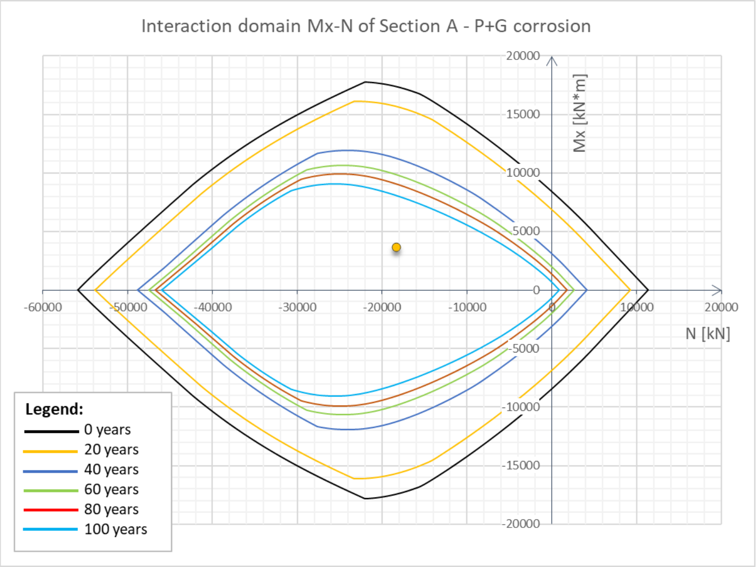

Figure 5.12: Interaction domain Mx-N of section A due to general and pitting corrosion, including bond reduction effect.

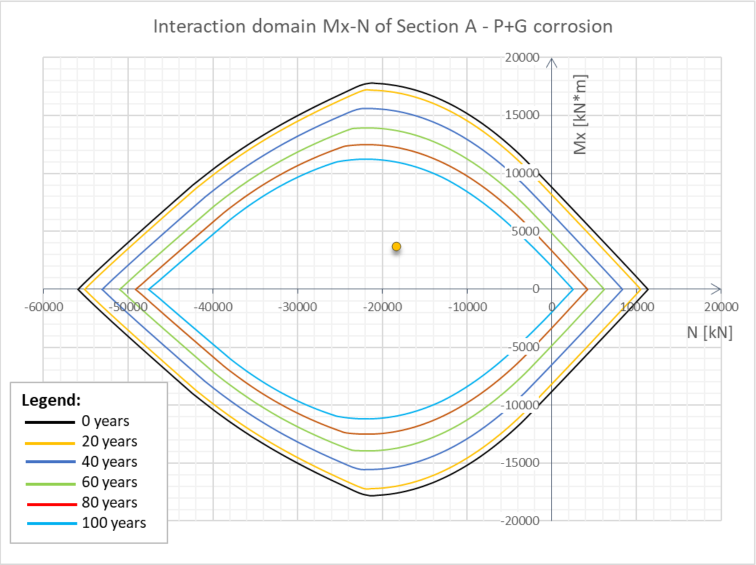

Figure 5.13: Interaction domain Mx-N of section A due to general and pitting corrosion (De Gaetano, 2019).

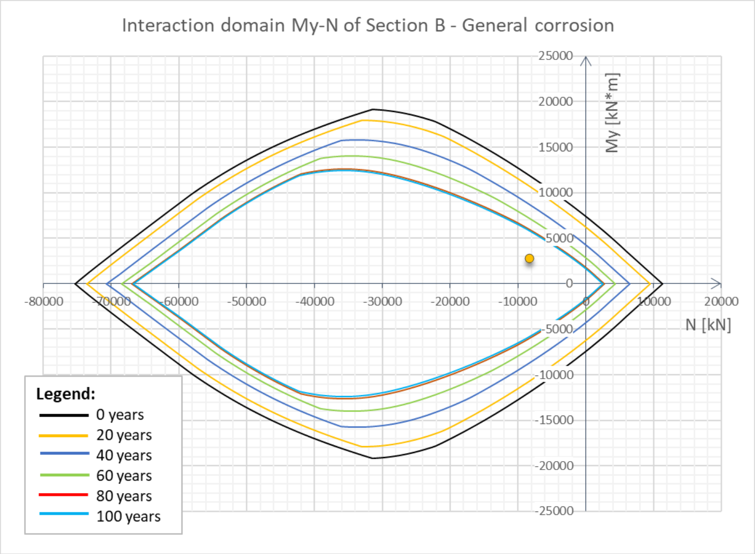

Figure 5.14: Interaction domain My-N of section B due to general corrosion, including bond reduction effect.

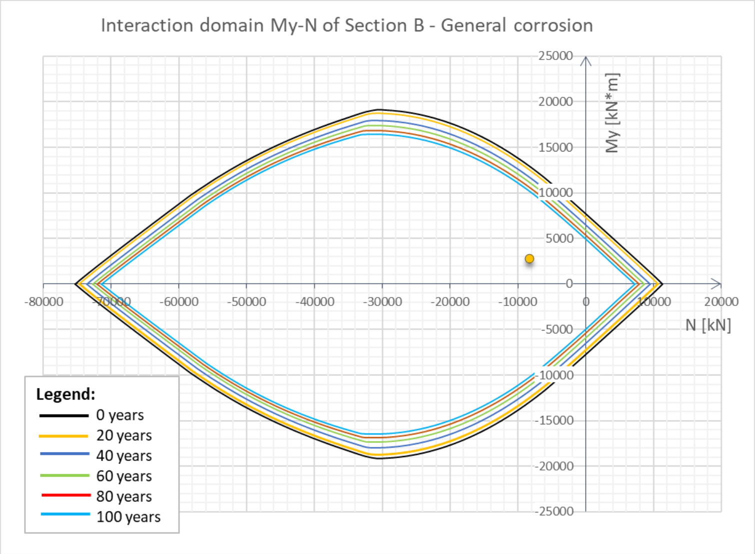

Figure 5.15: Interaction domain My-N of section B due to general corrosion (De Gaetano, 2019).

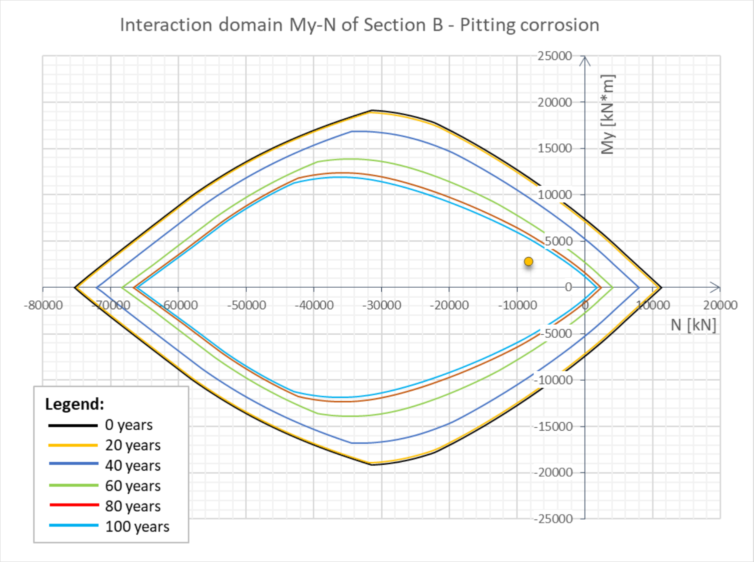

Figure 5.16: Interaction domain My-N of section B due to pitting corrosion, including bond reduction effect.

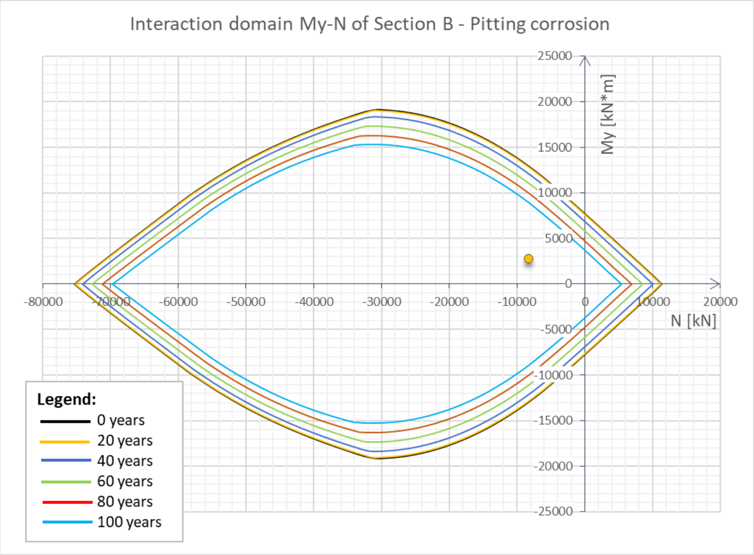

Figure 5.17: Interaction domain My-N of section B due to pitting corrosion (De Gaetano, 2019).

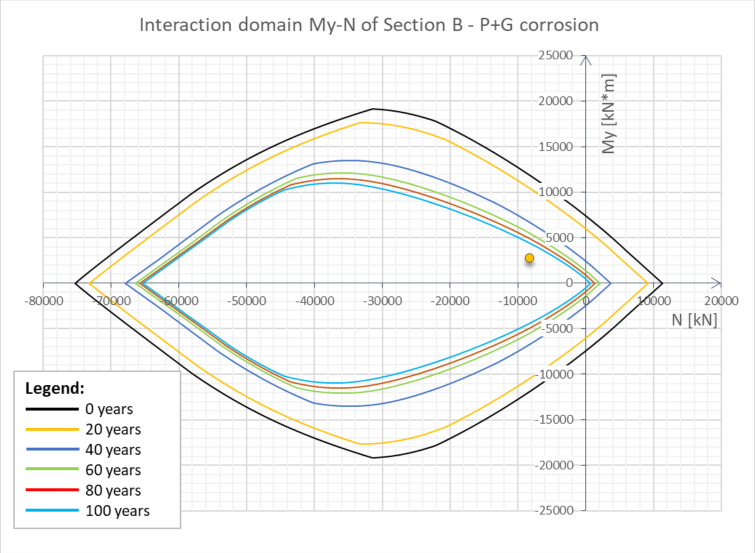

Figure 5.18: Interaction domain My-N of section B due to general and pitting corrosion, including bond reduction effect.

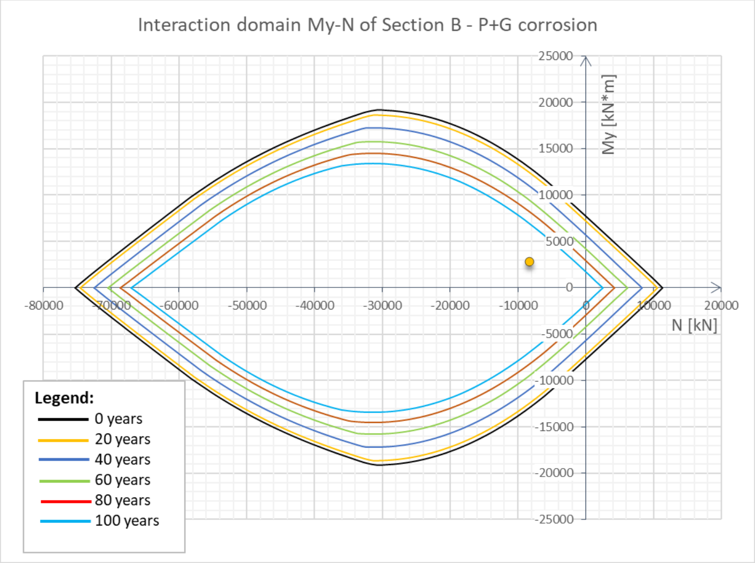

Figure 5.19: Interaction domain My-N of section B due to general and pitting corrosion (De Gaetano, 2019).

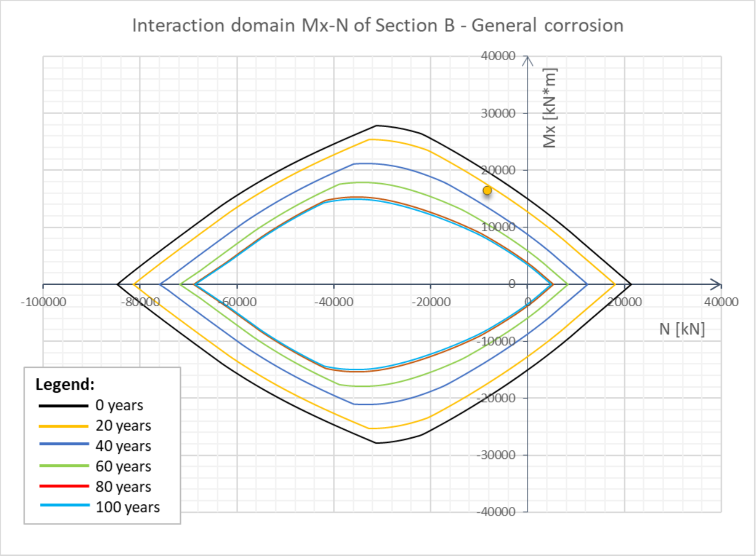

Figure 5.20: Interaction domain Mx-N of section B due to general corrosion, including bond reduction effect.

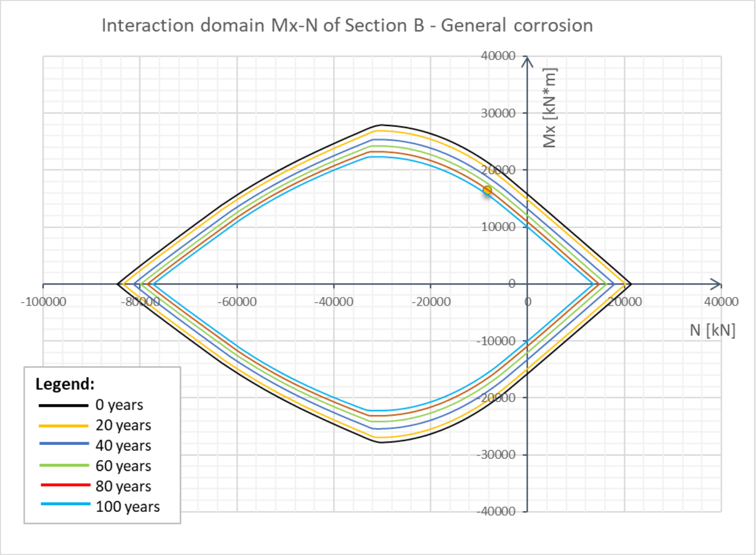

Figure 5.21: Interaction domain Mx-N of section B due to general corrosion (De Gaetano, 2019).

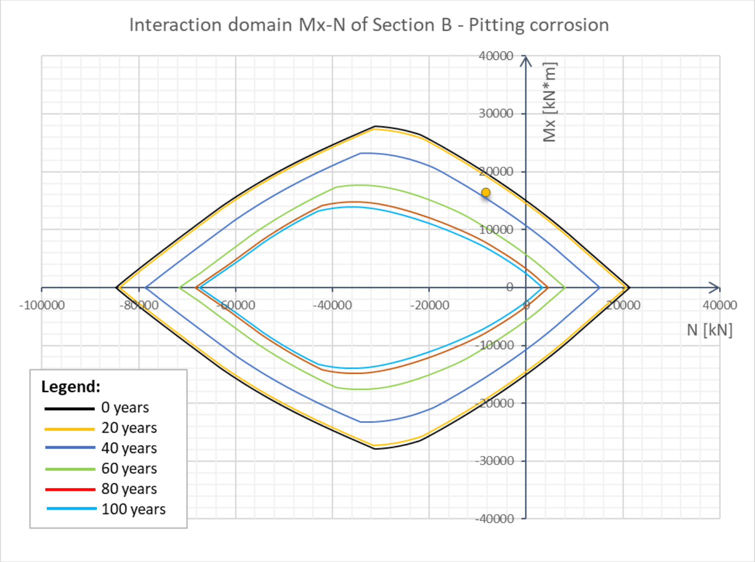

Figure 5.22: Interaction domain Mx-N of section B due to pitting corrosion, including bond reduction effect.

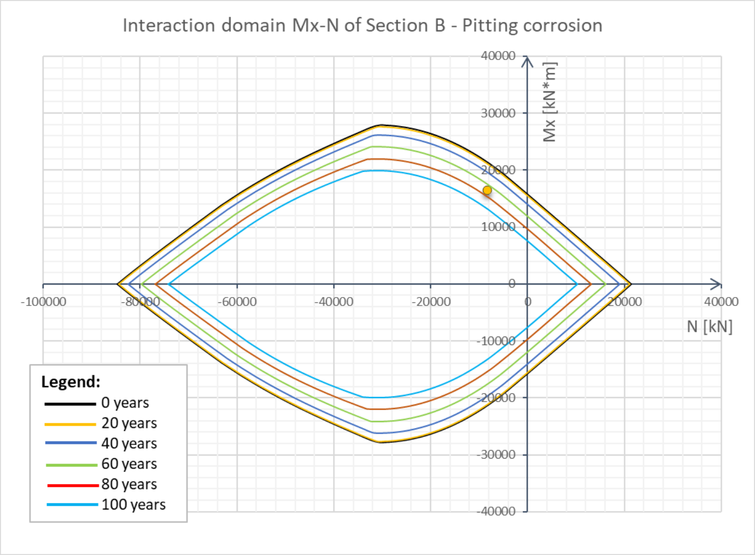

Figure 5.23: Interaction domain Mx-N of section B due to pitting corrosion (De Gaetano, 2019).

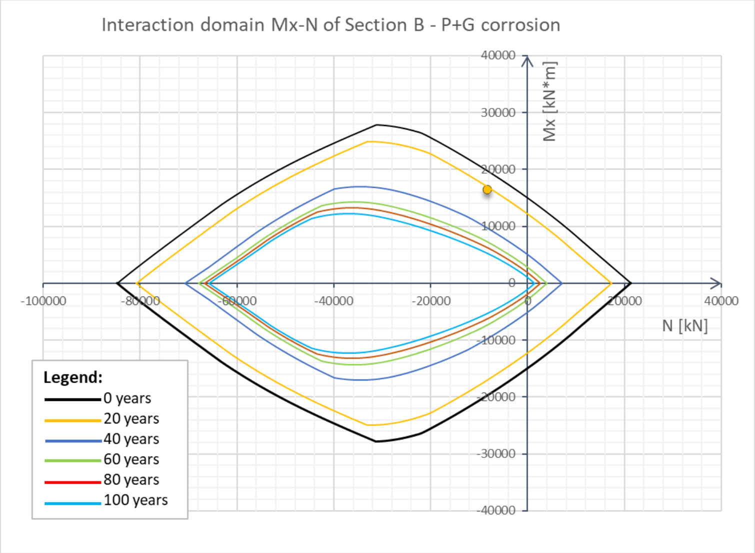

Figure 5.24: Interaction domain Mx-N of section B due to general and pitting corrosion, including bond reduction effect.

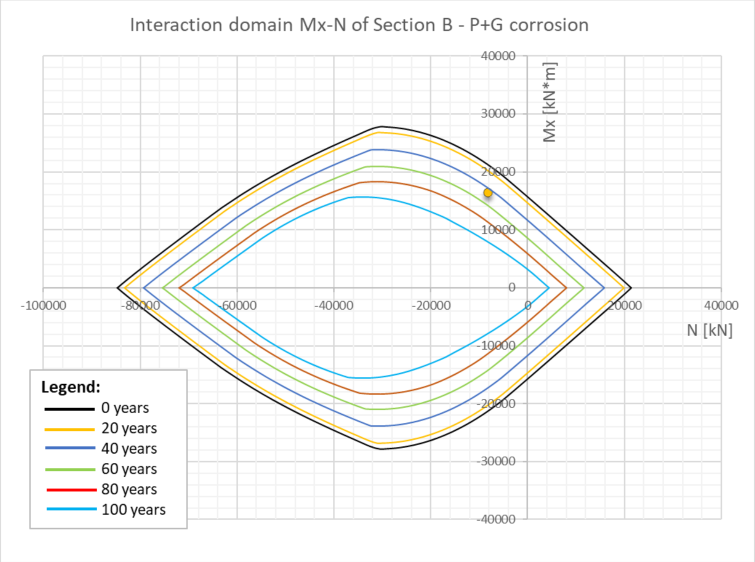

Figure 5.25: Interaction domain Mx-N of section B due to general and pitting corrosion (De Gaetano, 2019).

Bresler's domain is used to evaluate the strength of an element subjected to biaxial bending and axial load. The 2D plot is obtained for a fixed value of axial load (maximum load acting on the section) and presents on the axis the resistant moments in y and x directions.

The resistant domain is strongly reduced if the effect of bond deterioration is considered. Figures 5.26-5.31 show the graphs where the domains obtained from the study of De Gaetano, 2019 (100 years NB= no bonding effect) and of this research have been compared. The black line represents the domain of the no corroded section. The grey and the coloured ones represent the resistant domains after 100 years, considering the area loss effect and the area loss and bond strength reduction effects respectively. As done for the interaction domains, Bresler's domains have been constructed for section A and B and for the three corrosion cases.

Early failure of section A is expected when subjected to all different types of corrosion if the degradation of bond strength is considered, while it occurs only in the case of pitting and general corrosion acting simultaneously if only steel area loss effect is taken into account. Differently, the results forecast the failure section B for any corrosion attack typology in both the researches developed.

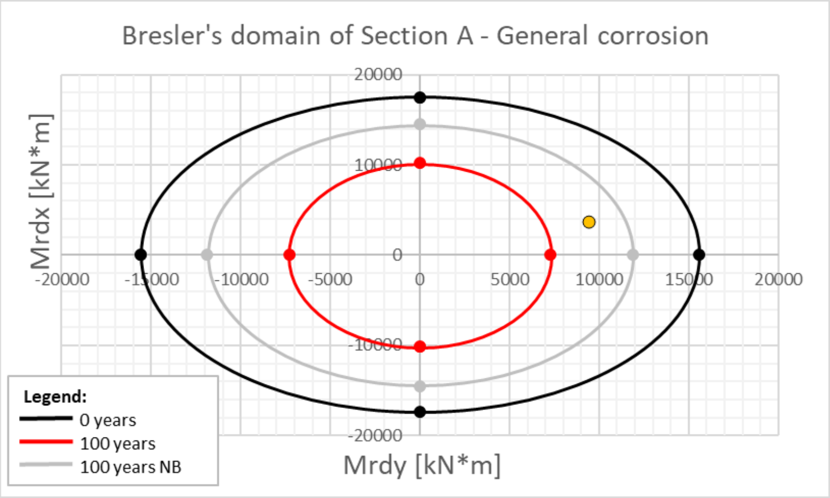

Figure 5.26: Bresler's domain of section A due to general corrosion.

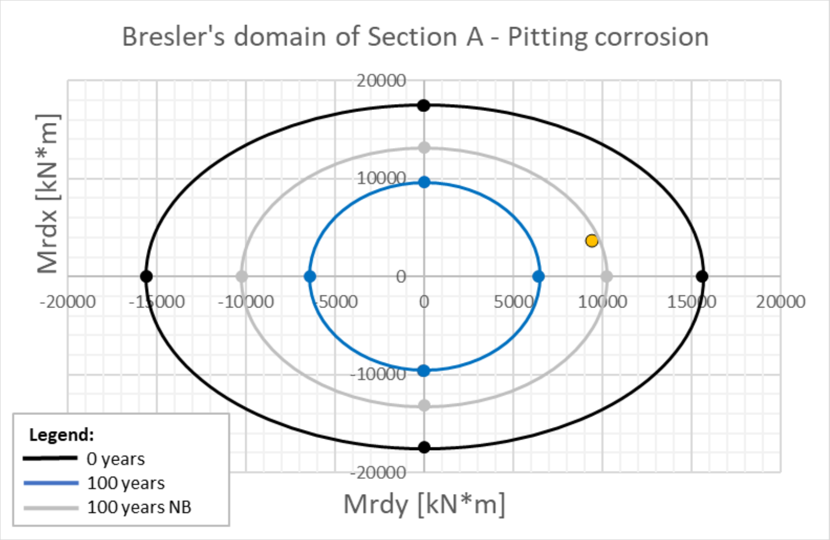

Figure 5.27: Bresler's domain of section A due to pitting corrosion.

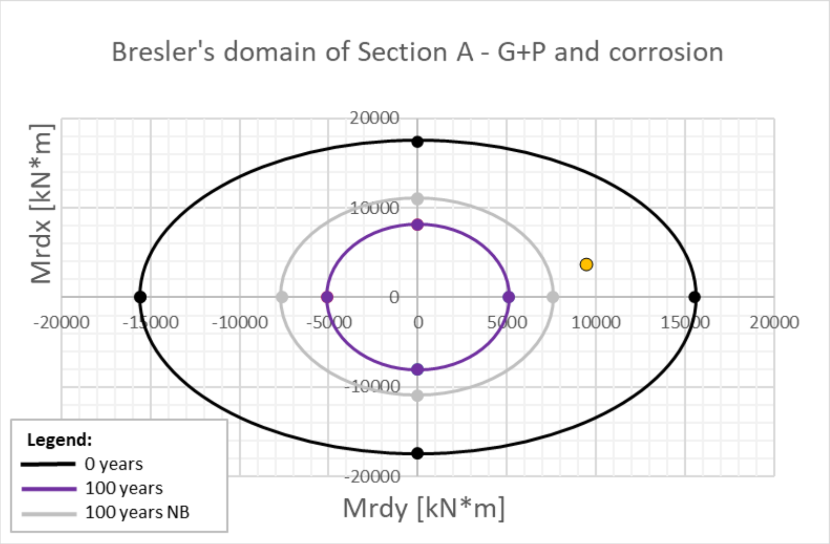

Figure 5.28: Bresler's domain of section A due to general and pitting corrosion.

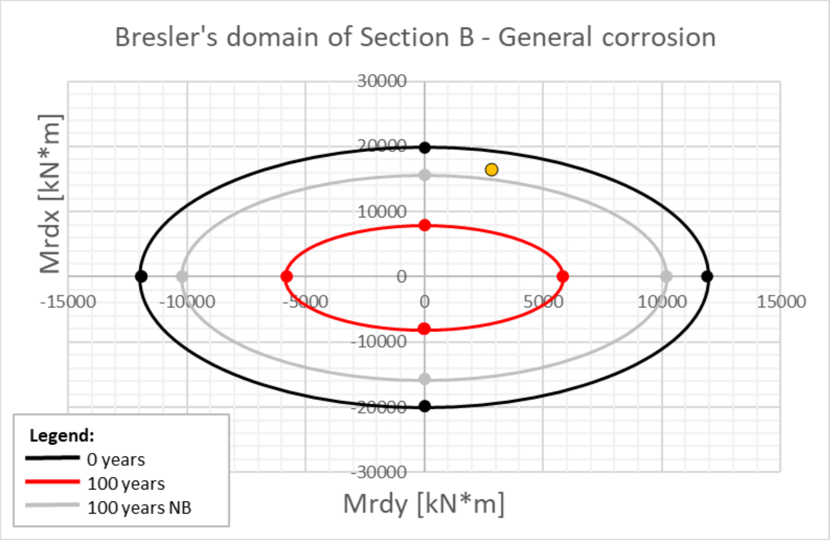

Figure 5.29: Bresler's domain of section B due to general corrosion.

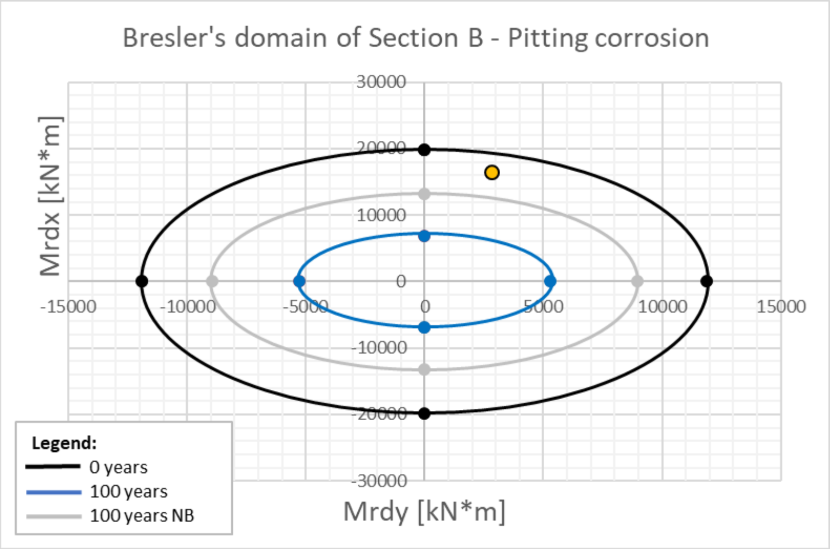

Figure 5.30: Bresler's domain of section B due to pitting corrosion.

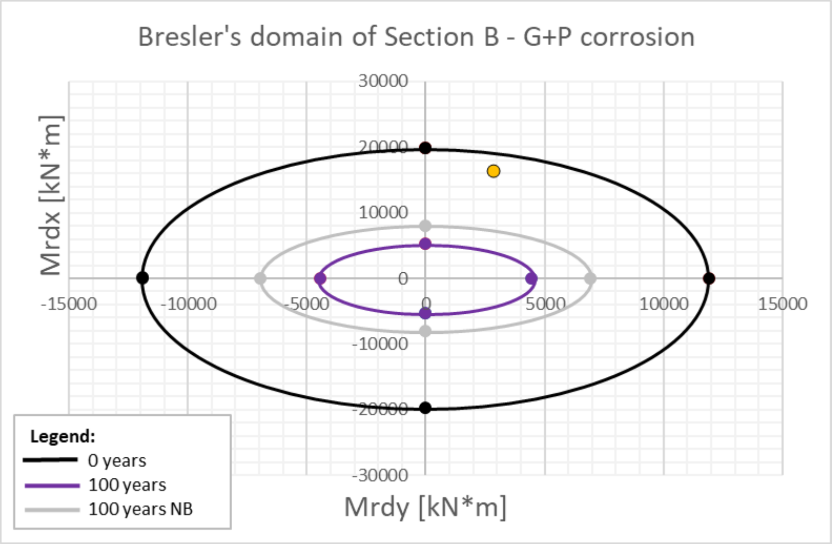

Figure 5.31: Bresler's domain of section B due to general and pitting corrosion.

5.2 Moment-Curvature Diagrams

It is important to know how the ductility of the pier changes in time and an useful tool to have this information is the Moment-curvature diagram. It represents the variation of resistant moment with respect to curvature and it is computed for a specific value of axial load. In seismic design ductility is considered a fundamental property of structural elements. It is an indicator of the capability to reach high level of deformation before the failure, avoiding sudden collapse of the structure and allowing to intervene in advance. Through the moment-curvature diagram it is possible to estimate the curvature ductility of a reinforced concrete section, that is defined as:

$$\mu_\phi = \phi_u/\phi_y$$

- ϕ_u : ultimate curvature
- ϕ_y : yield curvature

The curvature ductility is influenced by several factors and the main are:

- Axial force
- Tensile and compressive reinforcement ratios
- Concrete and steel material ductility

The ductility of a reinforced concrete section depends on materials ductility, that is their capability of dissipating energy through plastic deformation. In a RC element this property is mainly due to the steel, that is characterized by high plastic deformation capacity. Moreover, it undergoes a consistent decrement with the increase of the axial load. For what concern the steel reinforcement, an higher amount in the tensed part decreases the ductility, while more steel in compression increases it.

In order to understand how corrosion affects this property, moment-curvature diagrams have been plotted for Section A of the bridge pier object of study, for different years. The graphs have been built first considering only the effect of steel area loss and then, summing to it the effect of the bond strength reduction. In the first case it is possible to observe that the curvature ductility increases and that the resistant moment decreases with time. In fact, the yield curvature undergoes a decrement, because of the decreasing effect of deterioration on the steel yield strength and so, also on the steel yield deformation. The slight increase of the ultimate curvature is explicable whit the decrease of the amount of steel in the section in time (Figure 5.32, 5.34, 5.36). Points in the plots highlight the steel yielding point and the failure point.

Then, the diagrams representing the case of section affected by steel area loss and bond deterioration have been plotted (Figure 5.33, 5.35, 5.37). It is possible to understand that with time the ductility is lost and the section exhibits a fragile behaviour. Even after 20 years the yield curvature is not reached. That is because it is supposed that the steel yield strength decreases proportionally to the bond strength and that the perfect bond condition corresponds to the maximum yield stress. Anyway, during the first years the steel yield strength is not reduced and the material can still reach the yielding point. This is due to the fact that the aggressive agents need some time to reach the steel rebars and to make the corrosion process to start (propagation phase).

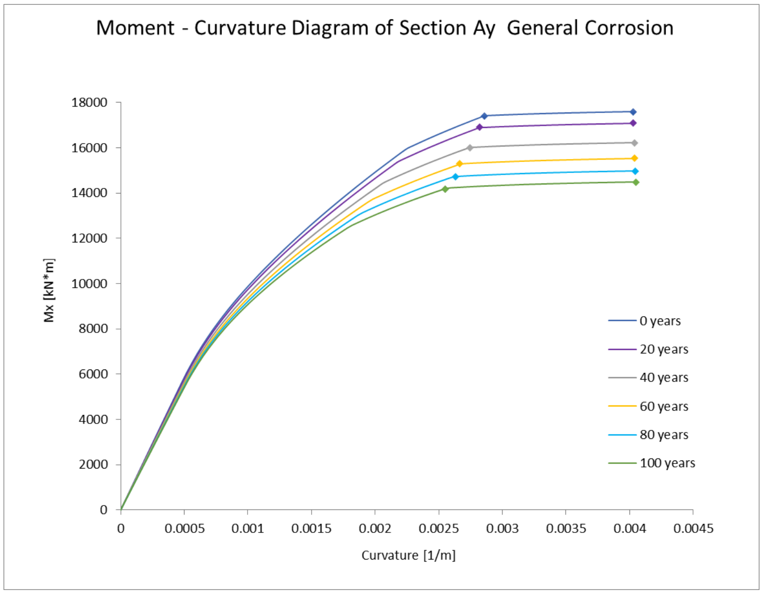

Figure 5.32: Moment-Curvature diagram for Section Ay due to general corrosion (Steel area loss effect).

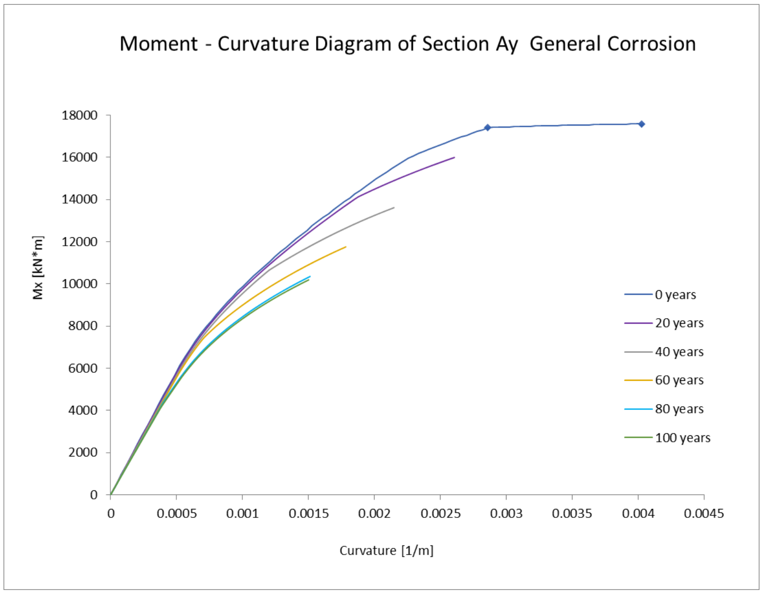

Figure 5.33: Moment-Curvature diagram for Section Ay due to general corrosion (Steel area loss and bond strength reduction effects).

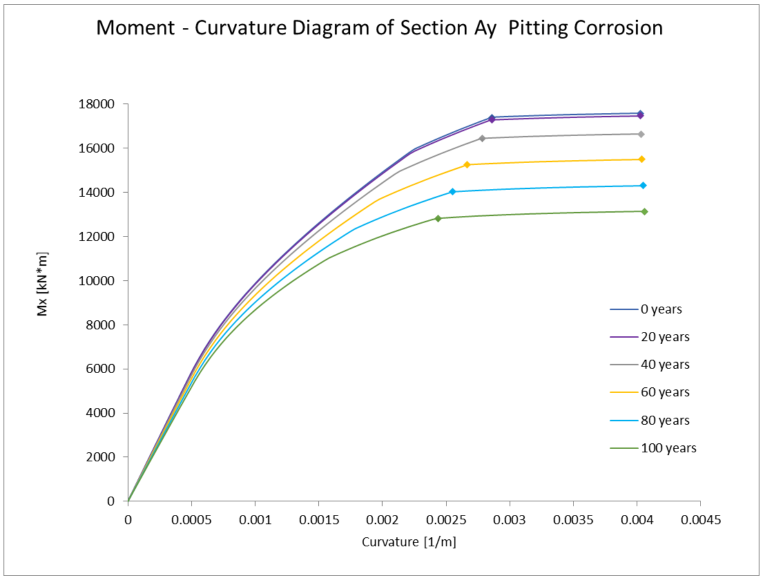

Figure 5.34: Moment-Curvature diagram for Section Ay due to pitting corrosion (Steel area loss effect).

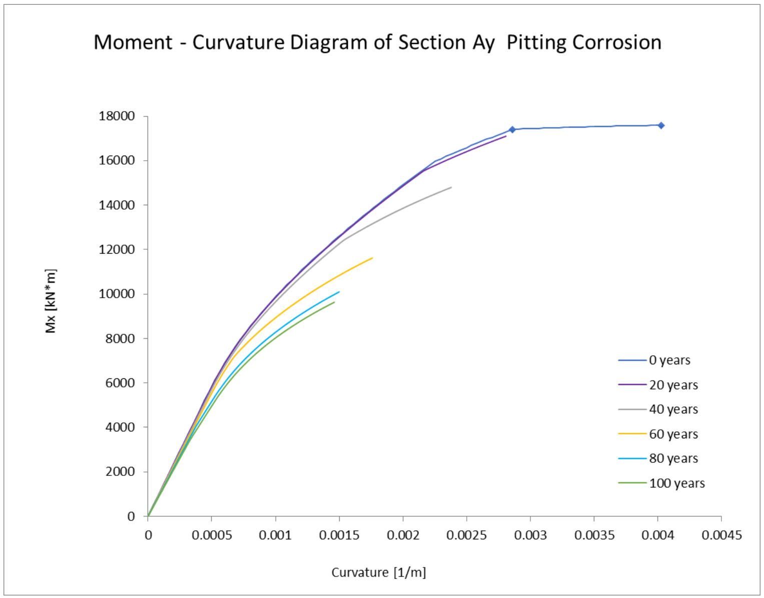

Figure 5.35: Moment-Curvature diagram for Section Ay due to pitting corrosion (Steel area loss and bond strength reduction effects).

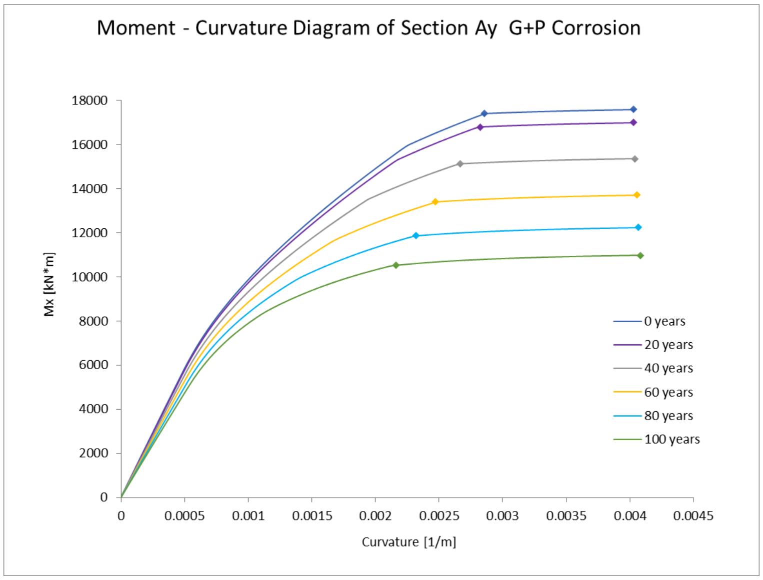

Figure 5.36: Moment-Curvature diagram for Section Ay due to G+P corrosion (Steel area loss effect).

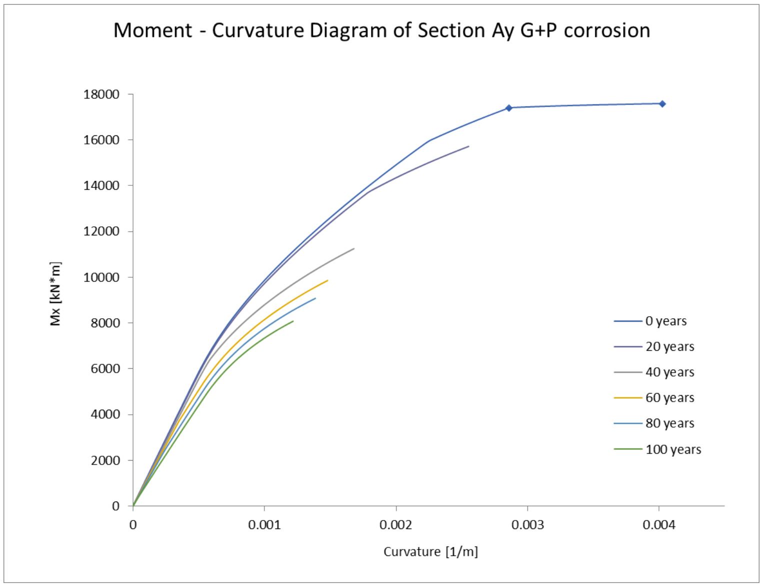

Figure 5.37: Moment-Curvature diagram for Section Ay due to G+P corrosion (Steel area loss and bond strength reduction effects).

Chapter 6

Corrosion protection methods

The aim of all protection methods is to delay as much as possible the beginning of the corrosion phenomenon. In fact, it is impossible to avoid it and what can be done is extending the structure service life through different types of design and interventions. For service life is intended the time during which the structure maintains its initial stability, functional and safety requirements without the need of maintenance. Tuutti's Model is commonly used to predict it and to represent the degradation of reinforced concrete structures (Figure 6.1).

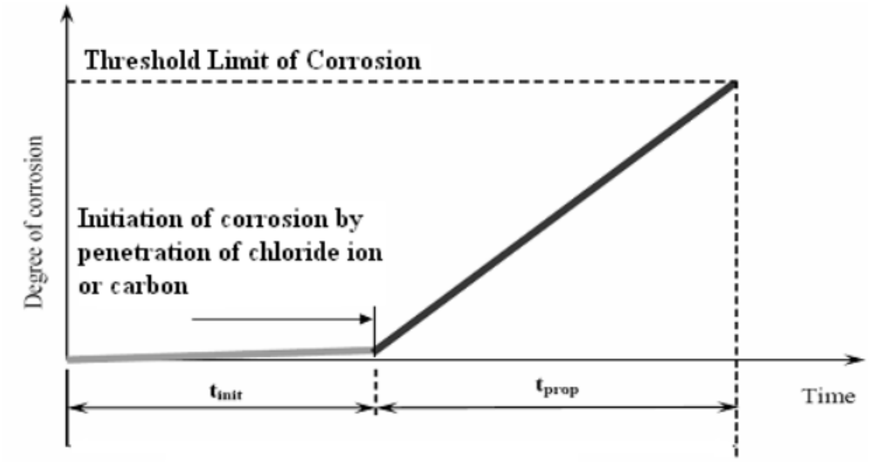

Figure 6.1: Tuutti's service life model (Tuutti, 1982).

In this model the service life is divided in two parts: the initiation and the propagation phases. The first one represents the time that carbon dioxide or chloride ions need to enter in the structure and reach steel rebars. The second phase is in between the beginning of the corrosion process and the cracking of the concrete. The first one is influenced by the concrete cover depth, concrete quality (water/cement ratio, curing time and cement type) and environmental factors (temperature, humidity and CO_2 and Cl^- ions concentration). The propagation is influenced by the presence of oxygen and water, concrete quality, pH of pore water, temperature and moisture content and resistivity of concrete (Bohni, 2005).

Table 6.1 reports a list of corrosion protection methods with related advantages and disadvantages, then a more detailed review is presented.

The typology of intervention changes in the case of new or existing construction. The main protective methods for the two cases are showed in Figure 6.2.

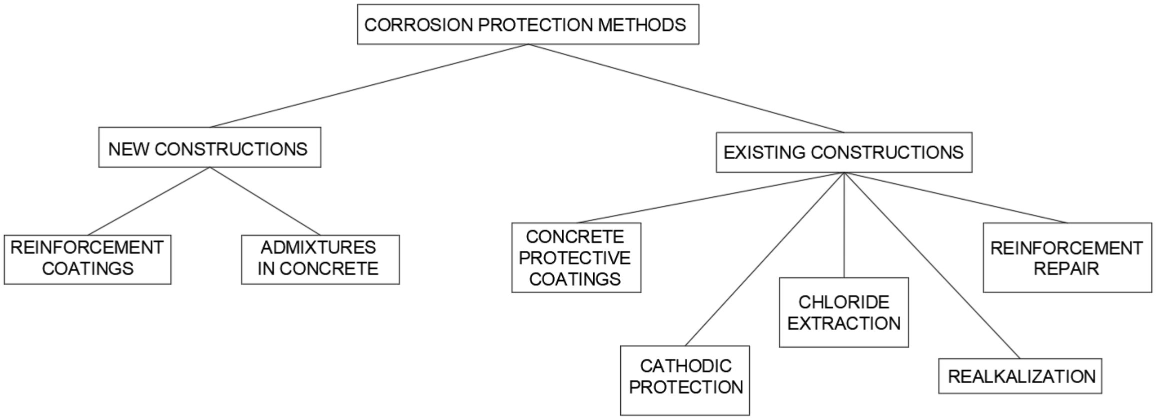

Figure 6.2: Summary of the main corrosion protective methods for RC structures.

6.1 Corrosion control in new RC structures

In order to build a structure provided of high corrosion resistance, first of all it is necessary to take precise design precautions. It is important to avoid the contact between two different metal and an efficient water drainage system is fundamental to prevent the stagnation of water that promotes the entrance of aggressive agents in the concrete. Moreover, the quality of the materials play an important role in the resistance of the structure to degradation. Higher is the quality of concrete and more difficult is for corrosion agents to enter and reach the steel rebars, de-passivating them.

The main protective methods used in new constructions are:

- Reinforcement coatings
- Admixture in concrete

Method	Advantage	Disadvantage
Increase the concrete cover of the reinforcement	• Costs • Handling (easy to realise) • Experience • Eventually higher critical chloride content for corrosion	• There are limits for the increase • Reduces the static height
Use of tighter (less porous) concrete	• Costs • Handling (partly) • Experience (partly)	• There are limits for the reduction of w/c ratio (workability) • Concrete remains, even at very low w/c ratios, a porous material • Low w/c ratios and mineral additions may not or may only slightly change the critical chloride content for corrosion. Some mineral addition may even reduce it.
Inhibitors as admixture for concrete	• Handling • Eventually a higher critical chloride content for corrosion	• Costs • Long-term efficiency and durability not proven
Surface protection systems	• Positive effect • Large variety of systems available • Appearance of the surface (colours) can be modified	• Costs • Handling (susceptibility to damages during work) • The efficiency has to be monitored • Need maintenance and repair modification of the appearance of the concrete surface
Zinc-coated steel	• Costs • Handling • Performance in carbonated concrete	• Limited efficiency and durability in highly chloride-contaminated concrete and in cracks • No or only a slight influence on the critical chloride content
Epoxy coated steel	• Costs • deliverability	• Handling on construction sites (susceptibility to damages during work) • Mixture between coated and ordinary (non-coated) reinforcement critical • Long term efficiency and durability not proven (delamination of the coating and corrosion underneath the coating) • No or only a slight influence on the critical chloride content
Stainless steel	• Handling • Higher critical chloride content for corrosion (dependent on the steel quality) • Mixture between stainless and ordinary reinforcement without any restriction or additional measures possible	• Costs • Restricted deliverability, availability, delivery forms, deadlines and amount of delivery • Experience
Cathodic protection	• Efficiency	• Costs • Handling (complicated) • Monitoring necessary
Waterproofing membranes	• Efficiency • Experience	• Costs • Handling (risk of damages) • Not always applicable

Table 6.1: Corrosion protection methods for reinfroced concrete structures (Bohni, 2005).

6.1.1 Reinforcement coatings

It consists in covering the steel rebar whit a corrosion resistant coating. It can be an organic coating, like epoxy coating (Figure 6.3), or metallic coating. This last type can be sacrificial or non-sacrificial. Zinc is an example of sacrificial metallic coating, in fact, having more negative potential then the steel, when the coating breaks it corrodes and continues to protect the reinforcement (anode). While, nickel and copper (noble metals) are used as non-sacrificial metallic coatings. They are characterized by high corrosion resistance but, in this case, the steel is protected only until the breaking of the coating (Virmani et al. 1998).

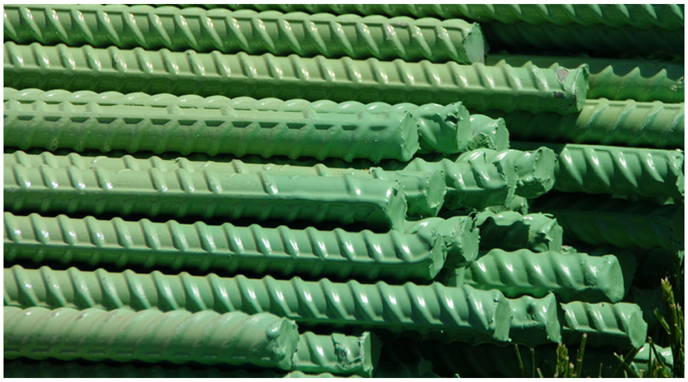

Figure 6.3: Epoxy-coated reinforcement rebar (National Precast Concrete Association).

6.1.2 Admixture in concrete

This method consists in the addition of substances in the concrete mix. These can be corrosion inhibitors, that are inorganic and organic chemicals whit the capability to increase the alkalinity of concrete. An alternative is the addiction of substances able to enhance the structural properties of concrete (silica fume, fly ash, slag...) that, basically, reduce the permeability of the material. The main types of corrosion inhibitors, categorized according to the mechanism of action, are:

- Anodic inhibitors
- Cathodic inhibitors
- Organic inhibitors

The fist ones passivate the steel creating a protective layer on the anodic surfaces and for the second type the film is formed on cathodic surfaces, while in the last case the protection is extended on the whole reinforcement surface (Virmani et al. 1998).

6.2 Corrosion control in existing RC structures

The most effective and used protective interventions against corrosion in existing structures are:

- Concrete protective coatings
- Cathodic protection
- Chloride extraction
- Realkalization
- Reinforcement repair

6.2.1 Concrete protective coatings

Coatings are applied on the concrete surface and the aim is to reduce the permeability of the material and the entrance of moisture and chlorides. It is fundamental to ensure the compatibility between the repair material and the concrete to avoid bond failures or unwanted chemical reactions. The installation requirements include specific characteristic of the concrete substrate and environmental conditions (ACI Commitee 546, 2004). In Table 6.2 the main types of surface treatments whit their characteristics and installation requirements are reported.

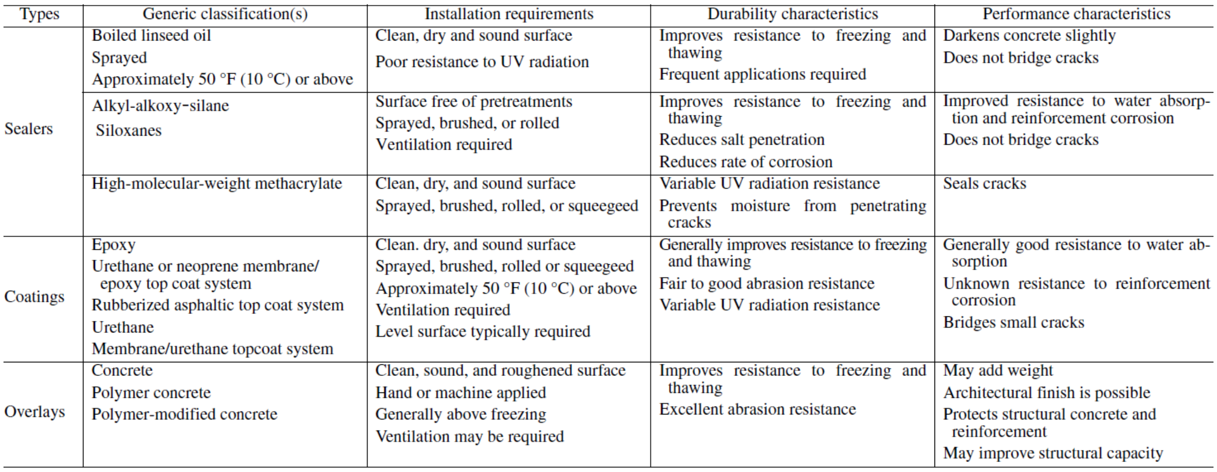

Types	Generic classification(s)	Installation requirements	Durability characteristics	Performance characteristics
Sealers	Boiled linseed oil Sprayed Approximately 50 °F (10 °C) or above	Clean, dry and sound surface Poor resistance to UV radiation	Improves resistance to freezing and thawing Frequent applications required	Darkens concrete slightly Does not bridge cracks
	Alkyl-alkoxy-silane Siloxanes	Surface free of pretreatments Sprayed, brushed, or rolled Ventilation required	Improves resistance to freezing and thawing Reduces salt penetration Reduces rate of corrosion	Improved resistance to water absorption and reinforcement corrosion Does not bridge cracks
	High-molecular-weight methacrylate	Clean, dry, and sound surface Sprayed, brushed, rolled, or squeegeed	Variable UV radiation resistance Prevents moisture from penetrating cracks	Seals cracks
Coatings	Epoxy Urethane or neoprene membrane/ epoxy top coat system Rubberized asphaltic top coat system Urethane Membrane/urethane topcoat system	Clean. dry, and sound surface Sprayed, brushed, rolled or squeegeed Approximately 50 °F (10 °C) or above Ventilation required Level surface typically required	Generally improves resistance to freezing and thawing Fair to good abrasion resistance Variable UV radiation resistance	Generally good resistance to water absorption Unknown resistance to reinforcement corrosion Bridges small cracks
Overlays	Concrete Polymer concrete Polymer-modified concrete	Clean, sound, and roughened surface Hand or machine applied Generally above freezing Ventilation may be required	Improves resistance to freezing and thawing Excellent abrasion resistance	May add weight Architectural finish is possible Protects structural concrete and reinforcement May improve structural capacity

Table 6.2: Types of concrete surface treatments (ACI Committee 546, 2004).

6.2.2 Cathodic protection

It is an electrochemical technique that protects steel from corrosion providing direct continuous electrical current that goes from an anode to the steel rebar. The aim is to make the reinforcing steel cathodic so that it is protected from corrosion. This is possible electrically connecting the steel to another metal that become the anode. Two different systems can be identified:

- Impressed current system protection
- Sacrificial (galvanic) cathodic protection

The first one consist in providing a current flow through an electric power source, from an external anode to the steel rebar. It is constituted by an anode (slow rate corrosion metal such as Platinum), a power source, connecting cables and monitoring and measuring devices.

Instead, in the second method the current is produced by coupling two different metals. It exploits the oxidation potential of the sacrificial anode (usually zinc), that is electrically connected to the steel through the concrete (electrolyte). The potential difference between the steel (cathode) and the anode creates a current flow that decreases consistently the corrosion attack. In fact, due to the more negative oxidation potential, the anode undergoes to corrosion more easily then the steel, protecting it.

This protection method is influenced by several factors such as concrete resistivity, moisture content, temperature, permeability, chloride content, pH and amount of reinforcing steel. The impressed current system needs continuous maintenance and monitoring, differently from the galvanic system where the current is regulated automatically when the environmental conditions change. Monitoring stations can be installed to compute the remaining service life of the anode. They are connected to both, the anode and the cathode, and measure the current flow between them (ACI Committee, 2004). The use of cathodic protection is suitable for any type of reinforced concrete structures. It is important that the reinforcing steel is electrically continuous and that the concrete has good conductive properties (specific resistivity and moisture content). This method is used in new constructions too, placing anodes at level of reinforcement (ACI Committee, 2005).

The types of sacrificial passive cathodic systems are:

- Zinc hydrogel anodes (zinc sheet anodes pre coated with conductive hydrogel adhesive applied to the concrete surface) (Figure 6.4)
- Sprayed zinc or zinc alloys
- Embedded galvanic anodes (localized galvanic protection where the anodes are attached to the steel and embedded in the repair concrete) (Figure 6.5)

The types of impressed current cathodic protections are:

- Surface-mounted anodes without concrete overlays
- Conductive mastic anodes (conductive coating with embedded anodes)
- Plate-type anodes (anode plates glued to concrete surface)
- Surface-mounted anodes with concrete overlays
- Mesh-type noble metal anodes (anodes fixed to concrete with pins and then covered with concrete)
- Conductive polymer concrete strips (anodes fixed to concrete and covered with cementitous overlay)
- Embedded anodes (anodes in concrete or at reinforcement level in case of new constructions)
- Saw slot anodes (slots filled with noble metal anodes and conductive polymer concrete on the concrete surface)

Figure 6.4: Surface applied galvanic anode system
(Vector corrosion technologies).

Figure 6.5: Galvanic embedded anodes (Vector corrosion technologies).

6.2.3 Chloride extraction

Electrochemical chloride extraction (ECE) consists of removing chlorides ions from the concrete through ion migration. This is possible applying on the surface of the concrete an anode that is connected to a power supply together with the steel reinforcement, so that they have opposite charge. In this way the chloride ions migrate through the anode because they are negatively charged, and go outside the concrete into the electrolyte that surround the anode. At the same time the production of hydroxyl ions at the steel rebar surface occurs, causing a pH increase and a repassivation of the rebar. After the treatment everything is removed from the concrete surface. Its duration depend on the quantity of chloride ions and of reinforcing steel, treatment density and concrete properties (permeability, electrical resistivity...) and it range between 3 and 8 weeks (ACI Committee, 2004).

6.2.4 Realkalization

It is an electrochemical treatment that increase the pH of concrete subjected to carbonatation. The application procedure is similar to ECE whit a shorter treatment time that goes from 3 to 10 days (ACI Committee, 2004).

6.2.5 Reinforcement repair

One possibility is the replacement of the steel bar. The damaged part is cut and then replacement bars are merged through welding or mechanical connections. If the reinforcement undergo a loss of cross-section an alternative to the total substitution can be the addition of supplemental reinforcement. Another type of intervention consists in treating the steel reinforcement with a coating. It can be epoxy, polymer-cement slurry or zinc-rich coating. The thickness of the protective layer should be lower then a certain value in order to avoid loss of bond strength between the steel and the concrete. In the case of prestressing steel it should be detensioned before the reparation and then tensioned again (ACI Committee, 2004).

Chapter 7

Corrosion monitoring techniques

An efficient and continuous monitoring of the structure plays a key role in the prevention and minimization of corrosion damages. In fact, when the damage is visible by eyes it means that the structure is in an advanced state of decay and a minimal intervention is not sufficient any more for its rehabilitation. It is fundamental to intervene on the structure at early stage of degradation so that a repair intervention can be less costly and easier to realize.

The control of the state of degradation of reinforced concrete elements can be done trough field and laboratory tests, performed on site, on the real structure, and in laboratory's specimens and models, respectively. Usually, both types of tests are carried out in order to have a clear and detailed description of the real conditions of the structure analysed. Another differentiation is between non-destructive and destructive tests, depending on how much the structure is affected by the test (Bien et al. 2019). Destructive methods give informations about the speed of corrosion, while non destructive methods about evolution of corrosion over time.

7.1 Destructive methods

The evaluation of the corrosion level through destructive techniques is usually avoided because of the induced damages in the structure. Basically they consist in drilling cores to create holes that permit direct access to the steel reinforcement. In this way the corrosion level in the rebars and the concrete state can be assessed. Many informations about concrete and steel conditions can be obtained with this method, but the destructive nature and the necessity to execute a repair operation after the test, have not allowed widespread use in the detection of corrosion phenomenon.

7.2 Non destructive methods

Many non-destructive techniques can be used to evaluate the corrosion level in steel reinforcement rebars. Verma et al. (2013) listed the most used methods to assess corrosion and concrete damages with relative advantages, disadvantages and functioning principles (Table 7.1). In this section are reviewed in detail the principle ones and some additional techniques commonly used.

7.2.1 Acoustic Emission Monitoring (AE)

It is considered as a passive structural health monitoring method. The sensors used in this technology are able to detect damages in the structures at early stage. In fact, the formation of microcracking in concrete causes strain energy release in form of elastic waves, that are detected from the sensors. These can be located on concrete surface or be embedded inside the concrete. Abouhussien et al. 2015, performing accelerated corrosion tests, demonstrate that the AE measured parameters can be easily correlated to the degree of degradation of the reinforced concrete (percentage of steel mass loss or crack width), permitting an early intervention and cost saving.

7.2.2 Infrared Thermography

This method can be used to detect a wide range of defects that can be present in RC structures. In the specific case of corrosion, it exploits the different thermal, electric and magnetic characteristics of rebars subjected and not to corrosion attack. It does not require direct contact with the embedded rebar, that is heated remotely from concrete (active method). Then, the heat is transferred from steel to concrete by conduction and the IR thermography is used to measure the temperature at concrete surface. IR camera is able to capture infrared radiations, converting them into electronic signals that are then used to create images, where different colours correspond to different IR radiation densities (Figure 7.1). Higher is the temperature and more are the radiations emitted, but the technique can be applied without surface heating too (passive method). Areas of the reinforcement subjected to corrosion can be identified because of the different IR emission density of non corroded parts (Baek et al. 2012).

7.2.3 X-ray/Gamma Radiography

Radiography permits to identify the concrete status and the presence of possible damages in the reinforcement. In this technique both X-rays and γ rays can be used. These pass through the material and are modified according to its nature and characteristics. Rays are transformed into visible light using a fluometallic converter so that defects in the structure can be localized (Song et al. 2007).

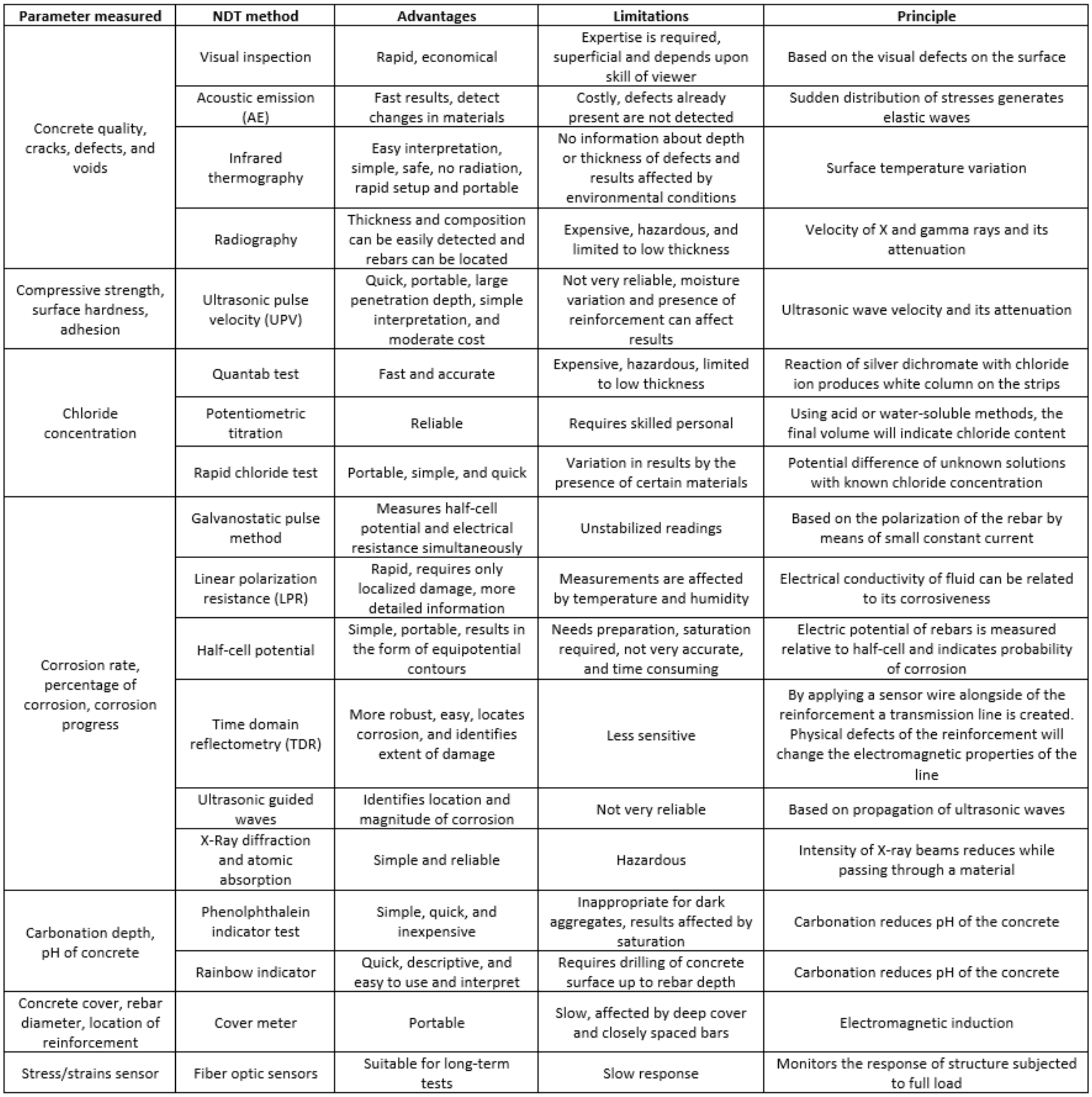

Parameter measured	NDT method	Advantages	Limitations	Principle
Concrete quality, cracks, defects, and voids	Visual inspection	Rapid, economical	Expertise is required, superficial and depends upon skill of viewer	Based on the visual defects on the surface
	Acoustic emission (AE)	Fast results, detect changes in materials	Costly, defects already present are not detected	Sudden distribution of stresses generates elastic waves
	Infrared thermography	Easy interpretation, simple, safe, no radiation, rapid setup and portable	No information about depth or thickness of defects and results affected by environmental conditions	Surface temperature variation
	Radiography	Thickness and composition can be easily detected and rebars can be located	Expensive, hazardous, and limited to low thickness	Velocity of X and gamma rays and its attenuation
Compressive strength, surface hardness, adhesion	Ultrasonic pulse velocity (UPV)	Quick, portable, large penetration depth, simple interpretation, and moderate cost	Not very reliable, moisture variation and presence of reinforcement can affect results	Ultrasonic wave velocity and its attenuation
Chloride concentration	Quantab test	Fast and accurate	Expensive, hazardous, limited to low thickness	Reaction of silver dichromate with chloride ion produces white column on the strips
	Potentiometric titration	Reliable	Requires skilled personal	Using acid or water-soluble methods, the final volume will indicate chloride content
	Rapid chloride test	Portable, simple, and quick	Variation in results by the presence of certain materials	Potential difference of unknown solutions with known chloride concentration
Corrosion rate, percentage of corrosion, corrosion progress	Galvanostatic pulse method	Measures half-cell potential and electrical resistance simultaneously	Unstabilized readings	Based on the polarization of the rebar by means of small constant current
	Linear polarization resistance (LPR)	Rapid, requires only localized damage, more detailed information	Measurements are affected by temperature and humidity	Electrical conductivity of fluid can be related to its corrosiveness
	Half-cell potential	Simple, portable, results in the form of equipotential contours	Needs preparation, saturation required, not very accurate, and time consuming	Electric potential of rebars is measured relative to half-cell and indicates probability of corrosion
	Time domain reflectometry (TDR)	More robust, easy, locates corrosion, and identifies extent of damage	Less sensitive	By applying a sensor wire alongside of the reinforcement a transmission line is created. Physical defects of the reinforcement will change the electromagnetic properties of the line
	Ultrasonic guided waves	Identifies location and magnitude of corrosion	Not very reliable	Based on propagation of ultrasonic waves
	X-Ray diffraction and atomic absorption	Simple and reliable	Hazardous	Intensity of X-ray beams reduces while passing through a material
Carbonation depth, pH of concrete	Phenolphthalein indicator test	Simple, quick, and inexpensive	Inappropriate for dark aggregates, results affected by saturation	Carbonation reduces pH of the concrete
	Rainbow indicator	Quick, descriptive, and easy to use and interpret	Requires drilling of concrete surface up to rebar depth	Carbonation reduces pH of the concrete
Concrete cover, rebar diameter, location of reinforcement	Cover meter	Portable	Slow, affected by deep cover and closely spaced bars	Electromagnetic induction
Stress/strains sensor	Fiber optic sensors	Suitable for long-term tests	Slow response	Monitors the response of structure subjected to full load

Table 7.1: Non destructive corrosion detection methods in reinforced concrete structures (Verma et al. 2013).

Figure 7.1: Digital photography (left) and IR camera photography (right) of a bridge.

7.2.4 Ultrasonic Pulse Velocity Measurement (UPV)

This method consists on measuring the speed of sound (ultrasonic) through materials and permits to identify damages and to measure material strength. In fact, eventual cracks or voids in the concrete increase the travel time of the pulse. It is necessary that the electro-acoustical transducer that produces the pulses is well connected to the material surface and sometimes the high roughness of concrete surface impedes this, making the technique difficult to be used. The pulse is received from another transducer that can be located in a opposite position (direct transmission), diagonally (diagonal transmission) or on the same surface (indirect transmission), respect to the other (Song et al. 2007).

Pulse velocity is computed as:

$$V = \frac{L}{T} \tag{7.1}$$

- L: distance between the transducers
- T: transmit time or time for the impulse to reach the receiver $[\mu s]$

The ultrasonic pulse velocity values associated to different concrete quality categories and concrete compressive strengths are reported in Table 7.2.

7.2.5 Galvanostatic Pulse Transient Method

This technique involves the use of an electrode, placed on concrete surface, that creates a current pulse up to 10 seconds, so that the reinforcement is polarized (Song et al. 2007). A reference electrode measures the change in the reinforcement potential, that at a fixed time can be computed as:

$$V_t(t) = I_{app}[R_p[1 - exp(-t/RpC_{dl})]] + R_\Omega \tag{7.2}$$

- R_p: polarization resistance

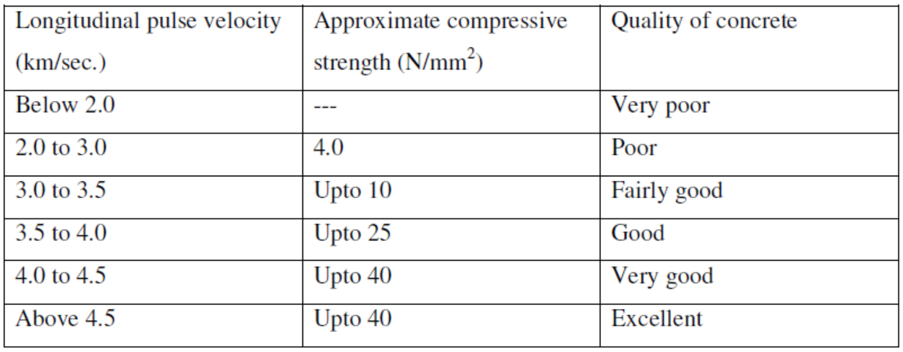

Longitudinal pulse velocity (km/sec.)	Approximate compressive strength (N/mm^2)	Quality of concrete
Below 2.0	---	Very poor
2.0 to 3.0	4.0	Poor
3.0 to 3.5	Upto 10	Fairly good
3.5 to 4.0	Upto 25	Good
4.0 to 4.5	Upto 40	Very good
Above 4.5	Upto 40	Excellent

Table 7.2: Ultrasonic pulse velocity and concrete quality (Song et al. 2007).

- C_{dl}: double layer capacitance
- R_{Ω}: ohmic resistance

These values are obtained from experimental results.

7.2.6 Linear Polarization Resistance Measurement (LPR)

This method is considered more accurate and less intrusive than the previous described. In fact, the measurements provide much more informations and it is necessary just one connection to the steel rebar. This technique consists in changing the potential of the reinforcement of a small amount (ΔE) and measuring the current decay (ΔI), or applying a small current (ΔI) to the reinforcement and measuring the change in the potential (ΔE) after a fixed time. In both cases an electrode applied on the concrete surface is used. Then the polarization resistance is computed as:

$$R_p[k\Omega cm^2] = \Delta E/\Delta I \tag{7.3}$$

And then the corrosion rate is obtained as:

$$I_{corr}[\mu A/cm^2] = B/R_p \tag{7.4}$$

B: Ster-geary constant (25 mV for active steel and 50 mV for passive steel)

The corrosion current density is calculated dividing the corrosion rate by the polarized steel area:

$$i_{corr} = I_{corr}/A \tag{7.5}$$

In order to have accurate measurements it is necessary to know exactly which one is the polarized area and the most used method consists in the use of a guard ring that is able to confine the current in a specific area (Martinez et al. 2009). The measurement of corrosion current density can be correlated to the reinforcement section loss and an estimation of the structure remaining service life can be done. Table 7.3 reports the corrosion current values and the rebar conditions associated. It is necessary to take into account that the measurements are affected by temperature and humidity.

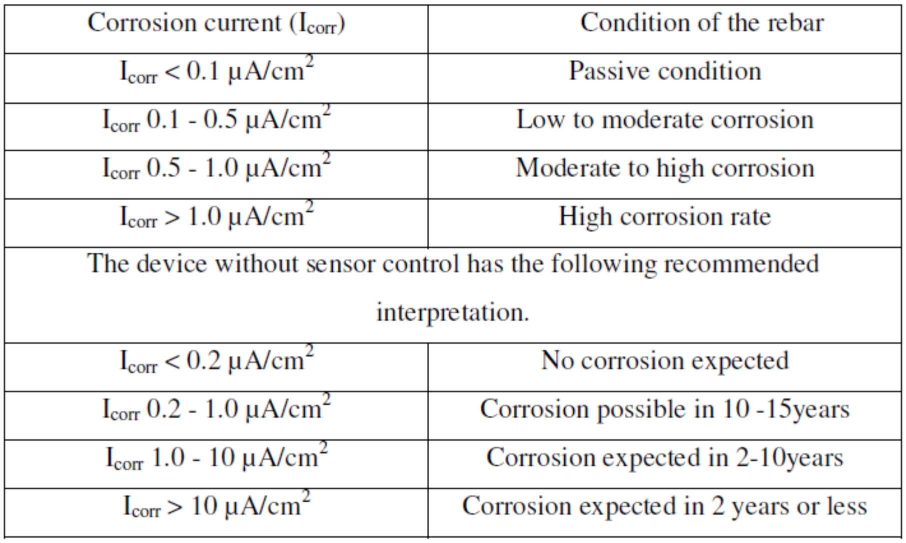

Corrosion current (I_{corr})	Condition of the rebar
$I_{corr} < 0.1\ \mu A/cm^2$	Passive condition
I_{corr} 0.1 - 0.5 $\mu A/cm^2$	Low to moderate corrosion
I_{corr} 0.5 - 1.0 $\mu A/cm^2$	Moderate to high corrosion
$I_{corr} > 1.0\ \mu A/cm^2$	High corrosion rate
The device without sensor control has the following recommended interpretation.	
$I_{corr} < 0.2\ \mu A/cm^2$	No corrosion expected
I_{corr} 0.2 - 1.0 $\mu A/cm^2$	Corrosion possible in 10 -15years
I_{corr} 1.0 - 10 $\mu A/cm^2$	Corrosion expected in 2-10years
$I_{corr} > 10\ \mu A/cm^2$	Corrosion expected in 2 years or less

Table 7.3: Corrosion current values and the associated rebar conditions (Song et al. 2007).

7.2.7 Open Circuit (Half - cell) Potential Measurements

This method is based on the measurement of the difference in corrosion potential of steel rebar whit respect to a reference electrode (half - cell) that is positioned on the concrete surface. It is necessary to connect the electrode to the reinforcement through a voltmeter. The potential vary according to the characteristic of the surrounding environment, in this case represented by the concrete. It is the most widespread electrochemical technique in the measurement of corrosion, but it can give information only about the corrosion probability of the reinforcement (Verma et al. 2014). Moreover, it is always necessary to combine the results of this analysis with the ones obtained from others methods, because they can be affected and altered by several factors.

Corrosion conditions associated whit specific potential ranges are reported in Table 7.4. The potential values are the differences in voltage between the rebar and the reference electrode. Both measurements, using saturated calomel (SCE) and copper/copper sulfate (CSE) electrodes, are shown.

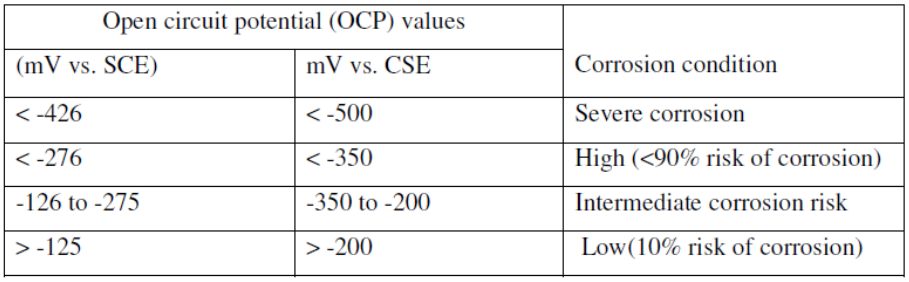

Open circuit potential (OCP) values		Corrosion condition
(mV vs. SCE)	mV vs. CSE	
< -426	< -500	Severe corrosion
< -276	< -350	High (<90% risk of corrosion)
-126 to -275	-350 to -200	Intermediate corrosion risk
> -125	> -200	Low(10% risk of corrosion)

Table 7.4: Relaionship between HCP measurements and corrosion conditions (Song et al. 2007).

7.2.8 Concrete Resistivity Measurements

The resistivity of concrete is a property strongly related with the corrosion process. In fact, higher is the concrete resistivity and slower is the corrosion, due to the more difficult passage of the current flow between anode and cathode zones. For the measurement, electrodes and surface and embedded probes are used. A known current (I) is generated on the outer probes and in the inner probes the potential drop (V) is measured, so resistance is obtained as:

$$R = V/I \tag{7.6}$$

And concrete resistivity is expressed as:

$$\rho = 2\pi a R \tag{7.7}$$

- a: inner electrodes distance [cm]
- R: resistance [ohm]

This property depend on concrete quality and on environmental conditions (humidity, temperature). Table 7.5 shows the concrete resistivity ranges and the associated corrosion risk (Song et al.2007).

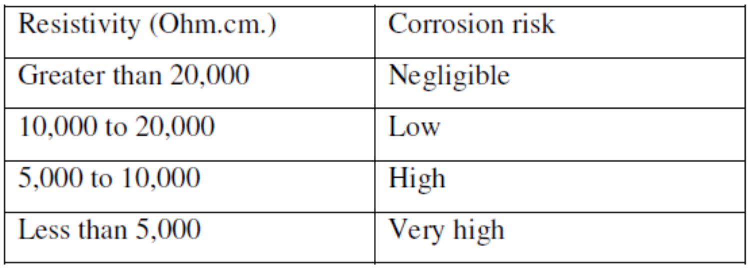

Resistivity (Ohm.cm.)	Corrosion risk
Greater than 20,000	Negligible
10,000 to 20,000	Low
5,000 to 10,000	High
Less than 5,000	Very high

Table 7.5: Concrete resistivity and correspondent corrosion risk (Song et al. 2007).

7.2.9 Electrochemical Impedance Spectroscopy (EIS)

In this technique an alternating voltage is applied to the reinforcement rebar and the current is measured for different frequencies. This method can provide more informations then the previous mentioned but needs more time to be performed and usually is done only in laboratories. The results are similar to the ones of linear polarisation method. The parameters measured are the same but the current is expressed in terms of time in the liner polarisation and in terms of frequency in this method.

Harmonic Analysis is an evolution of the impedance spectroscopy. In fact, it is based on the same principles but it requires less time to be carried out. A voltage perturbation is applied to the rebar at a single frequency and the current is measured (i_1). The first and second harmonics are measured too (i_2, i_3) and the corrosion rate is computed as:

$$I_{corr} = \frac{i_1^2}{\sqrt{48}\sqrt{2i_1 i_3 - i_2^2}} \tag{7.8}$$

A limitation of this technique is on the assumption of uniform corrosion. In fact, in case of localized corrosion the measurement has low accuracy (Song et al. 2007).

7.2.10 Embeddable Corrosion Monitoring Sensors (ECI)

This sensor type permits to obtain early and real time measurements of corrosion level in reinforcement and it is mainly used in new structures. All the values measured are transferred through a digital network. These instruments permit to measure many corrosion related parameters, such as corrosion potential, galvanic currents, concrete resistivity, water content and the corrosion rate. All the values obtained are transferred through a digital network.

Optical fibre sensors are used a lot because of they small size and capacity to resist in hard environmental conditions (Figure 7.2). The majority of these sensors are passive and are based on the principle of reflectometry, that consist in transmitting a light ray or wave into the fiber and then to process the backscattered signals using a photodetector. If the fiber presents deformation due to strain of cracks in the material, the signal will detects it, showing differences from the emitted one.

Figure 7.2: Optical fiber sensors on a reinforcement concrete column.

7.2.11 Cover Thickness Measurement

The instrument used is called covermeter of profometer and permits to measure concrete cover thickness,rebar size and position, moving it on concrete surface (Figure 7.3). This is possible creating a magnetic field though the use of a probe coil. Current flows in the coil and the voltage is altered in presence of metal objects. It changes as a function of concrete cover and bar diameter.

Figure 7.3: Covermeter

Conclusions

The aim of this research is to evaluate the effects of bond degradation between steel and concrete in corroded reinforced concrete structures. The study is carried out applying the empirical model ARC2010 for bond degradation to the bridge overpass designed by De Gaetano, 2019. In the previous study only the steel area loss effect on the bridge pier capacity was taken into account. Focusing on the additional aspect of adherence it is possible to highlight its influence in the determination of the corroded structure service life and to compare the results obtained if this aspect is considered or neglected. The bond between steel and concrete is essential for the characteristics of the two materials to be fully exploited, that is why a strong change in the RC element capacities is advisable if bond undergoes to degradation. This study confirms the expectations of a drastic reduction in strength capacity and ductility of the bridge pier if bond strength reduction is considered in addition to the steel area loss. The results obtained by De Gaetano, 2019, show an important reduction in the pier strength capacity, with halving of the structure service life.

The bond degradation has been considered decreasing in a proportional way the steel yield strength. This causes a further reduction of the pier strength and an earlier failure of the structure. Moreover, as corrosion progresses, the ductility of RC pier section is completely lost. In fact, according to the hypothesis done, the steel can reach yield strength and exhibits plastic behaviour only if the bond is in perfect conditions. So, the degradation of the bond transforms from ductile to fragile the behaviour of the reinforced concrete section. The absence of ductility in a RC element caused abrupt failure of the structure, in fact, if the material cannot enter in the plastic field, no deformation will be visible by eyes and the collapse of the structure will be unexpected without the possibility to repair it in time.

The bond degradation effect cannot be neglected in the study of a corroded structure in seismic zone. This study permits to estimates a possible failure time without any kind of in field investigation and in the situation in which no intervention is carried out on the structure during its service life. From the results obtained it is possible to understand that for a structure located in a zone close to the sea and of high seismic hazard, monitoring is necessary to control the corrosion process and to identify the best intervention to be carried out in order to avoid early failure of the structure.

Ringraziamenti

Voglio ringraziare tutte le persone che mi hanno aiutato e sostenuto per la realizzazione di questa tesi e durante il percorso di studi che mi ha permesso di arrivare fin qui.

Sono grata di aver avuto l'opportunità di partecipare ad un programma di scambio internazionale durante il quale ho iniziato il lavoro di tesi presso l'Universitat Politècnica de Catalunya.

Studiare presso due atenei diversi non solo mi ha permesso di frequentare due centri universitari all'avanguardia, ma anche di poter collaborare con il Professor Casas e il Professor Domaneschi per il progetto di tesi.

Ringrazio entrambi per il sostegno costante e l'aiuto che mi hanno dato. La loro continua disponibilità e i loro spunti mi hanno permesso di andare avanti nello svolgimento di questo lavoro. Li ringrazio per avermi guidata e per avermi insegnato molto, sia durante le lezioni che durante la scrittura della tesi.

Ringrazio anche Antonino, che non ho mai incontrato ma con la sua gentilezza e disponibilità mi ha sempre aiutata per qualsiasi dubbio sul lavoro di tesi e non solo. E' stato una guida per me durante questo ultimo anno e sono contenta di aver avuto l'opportunità di continuare la sua ricerca.

Ringrazio poi la mia famiglia e in particolare i miei genitori che mi sono sempre stati vicini nonostante la distanza, sempre pronti a festeggiare i miei successi e a sostenermi nei momenti più duri.

Un ringraziamento anche a Chiara, Matteo e Jacopo, la mia famiglia di Torino, e a tutti gli amici dell'università di Torino e di Firenze, che hanno sempre rappresentato un'ancora di salvezza nei momenti di scoraggimento di questo percorso. Senza di loro gli insuccessi e le preoccupazioni sarebbero stati più difficili da superare e i momenti di felicità non sarebbero stati tanto belli.

Grazie a tutte le persone che ho conosciuto a Barcellona in università e non, professori, colleghi, coinquilini e amici che hanno reso questa esperienza unica e bellissima.

E infine grazie a Chiara, Jasmine, Federico e Lorenzo, siete la mia casa in qualsiasi posto mi trovi.

Bibliography

Abouhussien A.; Hassan A., 2015, ’Evaluation of damage progression in concrete structures due to reinforcing steel corrosion using acoustic emission monitoring’. Journal of Civil Structural Health Monitoring, Vol. 5, pp.751-765.

ACI Committee 546, ’Concrete Repair Guide (ACI 546R-04)’. American Concrete Institute, Farmington Hills, Mich., 2004, pp. 39-40.

ACI Committee E 706, ’Installation of embedded galvanic anodes’. ACI RAP bulletin 8, 2005.

Al-Sulaimani, G.J., Kaleemullah, M., Basunbul, I.A., 1990, ’Influence of corrosion and cracking on bond behaviour and strength of reinforced concrete members’. ACI Structural Journal, Vol. 87, n° 2, pp. 220-231.

Angst U., 2019, ’Durable concrete structures: cracks & corrosion and corrosion & cracks’. 10th International Conference on Fracture Mechanics of Concrete and Concrete Structures, FraMCos-X (Bayonne, France).

Apostolopoulos C.; Koulouris K.; Apostolopoulos A., 2019, ’Correlation of Surface Cracks of Concrete due to Corrosion and Bond Strength (between Steel Bar and Concrete)’. Advances in Civil Engineering, Vol 2019.

Ashrafi H.; Bazli M.; Oskouei A., 2017, ’Enhancement of bond characteristics of ribbed-surface GFRP bars with concrete by using carbon fibre mat anchorage’. Construction and Building materials, Vol. 134, pp. 507-519.

Baek S.; Xue W.; Feng M. Q.; Kwon S., 2012, ’Nondestructive Corrosion Detection in RC Through Integrated Heat Induction and IR Thermography’. Journal of Nondestructive Evaluation, Vol.31, pp.181-190.

Bien J.; Kaminski T.; Kuzawa M., 2019, 'Taxonomy of non-destructive field tests of bridge materials and structures'. Archives of Civil and Mechanical Engineering, Vol. 19, pp.1353-1367.

Bilcik J.; Holly I., 2013, 'Effect of reinforcement Corrosion on Bond Behaviour'. Concrete and Concrete Structures 2013 Conference, Procedia Engineering, Vol. 65, pp. 248-253.

Bohni H., 2005, 'Corrosion in reinforced concrete structures'. Woodhead Publishing Ltd, Abington Hall, Abington Cambridge CB1 6AH, England, pp. 6-40.

Cairns J.; Dut Y.; Law D., 2008, 'Structural performance of corrosion-damaged concrete beams'. Magazine of concrete research, Vol 80, pp. 359-370.

Chen H.; Nepal J., 2014, Gamma process modelling for lifecycle performance assessment of corrosion affected concrete structures. The 2014 World Congress on Advances in Civil, Environmental, and Materials Research (ACEM14, Busan, Korea).

Chung, L., Jay Kim, J., Yi, S., 2008, 'Bond strength prediction for reinforced concrete members with highly corroded reinforcing bars'. Cement and Concrete Composites, Vol 30 , pp. 603-611.

Coronelli D., 2002, 'Corrosion cracking and bond strength modelling for corroded bars in reinforced concrete'. ACI Structural Journal, Vol. 99, pp. 267-276.

Coronelli D.; Gambarova P., 2004, 'Structural assessment of corroded reinforced concrete beams: Modeling guidelines'. Journal of Structural Engineering, Vol. 130, pp. 1214-1224.

Coronelli D.; Blomfors M.; Zandi K.; Lundgren K., 2018, 'Engineering bond model for corroded reinforcement'. Engineering Structures, Vol. 156, pp. 394-410.

De Gaetano A., 2019, 'Seismic performance of deteriorating concrete bridges'. Master's thesis, Politecnico di Torino.

Domaneschi M.; De Gaetano A.; Casas J.R.; Cimellaro G.P., 2020,'Deteriorated seismic capacity assessment of reinforced concrete bridge piers in corrosive environment'. Structural Concrete, pp. 1-16.

Domaneschi M.; Pellecchia C.;De Iuliis E.; Cimellaro G. P.; Morgese M.; Khalil A.A., Ansari F., 2020, 'Collapse analysis of the Polcevera Viaduct by the Applied Element Method'. Engineering Structures, Vol. 214, 110659.

Du C.; Twumasi J. O.; Tang Q.; Guo X.; Zhou J.; Yu T.; Wang X., 2018, 'All-Optical Photoacoustic Sensors for Steel Rebar Corrosion Monitoring'. Sensors, Vol. 18.

El Safty A.;Yousri K. M.;El Din H. S., 2019,'Concrete repair and cathodic protection of corroded reinforced concrete structure'. The 2009 PCI Convention and National Bridge Conference, San Antonio, Texas.

FIB 1990, Model Code for Concrete Structures 1990. Federation Internationale du Beton. Laussane.

FIB 2010, Model Code for Concrete Structures 2010. Federation Internationale du Beton. Lausanne.

Fischer C.; Ozbolt J., 2013, 'An appropriate indicator for bond strength degradation due to reinforcement corrosion'. VIII International Conference on Fracture Mechanics of Concrete and Concrete Structures FraMCoS-8 (Toledo, Spain).

Gonzalez F.; Fernandez J.; Agranati G.; Villanueva P., 2018, 'Influence of construction conditions on strength of post installed bonded anchors'. Construction and Building Materials, Vol. 165, pp. 272-283.

Gudonis E.; Kacianauskas R.;Gribniak V.; Weber A.;Jakubovskis R.; Kaklauskas G., 2014, 'Mechanical Properties of the Bond Between GFRP Reinforcing Bars and Concrete'. Mechanics of Composite Materials, Vol. 50, pp. 457-466.

Kabir M.; Islam M., 2014, 'Bond stress behaviour between concrete and steel rebar: Critical investigation of pull-out test via Finite Element Modeling'. International Journal of Civil and Structural Engineering, Vol. 5, pp. 80-90.

Kivell, A.R.L., 2012. Effects of bond deterioration due to corrosion on seismic performance of reinforced concrete structures (Master's thesis in faculty of Civil Engineering, University of Canterbury).

Lin H.; Zhao Y., 2016, 'Effects of confinements on the bond strength between concrete and corroded steel bars'. Construction and Building Materials, Vol. 118, pp. 127-138.

Lundgren K., 2005, 'Bond between ribbed bars and concrete. Part 1: Modified model'.

Magazine of concrete research, Vol. 57, pp. 371-382.

Lundgren K., 2005, 'Bond between ribbed bars and concrete. Part 2: The effect of corrosion'. Magazine of Concrete Research, Vol. 57, pp. 383-395.

Lundgren K.; Kettil P.; Zandi Hanjari K.; Schlune H.; Soto San Roman A., 2012, 'Analytical model for the bond-slip behaviour of corroded ribbed reinforcement'. Structure and Infrastructure Engineering, Vol. 8, pp. 157-169.

Martinez I.; Andrade C., 2009, 'Examples of reinforcement corrosion monitoring by embedded sensors in concrete structures'. Cement and Concrete composites, Vol. 31, pp.545-554.

Moodi Y.; Sohrabi M.; Mousavi S., 2020, 'Effects of stirrups in spliced region on the bond strength of corroded splices in reinforced concrete (RC) beams'. Construction and building materials, Vol 230.

Morgese M.; Ansari F.; Domaneschi M.; Cimellaro G. P., 2020, 'Post-collapse analysis of Morandi's Polcevera viaduct in Genoa Italy'. Journal of Civil Structural Health Monitoring, Vol. 10, pp. 69-85.

National Academies of Sciences, Engineering, and Medicine, 2013. 'Design Guide for Bridges for Service Life'. Washington, DC: The National Academies Press.Chapter 5, pp. 235-250.

RILEM TC, 1994, 'RC 6 Bond test for reinforcement steel. 2. Pull-out test, 1983'. RILEM Recommendations for the Testing and Use of Constructions Materials, pp. 218-220.

RILEM TC, 1994, 'RC 5 Bond test for reinforcement steel. 1. Beam test, 1982'. RILEM Recommendations for the Testing and Use of Constructions Materials, pp. 213-217.

Song H.; Saraswathy V., 2007, 'Corrosion Monitoring of Reinforced Concrete Structures-A review'. International Journal of Electrochemical Science, Vol 2, pp. 1-27.

Spinella N.; Colajanni P.; Recupero A.; Tondolo F., 2019, 'Ultimate Shear of RC Beams with Corroded Stirrups and Strengthened with FRP'. Buildings, Vol. 9, pp. 1-14.

Tuutti K., 1982, 'Corrosion of steel in concrete'. Swed. Cem. Conc. Res. Ins. PhD Thesis.

Verma S.; Bhadauria S.; Akhtar S., 2013, 'Review of Nondestructive testing methods for condition Monitoring of Concrete Structures'. Journal of construction Engineering, Vol 2013, pp.1-11.

Verma S.; Bhadauria S.; Akhtar S., 2014, 'Monitoring Corrosion of Steel Bars in Reinforced Concrete Structures'. The Scientific World Journal, Vol 2014.

Virmani Y. P.; Clemena G., 1998,'Corrosion protection - Concrete bridges'. Technical report Turner-Fairbank highway research center.

Yang Y.; Nakamura H.; Miura T.; Yamamoto Y., 2019, 'Effect of corrosion-induced crack and corroded rebar shape on bond behaviour'. Structural Concrete, Vol. 20, pp. 2171-2182.

Zandi Hanjari K.; Lundgren K.; Kettil P. et al., 2008, 'Structural behaviour of corroded reinforced concrete structures'. The Fourth International Conference on Bridge Maintenance, Safety, Management, Health Monitoring and Informatics pp. 481 (Seoul, Korea).

Zhao Y.; Lin H.; Wu K.; Jin W., 2013, 'Bond behaviour of normal/recycled concrete and corroded steel bars'. Construction and Building Materials, Vol. 48, pp. 348?359.

Zhao Y.; Lin H., 2018, 'The Bond Behaviour between Concrete and Corroded Reinforcement : State of the Art'. Sixth International Conference on the Durability of Concrete Structures (Leeds, United Kingdom).